Title

Impact of Maximal Overexpression of a Non-toxic Protein on Yeast Cell Physiology

Authors

Yuri Fujita[1], Shotaro Namba[1], Yoshiaki Kamada[2,3], Hisao Moriya[4]

Affiliations

[1]Graduate School of Environmental, Life, Natural Science and Technology, Okayama University

[2]National Institute for Basic Biology, Okazaki, Japan

[3]Graduate University for Advanced Studies (SOKENDAI), Hayama, Kanagawa, Japan

[4]Faculty of Environmental, Life, Natural Science and Technology, Okayama University

Competing interests

The authors declare that there are no competing interests.

Author contribution

YF and HM conceived and designed the experiments, YF and YK performed experiments, YF, SN, and HM analyzed the data, and YF and HM wrote the paper.

Summary

While it is recognized that excess expression of non-essential proteins burdens cell growth, the physiological state of cells under such stress is largely unknown. This is because it is challenging to distinguish between adverse effects arising from the properties of the expressed excess protein (cytotoxicity) and those caused solely by protein overexpression. In this study, we attempted to identify the model protein with the lowest cytotoxicity in yeast cells by introducing a new neutrality index. We found that a non-fluorescent fluorescent protein (mox-YG) and an inactive glycolytic enzyme (Gpm1-CCmut) showed the lowest cytotoxicity. These proteins can be expressed at levels exceeding 40% of total protein while maintaining yeast growth. The transcriptome of cells expressing mox-YG to the limit indicated that the cells were in a nitrogen source requirement state. Proteome analysis revealed increased mitochondrial protein and decreased ribosome abundance, similar to the inactivated state of the TORC1 pathway. The decrease in ribosome abundance was presumably due to defective nucleolus formation, partially rescued by a mutation in the nuclear exosome. These findings suggest that massive overexpression of excess protein, termed protein burden, causes nitrogen source starvation, a metabolic shift toward more energy-efficient respiration, and a ribosomal biosynthesis defect due to an imbalance between ribosomal protein and rRNA synthesis in the nucleolus.

Introduction

Expression levels of proteins are optimized to maximize the fitness of organisms, and the evolutionary principle that determines those levels is considered to be demand and constraint (Bruggeman et al., 2020) (Figure 1A). Demand is the evolutionary pressure that works to increase the expression of a protein to meet the requirements of its function, and constraint is the evolutionary pressure that works to decrease the expression of a protein to avoid the negative effects produced by excess protein. Constraints appear as disturbances in cellular function when the protein is overexpressed (Figure 1A, the red arrow). The mechanisms of constraining expression levels, or defects due to overexpression, can be roughly classified into four major categories (Moriya, 2015) (Figure 1B). “Resource overload” (also called “burden”) (Kastberg et al., 2022) is a disorder in which intracellular resources used for protein processing, such as synthesis, localization, degradation, and modification of proteins, are depleted or monopolized by the processing of that protein, resulting in a disruption of processing of other proteins (Dong et al., 1995; Eguchi et al., 2018; Kintaka et al., 2020, 2016; Stoebel et al., 2008). This phenomenon occurs in proteins with high expression levels. “Stoichiometry imbalance” is a disorder triggered by an imbalance of amounts between constituents within complexes, leading to untimely activation or inactivation (pathway modulation), degradation (resource overload), aggregation (promiscuous interaction), etc. (Kaizu et al., 2010; Makanae et al., 2013; Papp et al., 2003). This occurs due to the overexpression of proteins that form complexes. “Pathway modulation” is a disorder in which pathways are untimely activated or inactivated. This occurs especially with overexpression of proteins involved in pathway regulation, such as metabolic enzymes, kinases and phosphatases, and transcription factors (Prelich, 2012; Youn et al., 2017). “Promiscuous interaction” is a disorder in which weak interactions are enhanced by mass action to form complexes or aggregates that are not normally formed. This damages cellular function by inactivating essential proteins or overloading degradation resources, and is caused by overexpression of intrinsically disordered proteins or liquid-liquid phase-separating proteins (Bolognesi et al., 2016; Ma et al., 2010; Vavouri et al., 2009).

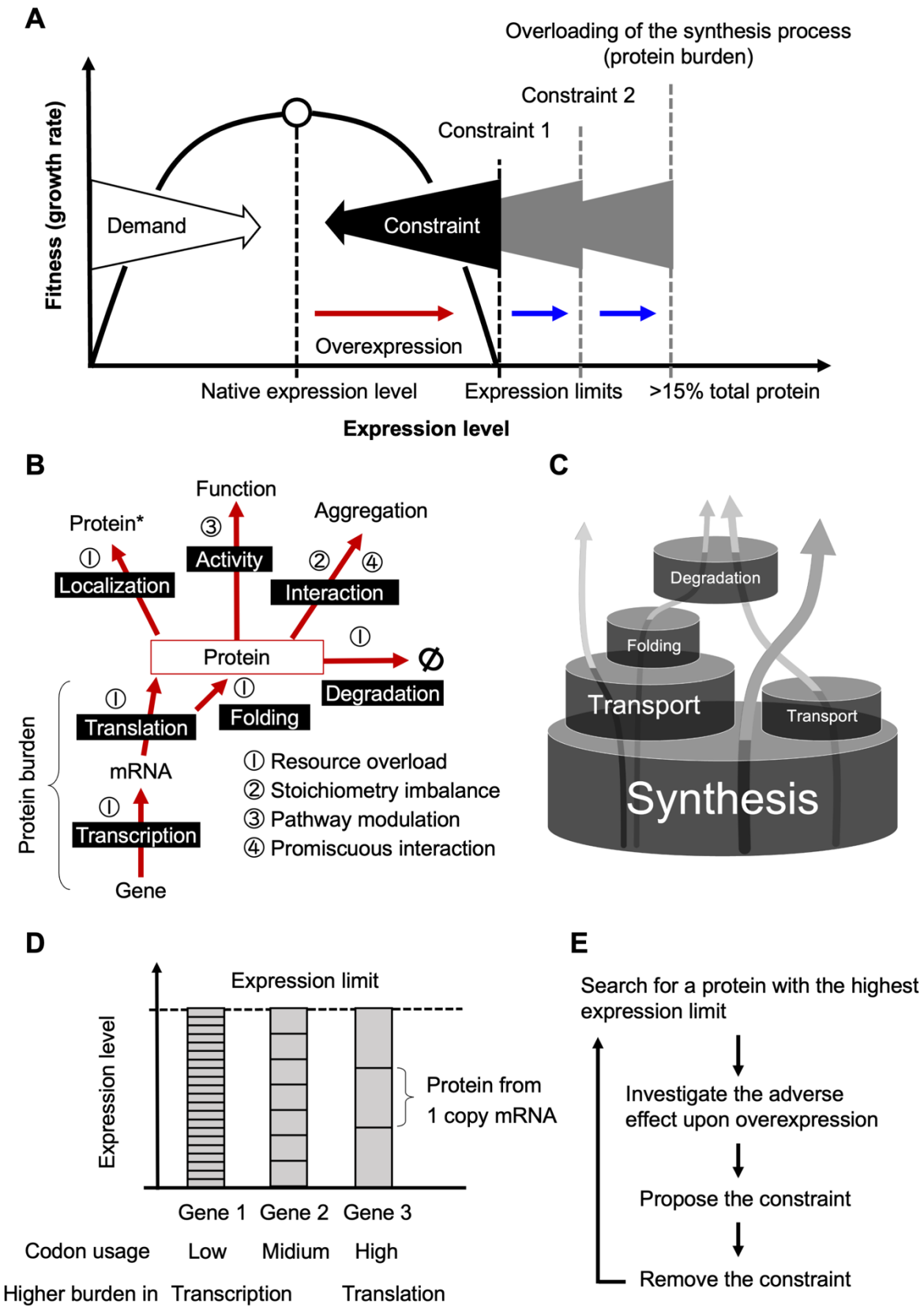

Figure 1. Schematic diagrams illustrating the constraints on protein expression levels.

63 **A**) Protein expression levels are determined by demand and constraints (created by the authors, inspired
64 by the work by Keren *et al*. (Keren et al., 2016). The existence of this evolutionary principle is revealed
65 by the relationship between fitness (growth rate) and expression level when the expression level is
66 altered, and in general, the native expression level provides the highest level of fitness for the organism
67 (Bruggeman et al., 2020). The existence of constraints is revealed by a decrease in fitness upon
68 overexpression (red arrow). Constraints determine the expression limit of the protein, i.e., the
69 expression level at which growth inhibition occurs (dotted lines), but there can be multiple constraints
70 for a single protein. The constraint that exists at the highest expression limit is protein burden.
71 **B)** Four major mechanisms that constrain protein expression levels. The figure outlines the fate of
72 proteins and shows what adverse effects occur upon overexpression (red arrows). The resource overload
73 that occurs within the synthesis process (transcription and translation) is specifically referred to as
74 protein burden. This diagram is a more concise redrawing of the author's earlier one (Moriya, 2015).
75 That asterisk means differentially localized proteins.
76 **C**) A barrel model for resource overload (modified from the author's earlier one) (Kintaka et al., 2020).
77 The size of the barrels represents the capacity of each process, and the arrows represent the fate of the
78 proteins processed there. The expression limit of a protein is defined by the lowest-capacity process
79 that processes the protein. Among these processes, synthesis, which processes all proteins, is considered
80 to have the largest capacity. Thus, proteins processed only by synthesis would have the highest
81 expression limits, and their overexpression would overload synthesis (i.e., cause protein burden).
82 Previous studies by the authors, conducted in this context, estimated that protein burden occurs at more
83 than 15% of total protein (Eguchi et al., 2018).
84 **D)** Difference in burden due to gene structure (codon optimization). The amount of transcription
85 required to achieve the same protein expression limit depends on the degree of codon optimization. This
86 may change whether transcription or translation results in a higher burden.
87 **E)** An ideal framework for protein burden studies. See text for details.

88

---

89 As the expression level of a protein increases, it eventually encounters one of the barriers created by
90 either these specified constraints or others that are unknown, all of which are related to the function and

91 physicochemical properties of the protein, and damage cellular function. The expression level at which
92 this occurs is referred to as the "expression limit" in this paper (see Figure 1A). If the constraints could
93 be removed from the protein, the expression limit would increase. For example, if components of a
94 complex are simultaneously expressed to resolve a stoichiometry imbalance, the expression limits of
95 those proteins will be increased (Kaizu et al., 2010; Makanae et al., 2013). In this manner, when (one)
96 constraint is removed from a protein, the expression limit would increase until the next constraint barrier
97 is hit (Figure 1A, dotted lines). The amount of expression limit created by a constraint barrier depends
98 on the type of constraint. Stoichiometry imbalances, pathway modulations, and promiscuous
99 interactions would create different expression limits for each protein. This is because they are
100 determined by the activity, regulatory mechanism, and physicochemical properties of each protein. On
101 the other hand, resource overload is presumed to be determined to some extent by the capacities of the
102 processes in the cell (Kintaka et al., 2020) (Figure 1C). Essentially, the synthesis, in which all proteins
103 are processed, should have the largest capacity, while processes such as transport, folding, and
104 degradation, in which only a fraction of proteins are processed, should have smaller capacities. In fact,
105 adding transport or degradation signals to a cytosolic protein lowers the expression limit (Kintaka et al.,
106 2016). In that light, the final constraint barrier that emerges when all possible constraints are removed
107 is the overloading of the synthesis process.
108
109 Overloading of the synthesis process is specifically referred to as "protein burden" or "protein cost"
110 (Eguchi et al., 2018; Kafri et al., 2016). It has long been the subject of study, mainly as an effect on
111 growth produced by excess (gratuitous) proteins that are not necessary for cellular function (Bruggeman
112 et al., 2020; Scott et al., 2010). This idea was first proposed in studies of the cost of unnecessary
113 induction of the *lac* operon in *Escherichia coli* (Koch, 1983). In recent years, much attention has been
114 paid to the actual mechanisms by which massive expression of excess protein inhibits growth and the
115 response of cells (Farkas et al., 2018; Kafri et al., 2016; Metzl-Raz et al., 2020). During protein burden,
116 it is presumed that depletion of the materials, machinery, and factors necessary for transcription and
117 translation occurs, along with competition from these monopolies. In particular, amino acids and
118 aminoacyl-tRNAs are major candidates for depletion (Kastberg et al., 2022). In addition, ribosomes,

119 which are crucial for protein synthesis, themselves require significant resources for their synthesis and
120 have therefore been considered major candidates for depletion during protein burden, as they compete
121 for these limited resources (Metzl-Raz et al., 2017). Mechanistic analysis of protein burden in budding
122 yeast, a model eukaryotic cell, has been intensively conducted by Barkai and colleagues, who reported
123 that transcription is rate-limiting in phosphate starvation and translation in nitrogen source starvation
124 (Kafri et al., 2016), and that basic transcription factors are limiting resources (Metzl-Raz et al., 2020).
125 In addition, a cellular response in the form of increased cell size and enhanced protein synthesis capacity
126 has been observed (Kafri et al., 2016). Thus, the previously expected decrease in ribosomes has not
127 been detected.
128
129 As mentioned above, to investigate protein burden, we need to overexpress proteins with minimal
130 constraints. This is because overexpressing proteins with additional constraints cannot overload the
131 synthetic process, as the additional constraints reduce the expression limits (Figure 1A). Also, the
132 cellular damage and cellular response generated by the constraint mask the protein burden response.
133 However, it remains unclear which proteins are not subject to constraints other than protein burden.
134 Proteins that would induce protein burden have been determined by assuming that they would be
135 minimally constrained based on their properties, and this assumption has been confirmed
136 experimentally. Model proteins selected in this manner in yeast include fluorescent proteins (FPs) and
137 certain glycolytic enzymes (Eguchi et al., 2018; Farkas et al., 2018; Kafri et al., 2016; Kintaka et al.,
138 2020, 2016). FPs do not have a specific function or interaction partner in yeast cells and are not actively
139 sorted into cellular compartments other than the cytosol. On the other hand, glycolytic enzymes are
140 naturally expressed at very high levels and are thus considered to be less constrained. Notably, these
141 proteins exhibit an expression limit of approximately 15% of total protein in yeast cells (Eguchi et al.,
142 2018). However, it is not clear whether these proteins are free from constraints other than protein burden.
143 This is because there may be unknown constraints, and there is no evidence that the measured
144 expression limit is the "true limit" at which protein burden occurs.
145

146 In addition to the protein (amino acid sequence) itself, there is another aspect to be considered when
147 selecting a model for protein burden. That is the nucleotide sequence of the gene used for expression,
148 i.e., transcriptional, and translational regulatory sequences, codon usage, and so on (Figure 1D). For
149 example, if a protein is to be expressed to the limit by a less codon-optimized and thus less
150 translationally efficient mRNA, a large amount of mRNA would be required, which would induce a
151 greater burden on transcription. Conversely, a similar attempt by an mRNA with high translation
152 efficiency would induce a greater burden on translation. These are the constraints inherent in protein
153 synthesis itself. Although there is some evidence that protein synthesis in nature is economically
154 designed to optimally load transcription and translation (Frumkin et al., 2017; Hausser et al., 2019;
155 Mahima and Sharma, 2023), it still needs to be determined what the genetic design should be to
156 minimize the burden.
157
158 Considering the above circumstance, a realistic approach to protein burden requires more than just
159 drawing straightforward conclusions from the overexpression of a single model protein (or gene).
160 Rather, it requires experimentally identifying proteins with the highest possible expression limits,
161 investigating the negative impacts of their overexpression, and, if any constraints are revealed,
162 examining whether their removal can increase expression limits. Through successive iterations, this
163 process gradually deepens our understanding of protein burden (Figure 1E). In each iteration, the least
164 constrained protein (and its gene) will be generated and utilized as a benchmark for further investigation
165 into proteins with high (or low) expression limits and the adverse effects of their overexpression. This
166 will (unintentionally) elucidate a new mechanism of constraint. Indeed, the enhanced green fluorescent
167 protein (EGFP), which we have used as a model for protein burden (Kintaka et al., 2020, 2016; Makanae
168 et al., 2013), was found to form a chaperone-entrapped aggregate upon overexpression and trigger the
169 heat shock response due to its low folding ability (Namba et al., 2022). Its overexpression also causes
170 abnormal yeast cell morphology through proteasomal stress as it contains cysteines. The moxGFP
171 (mox), which improved folding properties and lacks cysteine residues (Costantini et al., 2015), showed
172 a higher expression limit and no longer induced abnormal morphologies. However, even when

overexpressing mox, the anticipated depletion and competition for factors, or cellular responses to them have not been observed (Namba et al., 2022).

In this study, we found that a mutation causing loss of fluorescence in mox, and other fluorescent proteins increased the expression limit up to 3-fold, to more than 40% of total protein. Introducing a neutrality index (NI) to assess protein constraint, we found that non-fluorescent mox (mox-YG) and enzymatically inactive Gpm1 (Gpm1-CCmut) are currently the least constrained. Upon overexpression of mox-YG, depletion of amino acid or nitrogen sources, decreased ribosomal expression, and a metabolic shift from glycolysis to oxygen respiration were observed. Thus, physiological states, as anticipated with such protein burdens, are only generated by massive overexpression of proteins with significantly lower constraints. Some of the responses found appear to be due to inactivation of the TORC1 pathway, suggesting that eukaryotic cells use this regulatory pathway to buffer protein burden. In the burdened cells, the nucleolus was dysplastic, and mutations in the nuclear exosome partially restored this. Thus, the abnormal formation of liquid-liquid phase-separated organelles due to dilution may be one of the defects caused by the strong protein burden.

188 # Results

189 **Fluorescent property is a constraint on the expression of fluorescent proteins.**

190 To evaluate the expression limits of FPs, we overexpressed FPs to levels that induced growth inhibition.
191 Gene constructs, in which the *TDH3* promoter controls the target protein genes, were incorporated into
192 plasmids designed for the genetic-tug-of-war (gTOW) method (Figures 2A and Figure 2—figure
193 supplement 1A) (Moriya et al., 2006). Subsequently, yeast cells were transformed and cultured in a
194 medium depleted of leucine. The maximum growth rate (MGR) of cells was calculated from serial
195 measurements of optical density at 660 nm (OD_{660}). Protein levels were determined through the analysis
196 of proteins from cells in the logarithmic growth phase (Figure 2—figure supplement 1B). For each
197 protein, we also analyzed a mutant in which the Tyr residue forming the fluorophore was replaced with
198 Gly (YG mutation), resulting in a loss of fluorescence. This is because we unexpectedly found that this
199 mutation substantially increased the expression limits of FPs (see below).

200

201 Overexpression of the FPs and mutants all caused growth inhibition (Figure 2B, C). EGFP and mox
202 were expressed at about 15% of the total protein as previously reported (Kintaka et al., 2016), but
203 mCherry (mChe) and YG mutants were expressed at higher levels. Mox-YG expressed 44% of the total
204 protein (Figures 2D, E). Our previous work had evaluated only expression limits (Eguchi et al., 2018),
205 but we realized that we could not properly assess the constraints on each protein if the growth rates at
206 the expression limit were different. For example, the mChe's expression limit (20%) is higher than that
207 of sfGFP (17%), but the relative MGRs are 20% and 80%, respectively, which is much lower for mChe.
208 The relationship between %MGR and %protein level when the control is set at 100% is shown in the
209 scatter plot in Figure 2F. The lower left indicates more constraint as lower expression levels lead to
210 growth inhibition, and the upper right indicates less constraint as higher expression levels do not cause
211 growth inhibition. Here, we describe “unconstrained” as “neutral” and calculate the neutrality index
212 (NI) as the product of %MGR and %protein level.

213

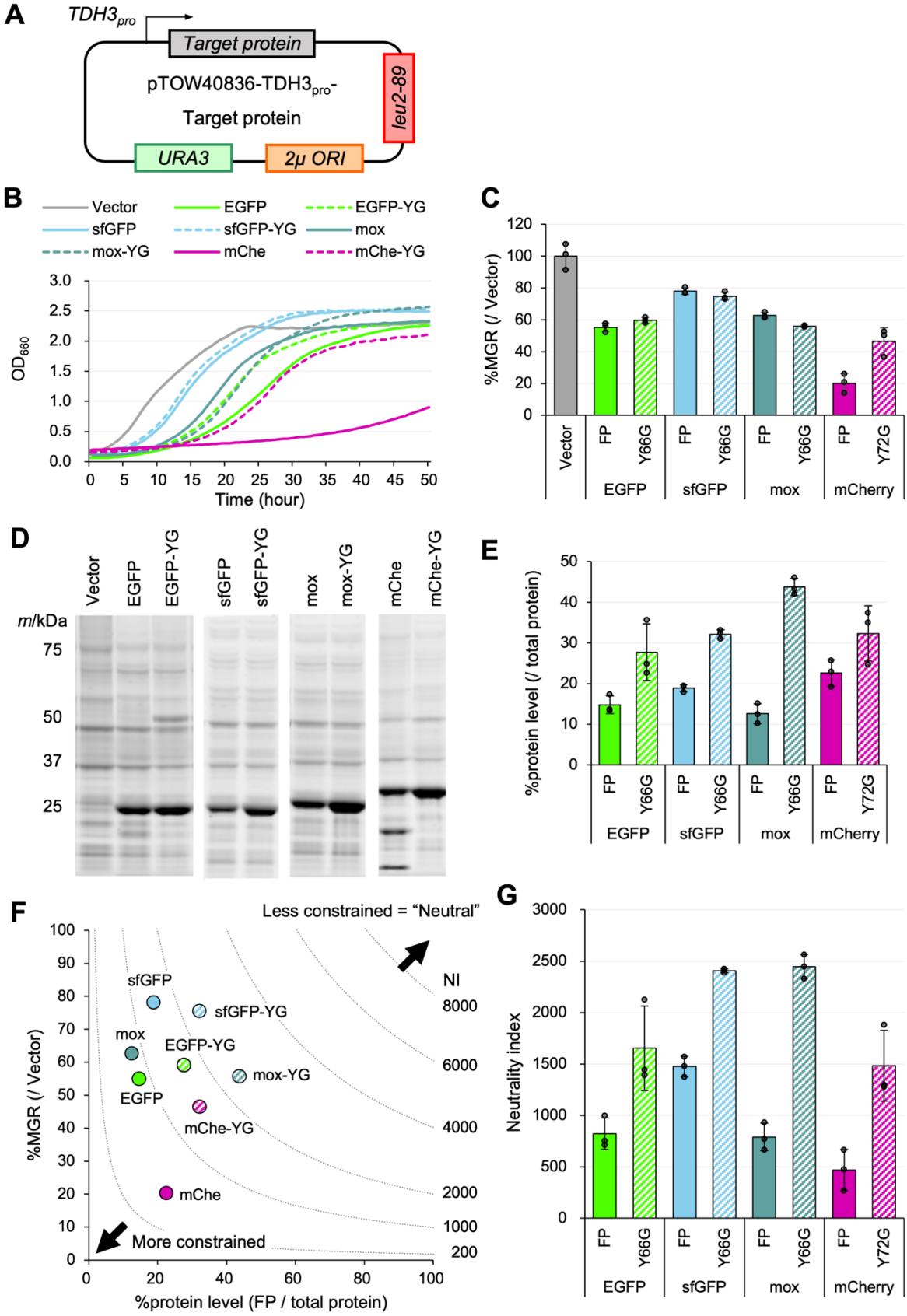

Figure 2. Evaluation of expression constraint (or neutrality) of fluorescent proteins.

216 **A**) Experimental setup of the analysis. Target proteins were expressed under the control of the *TDH3*
217 promoter ($TDH3_{pro}$) using the multicopy plasmid pTOW40836. The cells were pre-cultured under –Ura
218 conditions, and then cultured in –LeuUra conditions.
219 **B**) Growth curves of the vector control and cells overexpressing FPs and their mutants in synthetic
220 medium (–LeuUra). The solid or dotted lines show the average calculated from three biological
221 replicates. Growth curves with the standard deviations (SD) of replicates are shown in Figure 2—figure
222 supplement 2.
223 **C**) MGR of cells overexpressing FPs and their mutants (percent over the vector control).
224 **D**) Gel images of SDS-PAGE-separated proteins extracted from cells overexpressing FPs. All proteins
225 were separated after staining with a fluorescent dye.
226 **E**) Protein level of the target protein (percent over the total protein). The amount was calculated from
227 the intensity of the target bands separated by SDS-PAGE of **D**. See Figure 2—figure supplement 1B
228 for the method of FP and total protein quantification. Note that EGFP-YG and mCherry may not be
229 accurately measured due to dimerization and cleavage of the protein, respectively.
230 **F**) Relationship between MGR and the protein level. MGR data are the same as in **C**, and the protein
231 level data are the same as in **E**. The neutrality indexes (NIs), calculated from the products of MGR and
232 protein levels, are indicated by the lines. If the investigated proteins have the same NI, they are located
233 on the same dotted line segment.
234 **G**) The neutrality index for the FPs and mutants. The neutrality index is the product of %MGR (/Vector)
235 and %protein level (/total protein).
236 The bars and error bars in **C**, **E**, and **G** show the means and SDs calculated from three biological
237 replicates. The raw data is shown with dot plots.

238

---

239 Note that the regime of NI in Figure 2F shows a theoretical neutrality distribution but does not show
240 the relationship between growth rate and the expression level when the expression level of a protein
241 with a particular neutrality is increased or decreased. For example, 20% of the growth rate would be
242 maintained when the expression of mox-YG (NI = 2,400) is increased to 100%, but this is not realistic.
243 We also note that in this study, we calculated NI using the percentage of the target protein among total

244 cellular proteins separated by SDS-PAGE. Therefore, to calculate NI, the expression limit of the target
245 protein must be sufficiently high to be detectable by this method. On the other hand, if detection
246 sensitivity is improved, for example by using Western blotting, it becomes possible to estimate the NI
247 even for proteins under strong constraints—i.e., those that exhibit cytotoxicity. In fact, when we
248 recalculated the NI for EGFPs fused with various localization signals from our previous study (Kintaka
249 et al. 2016), all values were found to be below 100 (Figure 2−figure supplement 3).
250
251 The NI of each protein indicates that introducing a non-fluorescent mutation in FPs uniformly increases
252 neutrality (Figure 2G), suggesting that "having fluorescence" is a constraint on the expression of FPs.
253 The most neutral proteins were sfGFP-YG and mox-YG, with NIs of about 2,400. Notably, despite
254 significant differences in the degree of growth inhibition and expression limits between the two proteins,
255 their NIs are nearly identical (Figures 2F, G). They differ only in two amino acid residues (Cys - Ser)
256 (Figure 2—figure supplement 4), which seem to generate differences in expression efficiency. However,
257 this does not appear to affect their NIs.
258
259 We also investigated the impact of expression efficiency on NI with another FP, mChe. The mChe used
260 in this study is codon optimized (the codon adaptation index (CAI) = 0.584) (Keppler-Ross et al., 2008),
261 while the mChe used by Kafri *et al.* for protein cost analysis (here referred to as mChe-Kafri) is not
262 codon optimized (CAI = 0.236) (Kafri et al., 2016). When overexpressed, mChe-Kafri (and mChe-
263 Kafri-YG) had lower expression and growth inhibition than mChe (and mChe-YG) (Figures 2—figure
264 supplement 5A-D). This may be due to the lower translation rate of mChe-Kafri mRNA. However, their
265 NIs were not significantly different, especially for the YG mutation (Figures 2—figure supplement 5E,
266 F). Thus, the constraints indicated by NI are apparently not affected by translation efficiency. In the
267 study using this mCherry-Kafri, it was also reported that the more mChe-Kafri was expressed, the more
268 the cells enlarged (Kafri et al., 2016). However, no cell enlargement was observed with mox-YG, which
269 can be expressed more than mCherry. Interestingly, the mChe-YG cells did not show enlargement

270 (Figures 2—figure supplement 6A, B), indicating that cell enlargement is a phenomenon that occurs
271 specifically when fluorescent mChe is overexpressed.
272
273 It should be noted that the growth inhibition caused by the overexpression of mox-YG in this study is a
274 burden on translation rather than on transcription. This is because overexpression of a frameshift mutant
275 (moxFS), in which four nucleotides were inserted directly after the ATG of the mox-YG gene, abolished
276 the notable growth delay (Figures 2—figure supplement 6C, D).
277
278 **Constraint on fluorescent protein expression arises from fluorophore properties.**
279 Next, we further analyzed the possibility that fluorescence constrains the expression of FPs. When yeast
280 was grown in the dark, the degree of growth inhibition of mox was the same (Figure 2—figure
281 supplement 7A) and the expression limit of mox was rather increased (Figure 2—figure supplement
282 7B). Phototoxicity does indeed exist when expressing mox with fluorescence. This is because, when
283 exposed to strong light, cells overexpressing mox show a reduced growth rate (Figure 2—figure
284 supplement 7C-E) and abnormalities in their internal structures (Figure 2—figure supplement 7F).
285 However, the expression limits of mox and mox-YG were almost unchanged by the light (Figure 2—
286 figure supplement 7G, H). Thus, the constraint was not due to phototoxicity itself.
287
288 The number of Tyr residues was also irrelevant because NI was like that of mox-YG when a single Tyr
289 was added to the C-terminus of mox-YG (Figure 2—figure supplement 8A-E). Reactive oxygen species
290 (H_2O_2) are generated during fluorophore formation. When H_2O_2 was added to the medium, stronger
291 growth inhibition occurred only in mox (Figure 2—figure supplement 8F-H). This suggests that the
292 reactive oxygen species generated during fluorophore formation are responsible for the constraint.
293 However, this possibility is not supported by the omics analysis described later (see Discussion). Mox-
294 YG, like mox, was present throughout the cytoplasm and did not cause any characteristic localization
295 or aggregation (Figure 2—figure supplement 9).
296

297 During this study, we examined a moxGFP (mox-T203I) in which Thr203 was accidentally replaced by
298 Ile (Figure 2—figure supplement 10). The fluorescence of this mutant is reduced to 78% of mox
299 (Figures 2—figure supplement 10A-C). The growth rate of the cells expressing this mox-T203I was
300 like that of mox and mox-YG (Figure 2—figure supplement 10E). Still, the expression limit was
301 intermediate between mox and mox-YG (Figure 2—figure supplement 10F), resulting in the NI
302 intermediate between mox and mox-YG (Figure 2—figure supplement 10G). This result further
303 supports that fluorescence is related to constraints. However, as mentioned above, fluorescence
304 emission itself should not be toxic (Figure 2—figure supplement 7). We next focused on the formation
305 process of the fluorophore: the tyrosine of the GFP fluorophore undergoes phenol and phenolate state
306 changes, with Thr203 stabilizing the phenol form and substitution to Ile reducing the phenolate form
307 (Kummer et al., 2000). Furthermore, in enhanced GFPs such as mox, substitution of Ser65 before Tyr66
308 for Thr anchors the phenolate form. To investigate the possibility that this is a factor determining the
309 limit of mox, we produced mox with Thr65 replaced with Ser and examined its expression limit. The
310 mox-T65S mutant was expressed 12% more than mox (Figures 2—figure supplement 10H, I),
311 suggesting that the phenol-type fluorophore can be a limiting factor for the expression level of the
312 fluorescent protein, while the concrete mechanism is still unclear.
313
314 **Overexpression of mox-YG causes an amino acid starvation response.**
315 To understand the cell physiology under protein burden, we next performed transcriptome (RNA-seq)
316 analysis of the cells overexpressing mox-YG, the least constrained protein. Although the expression
317 limit of mox-YG is about 3-fold higher than that of mox (Figure 2E), the growth rates at the expression
318 limits of both are not largely different (Figure 2C). Thus, by comparing transcriptomes upon their
319 overexpression, we may be able to distinguish and extract the general transcriptional response due to
320 reduced growth rates from the (protein burden) response associated with the massive expression of a
321 less constrained protein.
322
323 The expression changes under mox and mox-YG overexpression were calculated as fold change (FC)
324 over the vector control (Figures 3—figure supplement 1A, B). The overall trend of expression changes

325 was similar (r = 0.64, Figure 3A). This similar variation may include responses associated with the
326 expression system and reduced growth rate. On the other hand, there were also different transcriptional
327 responses between the two. Gene categories that showed significant expression changes in either mox
328 or mox-YG overexpression are shown in Figure 3B. In addition to the enhanced ribosome synthesis and
329 decreased glycolysis observed in previous mox overexpression (Namba et al., 2022), enhanced
330 oxidative phosphorylation was detected. Interestingly, "Ribosome biogenesis", which was elevated in
331 mox overexpression, showed a rather decreasing trend in mox-YG overexpression (Figure 3B). Indeed,
332 *IFH1*, which is involved in ribosomal gene transcription (Martin et al., 2004), was upregulated in mox,
333 but downregulated in mox-YG (Figure 3A). Different trends were also observed for "amino acid
334 metabolism" (Figure 3B). The amino acid transporter genes *AGP1* and *GAP1* were upregulated only in
335 mox-YG overexpression (Figure 3A, C). Expressions of specific amino acid and nitrogen source
336 transporter genes were strongly induced in mox-YG (Figure 3C). The expression of glucose transporter
337 genes was also very different (Figure 3C). These results suggest that mox and mox-YG induce similar
338 but distinct transcriptional responses, particularly that mox-YG overexpression may result in depletion
339 of amino acid and nitrogen sources and decreased ribosome synthesis.
340 The transcriptional responses in mox-YG overexpression obtained by RNA-seq were confirmed by
341 transcriptional reporter analysis (Figure 3D and Figure 3—figure supplement 2). In this reporter
342 analysis, we also tested overexpression of a frameshift mutant (moxFS) that imposes a burden on
343 transcription but not on translation (Figure 2—figure supplement 6C, D). As a result, most of the
344 responses observed under mox-YG overexpression were not observed under moxFS overexpression,
345 suggesting that these transcriptional responses are likely caused by a burden on translation. The only
346 exception was *TDH3pro*, whose activity decreased even under moxFS overexpression. Since *TDH3pro*
347 is used for driving overexpression in this system, this result suggests that transcriptional competition
348 may occur as a result of overexpression. Notably, in our gTOW experiments, leucine depletion is
349 employed to induce overexpression; however, we consider it unlikely that leucine depletion *per se* is
350 responsible for the induction of *GAP1*, because *GAP1* expression remained unchanged in the vector
351 control even under gradual leucine depletion (Figure 3—figure supplement 3).

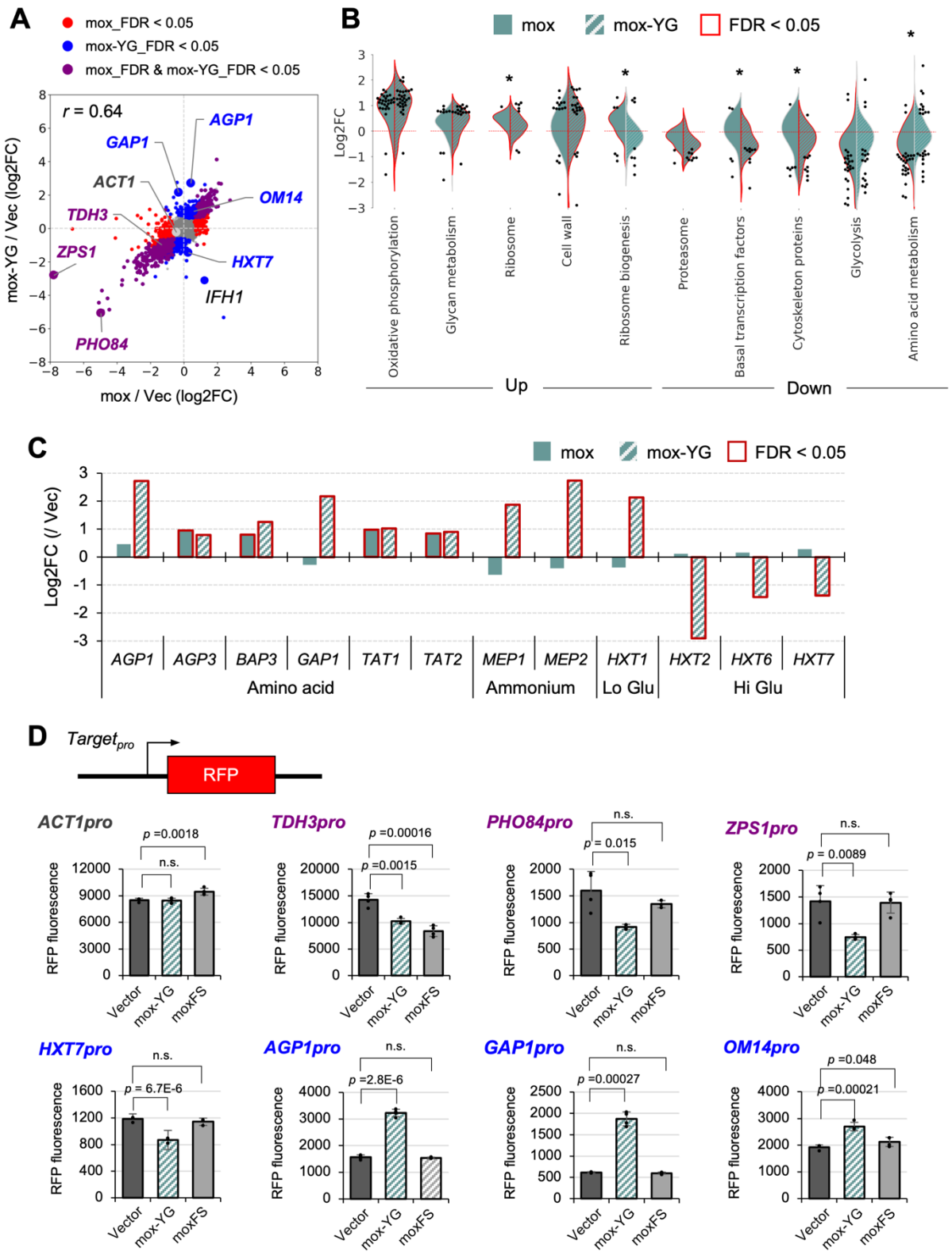

Figure 3. Transcriptional response of mox and mox-YG overexpression.

A) Comparison of transcriptional responses of mox and mox-YG overexpression. Genes that showed common or different transcriptional responses in mox and mox-YG overexpression are shown in

356 indicated colors. Genes that showed characteristic responses are also shown. FDR: false discovery rate.
357 *r*: Pearson correlation coefficient.
358 **B)** Gene groups that showed significant transcriptional changes. Among the KEGG orthology level 3
359 categories, gene groups in the category that were significantly up-regulated or down-regulated (FDR <
360 0.05) in mox or mox-YG overexpression are shown in the violin plots. Genes with significant expression
361 changes (FDR < 0.05) within the same category are shown by swarm plots. Asterisks indicate significant
362 differences (FDR < 0.05) between mox and mox-YG comparisons in gene groups belonging to the same
363 category. Comparisons for all categories are shown in Figure 3—figure supplement 1C.
364 **C)** Expression changes in representative amino acid, ammonium, and glucose transporters.
365 **D**) Verification of promoter activity by the reporter assay. Constructs used for promoter analysis with
366 transcription reporters and quantitative results of RFP fluorescence values (arbitrary unit) for each
367 promoter. "moxFS" means the frameshift mutant of mox-YG is overexpressed. Bars and error bars
368 indicate the mean and SD of maximum fluorescence values for RFP calculated from four biological
369 replicates. Raw data are shown as dot plots. The *p*-values were calculated by performing Welch's *t*-test
370 and applying Bonferroni correction. "n.s." means $p > 0.05$. Detailed constructs and time series data for
371 promoters other than those shown here are in Figure 3—figure supplement 2.
372
---
373 **Overexpression of mox-YG causes a proteomic response that partially overlaps with TORC1**
374 **inactivation.**
375 Protein burden is an overload on synthetic resources, and thus, when this overload occurs strongly, it is
376 expected that there would be a reduction in the amount of proteins other than those being overexpressed
377 due to competition for synthetic resources. Indeed, in cells overexpressing mox-YG, the amounts of
378 proteins other than mox-YG were reduced (Figure 4A). Interestingly, the total amount of protein per
379 cell remained almost constant, with the amount of other proteins decreasing as mox-YG was
380 overexpressed. This trend was generally true for the overexpression of other FP (Figure 4—figure
381 supplement 1). This suggests that there is a mechanism (or constraint) that maintains the overall cellular
382 protein levels.
383

384 The maintenance of total cellular protein levels under overexpression conditions may be due to
385 constraints such as intracellular space limitations or limitations in the availability of nutrients in the
386 medium. To investigate whether nutrient limitation contributes to this phenomenon, we attempted
387 overexpression of mox and mox-YG in YPD medium, which is considered to be more nutrient-rich than
388 the SC medium. Since leucine depletion could not be used to drive overexpression in this context, we
389 employed an alternative strategy using the aureobasidin A resistance marker (*AUR1d*) to increase
390 plasmid copy number (Figure 4—figure supplement 2A). In this experiment, mox-YG was expressed
391 at approximately 20% of the total cellular protein, with a corresponding increase in total protein content
392 per cell (Figure 4—figure supplement 2C, D). This result suggests that in nutrient-rich YPD medium,
393 cells may possess the capacity to buffer excess protein expression by increasing the total proteome.
394 However, under these expression conditions, no growth inhibition was observed (Figure 4—figure
395 supplement 2B), and thus the induction of mox-YG was not sufficiently strong. We therefore consider
396 it necessary to investigate the regime under conditions of stronger overexpression in future studies.
397
398 To examine changes in protein expression, proteomic analysis of mox-YG overexpressing cells (in the
399 SC medium) was performed. The distribution of intensities obtained from the analysis is shown in the
400 Proteomaps in Figure 4B. In mox-YG overexpressing cells, mox-YG accounted for 40% of the total
401 protein expression. Figure 4A suggests that in mox-YG overexpressing cells, proteins other than mox-
402 YG are overall reduced to about 60% compared to the vector. Therefore, we considered it necessary to
403 normalize the data overall to accurately represent changes in the per-cell proteome. However, in this
404 study, we used data without such correction to focus on how the composition of the proteome, other
405 than mox-YG, changed (see Materials and Methods and Figures 4—figure supplement 3A-C for more
406 details).
407
408 Figure 4C illustrates the categories that showed significant changes upon mox-YG overexpression (all
409 categories are shown in Figure 4—figure supplement 4). Elevated mitochondrial proteins, such as
410 oxidative phosphorylation and TCA cycle, and decreased ribosomal protein and ribosomal synthesis
411 were observed. Interestingly, the proteomic changes observed in mox-YG overexpressing cells showed

412 little correlation with the corresponding transcriptomic changes (Figure 4—figure supplement 3D). The
413 only notable exception was oxidative phosphorylation, which was upregulated at both the transcript and
414 protein levels (Figure 3B and 4C). In contrast, for example, ribosomal proteins were upregulated at the
415 transcript level but markedly downregulated at the protein level (Figure 3B and 4C). This discrepancy
416 may indicate a cellular state in which transcriptional responses are uncoupled from protein expression
417 as a result of protein burden.
418
419 As mentioned above, RNA-seq results suggested nitrogen source starvation in mox-YG overexpression.
420 Therefore, we investigated whether this response is influenced by the regulation through the TORC1
421 pathway, a primary mechanism responsive to nitrogen sources. By comparing expression changes due
422 to rapamycin (a TORC1 inhibitor) treatment (Gowans et al., 2018) and mox-YG overexpression, we
423 found that about 40% of the proteins with altered expression were congruent with the group of proteins
424 regulated by TORC1 (Figures 4—figure supplement 5A, B). Thus, the proteome expression changes
425 due to mox-YG overexpression may include responses due to inactivation of the TORC1 pathway as
426 well as other responses. Figure 4C shows which categories had significant expression changes when
427 separated into rapamycin-responsive (Rap) and rapamycin-non-responsive (Non-Rap) gene populations.
428 Carbohydrate metabolism, elevated TCA cycle, and decreased ribosome synthesis were suggested to be
429 responses due to TORC1 inactivation, while endocytosis, cytoskeleton, protein transport and lipid
430 synthesis, and glycolysis were suggested to be due to responses other than TORC1 inactivation (Figure
431 4—figure supplement 6). Oxidative phosphorylation included both Rap responses (12/32) and non-
432 responses (20/32) (Figure 4—figure supplement 6C). Indeed, mox-YG overexpression reduced the
433 sensitivity to rapamycin compared to the vector control (Figure 4—figure supplement 7A-E),
434 supporting the notion that TORC1 activity was diminished. However, we were unable to obtain direct
435 evidence demonstrating TORC1 inactivation. We examined the phosphorylation status of Atg13
436 (Kamada et al. 2000), a known TORC1 target, by Western blotting. In mox-YG overexpressing cells,
437 however, the total expression level of Atg13 was markedly reduced (Figure 4—figure supplement 7F).
438 Therefore, it remains inconclusive how the decreased expression of TORC1 targets affects downstream
439 signaling under these conditions.

440

441 Above transcriptome and proteome analyses suggested that mox-YG overexpression induces
442 mitochondrial development and a metabolic shift from fermentation to oxidative respiration. To verify
443 mitochondrial development, we performed fluorescence microscopy. Indeed, mitochondria labeled with
444 Rip1-mScarlet-I, a component of the oxidative phosphorylation pathway, were significantly more
445 developed in mox-YG overexpressing cells (Figure 4D, 4—figure supplement 8). Furthermore, oxygen
446 consumption was increased in these cells (Figure 4E, 4—figure supplement 9), supporting the notion
447 that they had undergone a metabolic shift toward oxidative respiration.

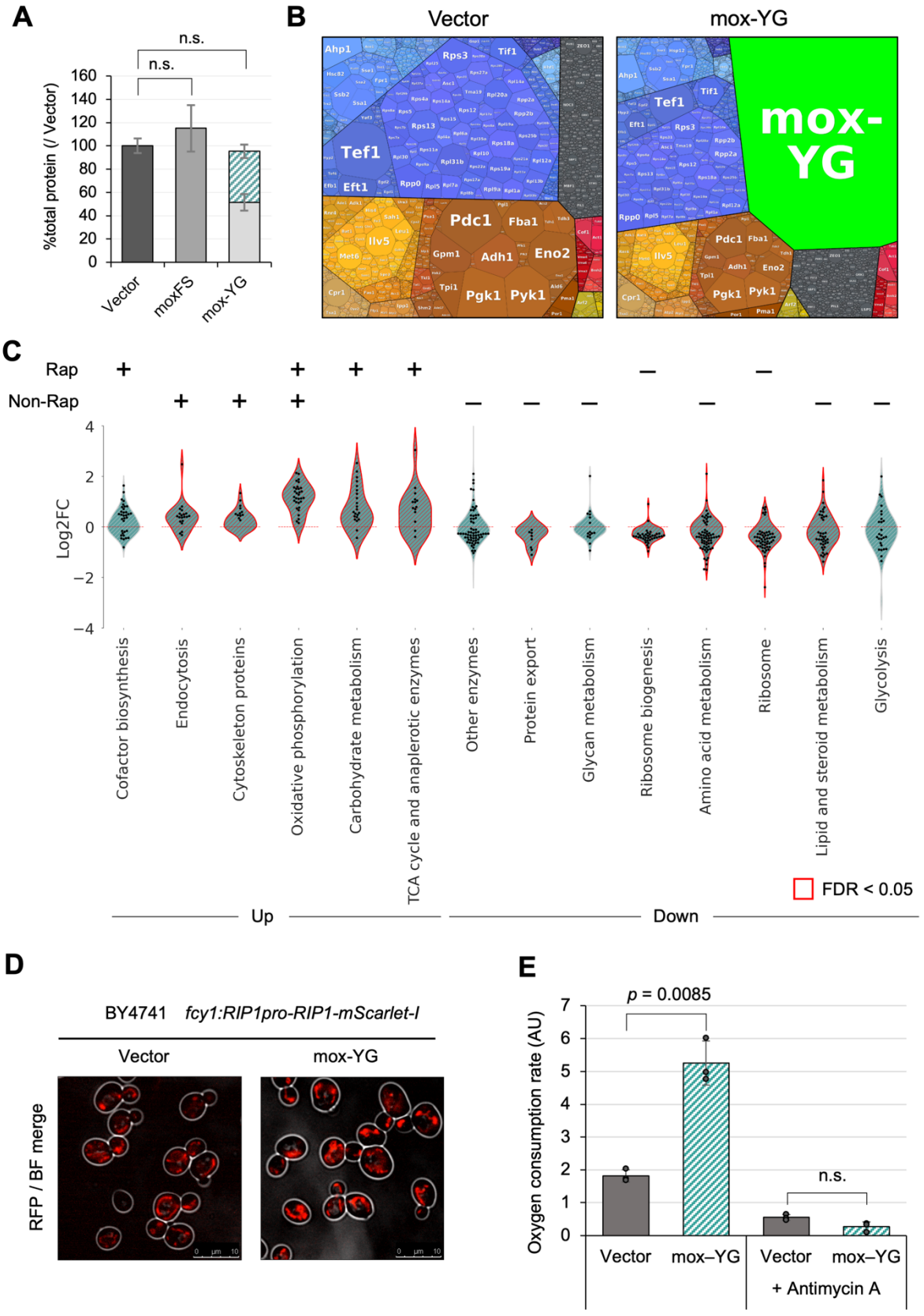

448

449 **Figure 4. Overexpression of mox-YG causes a proteome response like that of TORC1 inactivation.**

450 **A)** Ratio of the total protein level over the vector control. The colored area indicates the amount of
451 overexpressed protein. The amount was calculated from the intensity of the target bands separated by
452 SDS-PAGE. Bars and error bars indicate the mean and SD of protein levels calculated from three
453 biological replicates. The *p*-values were calculated by performing Welch's *t*-test and applying
454 Bonferroni correction. "n.s." means $p > 0.05$.
455 **B**) Visualization of the proteome of the vector control and mox-YG overexpressing cells using
456 Proteomaps (Liebermeister et al., 2014). Each polygon represents the mass fraction of the protein within
457 the proteome. Similar colors indicate similar or closely related pathways and proteins.
458 **C)** Violin plots showing groups of genes in the KEGG orthology level 3 category whose expression
459 was increased or decreased by mox-YG overexpression. Gene groups with significantly altered
460 expression (FDR < 0.05) in mox-YG overexpression are shown in red. Genes with significant
461 expression changes (FDR < 0.05) within the same category are shown by swarm plots. "+" and "–"
462 indicate the categories with significantly increased or decreased expression, respectively, when
463 separated into Rapamycin-responsive (Rap) and Rapamycin-non-responsive (Non-Rap) gene
464 populations. Comparisons for all categories are shown in Figures 4—figure supplement 6A, B.
465 Published data (Gowans et al., 2018) was used for comparison with the rapamycin response genes.
466 **D)** Fluorescence microscopy image showing the localization of Rip1-mScarlet-I. The vector control and
467 mox-YG overexpressing cells were observed in the log phase. Stationary phase cells, bright-field
468 images, quantitative results, and statistical analyses are shown in Figure 4—figure supplement 8.
469 **E)** Oxygen consumption rate in vector control and mox-YG overexpressing cells (arbitrary units, AU).
470 Antimycin A was added as a control for respiratory inhibition. Measurements were conducted with
471 three biological replicates. Bars and error bars indicate the mean and SD from three biological replicates.
472 Raw data are shown as dot plots. The *p*-values were calculated by performing Welch's *t*-test and
473 applying Bonferroni correction. "n.s." indicates $p > 0.05$. The measurement data are shown in Figure
474 4—figure supplement 9.

475

---

476 **Overexpression of mox-YG causes a dysplastic nucleolus, which is alleviated by mutations in the**
477 **nuclear exosome.**

478 Ribosomes are a crucial factor for protein burden because they are themselves protein synthesizers
479 while being synthesized in the highest amounts in the cell. Therefore, we further focused on the behavior
480 of ribosomes in mox-YG cells and expression changes were investigated in detail for each ribosomal
481 protein (Figure 5—figure supplement 1). While the majority of the 84 ribosomal proteins detected (45
482 of them significantly) decreased, six (Rps12, Rps31, Ppp0, Rpp2a, Rpl5, and Rpl12) showed significant
483 increases. Interestingly, all decreased ribosomal proteins are assembled into ribosomes in the nucleolus,
484 while all increased ribosomal proteins are assembled into ribosomes in the cytoplasm (Lafontaine,
485 2015). They constitute the "beak" of the 40S subunit and the "P-stalk" and the "central protuberance
486 (pc)" of the 60S subunit (Figure 5A). Electron micrographs showed an abnormal nucleolar formation
487 of mox-YG overexpressing cells (Figures 5B and Figure 5—figure supplement 3), in addition to reduced
488 ribosome density in the cytoplasm (Figure 5—figure supplement 2A). This abnormal nucleolar
489 formation was also confirmed by fluorescence microscopy images of Nsr1 (Nucleolin), the major
490 protein of the nucleolus (Figure 5—figure supplement 2B-D).
491
492 Based on these results, we hypothesized that overexpression of mox-YG creates an imbalance between
493 the amount of ribosomal protein synthesized in the cytoplasm and the amount of rRNA synthesized in
494 the nucleolus (Figure 5C, D). The imbalance may lead to the creation of misassembled ribosomes,
495 which are eventually degraded. We speculated that the primary enzyme degrading the misassembled
496 ribosome should be the nuclear exosome. This is because our previous genome-wide mutation analysis
497 identified exosome mutants (*dis3-1, mtr3-ts, mtr4-1, rpn42-ph, rpn45-ph, and ski6-ph*) as primary
498 mitigators of protein burden (Kintaka et al., 2020). We confirmed that the *mtr4-1* mutant does not show
499 growth retardation upon mox-YG overexpression (Figure 5E). In fact, in *mtr4-1* cells, there was no
500 difference in growth rate between the vector control and mox-YG overexpression (Figure 5—figure
501 supplement 5B), but rather a shorter lag time for the mox-YG overexpression than the vector control
502 (Figure 5E). We next quantified protein upon mox-YG overexpression in *mtr4-1* cells (Figure 5F).
503 Compared to the wild-type (Vector), the total protein content in *mtr4-1* (Vector) cells was reduced to
504 78%, which was likely related to the decreased growth. In the *mtr4-1* mox-YG overexpressing cells, the
505 amount of other proteins decreased (to 54%), overwhelmed by the 40% expression of mox-YG.

506 However, the overall protein content increased compared to the *mtr4-1* vector control, with a
507 composition like the wild-type mox-YG overexpressing cells. Therefore, in *mtr4-1* cells, even though
508 mox-YG overexpression reduced the amount of other proteins (to 54%) compared to the vector control
509 (78%), the growth rate was not reduced (Figure 5—figure supplement 5B). This suggests that mox-YG
510 overexpression restores the effect of growth inhibition caused by *mtr4-1*. Next, we observed the
511 composition of the nucleolus in *mtr4-1* (Figures 5G and Figure 5—figure supplement 5D, E). The
512 failure of nucleolus formation observed upon mox-YG overexpression was partially, but significantly,
513 rescued in the *mtr4-1* strain. This supports our hypothesis that misassembled ribosomes are degraded
514 by the exosome (Figure 5D), and with low exosome activity, nucleolus formation (and efficient
515 ribosome assembly) would be possible even with overexpression of mox-YG (Figure 5—figure
516 supplement 4D).
517
518 While experimenting with mox-YG overexpressing cells, we found that these cells stop growth earlier
519 (lower final density) at higher temperatures (38°C) than the vector controls (Figure 5H and Figure 5—
520 figure supplement 6A). Cells at this time did not show cell death such as cell bursting (Figure 5—figure
521 supplement 6B). Recently, it was reported that intracellular osmotic pressure increases at high
522 temperatures, resulting in less formation of liquid-liquid phase-separated structures such as nucleoli,
523 which are recovered when cells are placed in hyperosmotic conditions (Watson et al., 2023). We
524 hypothesized that the growth inhibition of mox-YG overexpressing cells at high temperatures may be
525 due to the enhanced failure of nucleolus formation, and thus cultured mox-YG overexpressing cells
526 under hyperosmotic pressure. At 30°C, hyperosmolarity caused the same decrease in growth for the
527 vector control and mox-YG overexpression (Figures 5I and Figure 5—figure supplement 6C). On the
528 other hand, at 38°C, hyperosmolarity caused a decrease in growth only in the vector control and no
529 further decrease in mox-YG overexpression cells (Figures 5J and Figure 5—figure supplement 6D).
530 The same trend was observed regarding the size of the nucleolus (Figures 5—figure supplement 6E, F).
531 Under the conditions with added sorbitol and under mox-YG overexpression, the size of the nucleoli
532 was smaller than the control at 30°C, whereas, at 38°C, it was rather larger than the control. This
533 suggests that mox-YG overexpression and hyperosmolarity may mitigate each other's growth-inhibitory

534 effects, and one explanation may be that hyperosmolarity suppresses the abnormal organization of the

535 nucleolus caused by mox-YG overexpression.

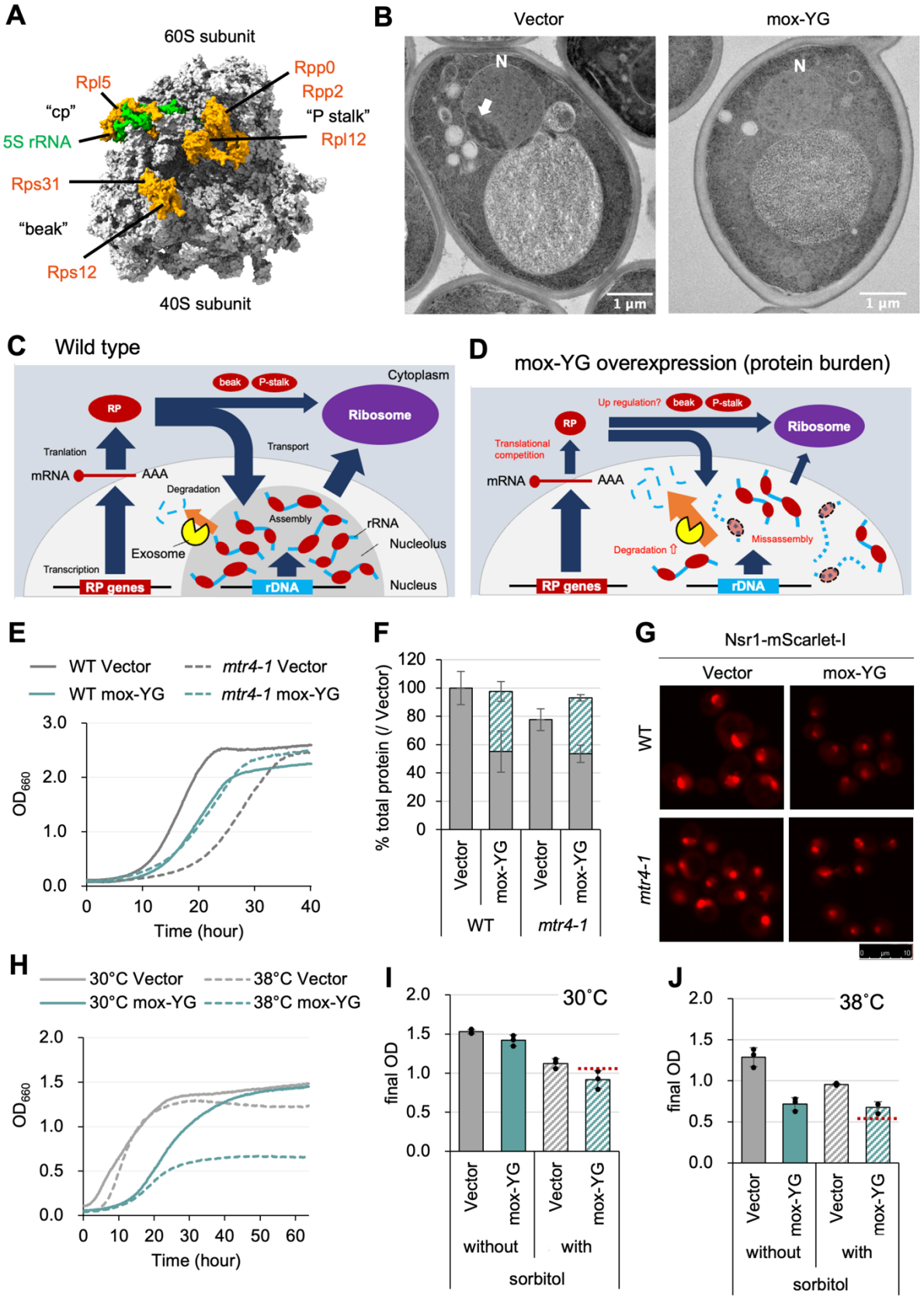

536

537 **Figure 5. mox-YG overexpression causes abnormal nucleolus formation.**

538 **A.** 3D structure of the ribosome. PDB model 6GQV (Pellegrino et al., 2018) is used for the base model
539 and colored using ChimeraX software (Meng et al., 2023). Ribosomal proteins with increased
540 expression upon mox-YG overexpression are shown with the named structures containing them. See
541 also Figure 5—figure supplement 1 for the quantitative data.

542 **B)** Electron microscope images of the vector control and mox-YG overexpressing cells. The arrow in
543 the image points to the nucleolus structure. N: nucleus. Images of other observed cells are shown in
544 Figure 5—figure supplement 3.

545 **C, D)** Model diagrams showing the hypothetical situation of the wild type (**C**) and mox-YG
546 overexpressing cells (**D**). In WT cells, enough ribosomal proteins (RPs) are produced, resulting in RP-
547 assembled rRNAs and the formation of nucleolus with normal morphology. On the other hand, in mox-
548 YG overexpressing cells, the amount of RP is reduced due to translation competition, increasing
549 misassembled rRNA. As a result, degradation of rRNA by exosomes may be accelerated, resulting in
550 abnormal nucleolus morphology.

551 **E)** Growth curves of WT and *mtr4-1* mutant cells with the vector control or upon overexpression of
552 mox-YG at 30˚C. The solid or dotted lines show the average calculated from three biological replicates.
553 Growth curves with SDs of replicates are shown in Figure 5—figure supplement 5A.

554 **F)** Ratio of total protein levels of WT and *mtr4-1* strains with the vector or upon mox-YG
555 overexpression, calculated the total protein level of WT cells with the vector as 100%. Gray bars
556 indicate expression levels of proteins other than mox-YG; green shaded bars indicate mox-YG
557 expression levels. Error bars were SDs calculated from three biological replicates. The *p*-values were
558 calculated by performing Welch's *t*-test. "n.s." means $p > 0.05$.

559 **G)** Fluorescence microscopy image of nucleolus-localized protein Nsr1-mScarlet-I of the WT and *mtr4-*
560 *1* mutant cells with the vector or mox-YG overexpression. Bright field and merged images, and
561 quantification of the nucleolus size are shown in Figures 5—figure supplement 5D and 5E.

562 **H)** Growth curves of the cells with the vector or under mox-YG overexpression cultivated at 30°C or
563 38°C. The solid or dotted lines show the average calculated from three biological replicates. Growth
564 curves with SDs of replicates are shown in Figure 5—figure supplement 6A.

565 **I, J)** Final OD of the cell culture with or without 1M sorbitol at 30°C (**I**) or 38°C (**J**). The bars and error
566 bars show the means and SDs calculated from three biological replicates. The red dotted line indicates
567 the final OD estimated from the product of (mox-YG without sorbitol) / (Vector without sorbitol) and
568 (Vector with sorbitol) / (Vector without sorbitol). Growth curves with SDs of replicates are shown in
569 Figures 5—figure supplement 6C, D.

570

571 **The Gpm1 mutant shows a similar NI to mox-YG, yet yields distinct phenotypes upon**
572 **overexpression.**

573 Thus far, our investigation has focused on heterologous fluorescent proteins. Finally, we turned to
574 endogenous yeast proteins to identify those with the lowest cytotoxicity and to examine the phenotypic
575 consequences of their overexpression. We previously investigated the expression limits of a group of
576 glycolytic enzymes in *S. cerevisiae*, with Gpm1 and its catalytic center mutant (CCmut) having the
577 highest expression limits (Eguchi et al., 2018). Here, we evaluated the neutrality of the wild types and
578 their CC-mutants of Tdh3 and Gpm1 (Figure 6A and Figure 6—figure supplement 1). The growth rates
579 at the expression limits were higher in the CCmut for both Tdh3 and Gpm1, and in Gpm1, the CCmut
580 grew two-fold faster (Figures 6—figure supplement 1A, C). The protein levels of wild types and
581 mutants of both proteins were not significantly different (Figures 6—figure supplement 1D, E). The
582 calculated NIs were highest for Gpm1-CCmut, which was equivalent to that of mox-YG (Figures 6A).
583 We previously concluded that the activities of glycolytic enzymes generally do not affect their
584 expression limits (Eguchi 2018), but their neutralities suggest that their activities can become
585 constraints in some way. This may be due to a disturbance in metabolism or a property of the active
586 enzyme, such as an effect of reactive amino acids (His or Cys, Figure 6—figure supplement 2).

587

588 Although Gpm1 and Gpm1-CCmut exhibited NIs comparable to that of mox-YG, suggesting that they
589 are similarly unconstrained, notable differences in cell morphology were observed (Figure 6B, 6—
590 figure supplement 3). Cells overexpressing Gpm1 appeared enlarged and spherical, while those
591 overexpressing Gpm1-CCmut did not show such hypertrophy but were still rounder than vector controls
592 or mox-YG overexpressing cells. The transcriptional responses observed in mox-YG overexpressing

593 cells, including the induction of *GAP1*, a marker of the amino acid starvation response, were not
594 detected in Gpm1-CCmut overexpression (Figure 6C and Figure 6—figure supplement 4). In Gpm1-
595 CCmut overexpressing cells, similar to mox-YG overexpression, the levels of proteins other than
596 Gpm1-CCmut were reduced, despite a slight, statistically non-significant increase in total protein
597 amount (Figure 6—figure supplement 1F). While mitochondrial development was observed in Gpm1-
598 CCmut cells using Rip1–mScarlet-I labeling (Figure 6—figure supplement 5), no increase in oxygen
599 consumption was detected (Figure 6D and Figure 6—figure supplement 6). The nucleolus, visualized
600 with Nsr1–mScarlet-I, appeared similarly shrunken in Gpm1-CCmut overexpressing cells as in mox-
601 YG overexpressing cells (Figure 6E and Figure 6—figure supplement 7). These results suggest that the
602 phenotypes observed in mox-YG overexpressing cells include both mox-YG–specific effects and
603 responses commonly associated with protein burden. Alternatively, as indicated by the abnormal cell
604 morphology, Gpm1-CCmut may possess unknown constraints or cytotoxic properties not captured by
605 the neutrality index, which could obscure the detection of phenotypes typically associated with protein
606 burden.

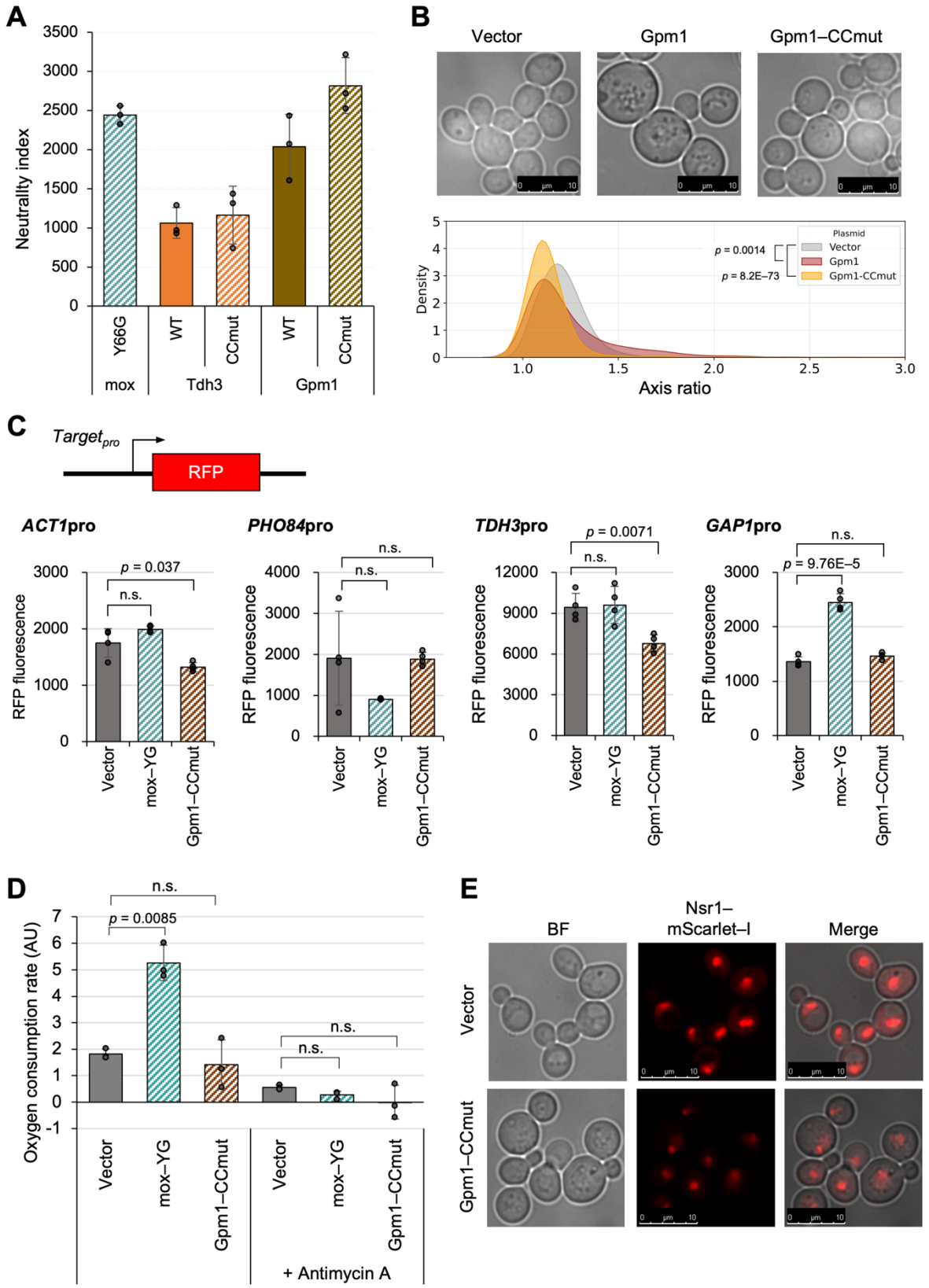

607

608 **Figure 6. The Gpm1 mutant shows a similar NI to mox-YG, yet yields distinct phenotypes upon**

609 **overexpression.**

610 A) The neutrality index for Gpm1, Tdh3, and their CCmuts. Data on growth rates and protein expression
611 levels used for the neutrality index calculation are presented in Figure 6—figure supplement 1.
612 B) Top images: representative microscopic images of cells overexpressing Gpm1 or Gpm1–CCmut.
613 Bottom graph: Distribution of cell axis ratios upon overexpression of Gpm1 and Gpm1–CCmut,
614 compared with the vector control. The *p*–values were calculated by the Mann–Whitney *U*–test.
615 Statistical analysis of cell size and comparison with mox-YG overexpressing cells are shown in Figure
616 6—figure supplement 3.
617 C) Promoter activity reporter assay. Constructs used for promoter analysis with transcription reporters
618 and quantitative results of RFP fluorescence values (arbitrary unit) for each promoter. Time series data
619 are in Figure 6—figure supplement 4.
620 D) Oxygen consumption rate in vector control, mox-YG, and Gpm1-CCmut overexpressing cells
621 (arbitrary units, AU). Antimycin A was added as a control for respiratory inhibition. The measurement
622 data are shown in Figure 6—figure supplement 6.
623 **E**) Fluorescence microscopy images of nucleolus with Nsr1–mScarlet–I. Log phase cells (OD_{660} = 1.0)
624 with the control vector or under Gpm1 or Gpm1–CCmut overexpression were observed. Statistical
625 analysis of nucleolar size is shown in Figure 6—figure supplement 7.
626 The bars and error bars in **A**, **C** and **D** show the means and SDs calculated from three biological
627 replicates. The raw data is shown with dot plots. The *p*-values were calculated by performing Welch's
628 *t*-test and applying Bonferroni correction. “n.s.” means $p > 0.05$.
629
630

Discussion

In this study, we found that the fluorescent properties of FPs constrain their expression limits. This fluorescence-induced cytotoxicity appears as different phenotypes depending on the FPs; an excess of fluorescent mCherry causes cell enlargement, but such a phenotype was not seen with green fluorescent proteins. On the other hand, the cause of the cytotoxicity is not clear currently. Fluorescence itself does not seem to constrain the expression limit, because the mox expression limit remained the same when cultured in the dark or under strong light (Figure 2—figure supplement 7). We also believe that H_2O_2 generated during fluorophore maturation (Craggs, 2009) is unlikely. In the presence of H_2O_2, mox overexpressing cells grew slightly slower than mox-YG overexpressing cells (Figure 2—figure supplement 8H). However, no transcriptional response to oxidative stress, including the catalase gene (*CTT1*), was seen with mox overexpression (FDR < 0.187, over the vector control, Data S1). Because *CTT1* expression was elevated in mox-YG overexpression (FDR < 0.006, over the vector control, Data S1), presumably due to enhanced respiration, mox-YG overexpression might rather increase oxidative stress tolerance. Conversely, "inactive" proteins might accumulate more without interfering with intracellular functions because both inactive fluorescent proteins and inactive glycolytic enzymes showed higher neutrality (Figures 2 and 6). However, our current data did not clarify the mechanism, and investigating more proteins and their variants would be required.

The currently least cytotoxic proteins, non-fluorescent mox-YG and inactive Gpm1 express more than 40% of the total protein, whereas yeast cells can maintain growth under these conditions (Figures 2 and 6). This is higher than the prediction in *E. coli*, which stops growing when 37% of the excess protein is expressed (Bruggeman et al., 2020). This may be due to the very low cytotoxicity of the proteins expressed in this study, or it may be because eukaryotic cells have greater capacity than prokaryotic cells. In the mox-YG overexpressing cells, we observed a previously expected but unobserved cellular physiology of the protein burden: depletion of protein synthesis resources (i.e., nitrogen source; Figure 3) and a decrease in other proteins (glycolytic enzymes and ribosomes; Figure 4), possibly due to competition for synthesis. In addition, metabolic conversion to mitochondria and failure of nucleolus

658 formation were observed (Figures 4 and 5). As a matter of fact, the nitrogen source depletion response
659 (Figure 3) itself is not self-evident. Because the total protein content in the mox-YG overexpressing
660 cells is the same as that in the vector control (Figure 4A), the intracellular nitrogen source used for
661 protein synthesis should not be depleted. Then, why does the nitrogen source depletion response occur?
662 Excess mox-YG may promote wasteful consumption of amino acids and nitrogen, or there may be
663 pathways that sense the amount of "useful proteins" and their ability to be synthesized, or there may be
664 depletion of specific amino acids in mox-YG excess. Another possibility is that there may be some
665 mechanism that maintains the amount of total protein in the cell even when the nitrogen source is
666 depleted. Depletion of nitrogen sources probably results in the inactivation of the TORC1 pathway
667 (Figure 4C), metabolic conversion from fermentation to respiration, and ribosome depression to an
668 economic mode. In *E. coli*, the ppGpp pathway plays this role (Shachrai et al., 2010). While the above
669 is thought to be a physiological response to protein burden, a defect in ribosome synthesis in the
670 nucleolus was also suggested (Figure 5B). This could be due to a conflict between nuclear rRNA
671 synthesis and cytoplasmic protein synthesis or to the negative effects of the inability to create a liquid-
672 liquid phase-separated structure due to dilution effects (see below). The partial restoration of nucleolus
673 formation by a mutation of the exosome (Figure 5G) supports this possibility.
674
675 When one type of protein is expressed as much as 40% of the total, as in the present study, the
676 cytoplasmic crowding, viscosity, pH, etc. may change due to the nature of the protein and the effect of
677 the reduced protein by competition. These may alter the movement of substances. It is known that when
678 ribosomes are reduced, the fluidity of large proteins changes (Delarue et al., 2018). Water activity-
679 osmotic pressure may change (Watson et al., 2023), and pH may also be affected. These may affect the
680 formation of liquid-liquid phase-separated structures (Delarue et al., 2018; Watson et al., 2023). The
681 failure of nucleolus formation observed in mox-YG overexpression (Figure 5B) may be due to such a
682 condition change. In fact, the growth of mox-YG overexpressing cells is significantly impaired at high
683 temperatures (Figure 5H), where liquid-liquid phase separation is less likely to occur (Watson et al.,
684 2023). In contrast, the effect appears to be reduced at high osmolarity (Figure 5J), where it is more
685 likely to occur (Watson et al., 2023). A mutation of the nuclear exosome restored nucleolus formation

686 (Figure 5G), which might be due to the reformation of the liquid-liquid phase-separated structure (i.e.,
687 nucleolus) by increasing the concentration of rRNA. These have not been considered phenomena that
688 occur with protein overexpression. The engineering of physicochemical properties of the cytoplasm
689 thus may be possible by mass expression of proteins with specific properties.
690
691 In this study, in addition to mox-YG, inactive Gpm1 was also expressed in large amounts as well (Figure
692 6). Both are globular proteins with relatively small molecular weight, but it is not yet clear what
693 characteristics are necessary for them not to be cytotoxic. Further investigation of the neutrality of
694 various proteins will clarify these features. In addition, while the overexpression of Gpm1-CCmut also
695 caused nucleolar shrinkage similar to that observed in mox-YG overexpressing cells, it did not induce
696 other phenotypes such as nitrogen starvation or enhanced respiration (Figure 6). Therefore, it remains
697 unclear which of the phenotypes observed in mox-YG overexpressing cells are general consequences
698 of "protein burden" and which are specific to mox-YG. As noted in the Introduction (Figure 1E), it is
699 essential to continue investigating multiple proteins that appear to be "unconstrained" in order to
700 address this issue. In this study, expression limits were investigated, but no experiments were performed
701 to gradually increase expression levels. For example, it would be meaningful to investigate at what
702 expression level of mox-YG a shift to the economy mode or failure of nucleolus formation occurs. Also,
703 due to the limitations of the experimental system, it may not be possible to express mox-YG to its true
704 limit. The expression of one specific protein cannot be 100% of the total protein, and there is always a
705 limit. As the number of ribosomes continues to decrease due to competition for synthesis, the excess
706 proteins cannot be synthesized either. Thus, there must be a final equilibrium point. A more powerful
707 and controllable expression system would be needed to investigate this. Although the translation system
708 appears to be the primary target of burden in mox-YG overexpression (Figure 2—figure supplement
709 6C, D), the bottleneck in the expression system may also differ depending on gene design (Figure 1D)
710 (Hausser et al., 2019).

711 # Materials and Methods

712 **Strains, growth conditions, and yeast transformation**

713 BY4741 (*MATa his3Δ1 leu2Δ0 met15Δ0 ura3Δ0*) (Brachmann et al., 1998) was used as the host strain
714 for the experiments. Yeast culture and transformation were performed as previously described (Amberg
715 et al., 2005). A synthetic complete (SC) medium without uracil (Ura) or leucine (Leu), as indicated,
716 was used for yeast culture. Other strains used in this study are listed in the Key Resource Table.

717

718 **Plasmid construction**

719 The plasmids were constructed by homologous recombination activity of yeast cells (Oldenburg 1997),
720 and their sequences were verified by DNA sequencing. Plasmids used in this study are listed in the Key
721 Resource Table.

722

723 **Genetic tug-of-war**

724 To overexpress a target protein to a level that causes growth inhibition (in this study this is referred to
725 as "expression limit"), we used gTOW (Figure 2—figure supplement 1A) (Moriya et al., 2012, 2006).
726 The gene of the target protein is incorporated into the gTOW plasmid (here, pTOW40836) and
727 introduced into yeast cells lacking *ura3* and *leu2* genes. The selection marker in this case is uracil (–
728 Ura conditions). Since this plasmid has the replication origin of 2 μm plasmid (*2 μ ORI*), this plasmid
729 becomes multicopy in the cell (about 30 in the case of the vector). When yeast cells carrying the plasmid
730 are transferred to a medium without leucine and uracil (–Leu/Ura conditions), the copy number of the
731 plasmid in the cells increases (to about 120 in the case of the vector). This is because *leu2-89* on the
732 plasmid is a *LEU2* allele with a large deletion in its promoter, so cells with higher plasmid copy numbers
733 will grow faster in –Leu/Ura conditions. In other words, *leu2-89* acts as a bias to raise the plasmid copy
734 number in –Leu/Ura conditions. If overexpression of the target protein inhibits growth, the plasmid
735 copy number will be lower than the copy number that gives rise to the critical expression of that protein.

736 In other words, the target gene acts as a bias to lower the plasmid copy number. The resulting tug-of-
737 war between the selection biases created by the two genes leads to a target protein being expressed at
738 close to the critical expression level in –Leu/Ura conditions (the green-colored area in Figure 2—figure
739 supplement 1A). By using a version of the aureobasidin A resistance gene (*AUR1*) with a deletion in its
740 promoter (*AUR1d*) as a bias to increase plasmid copy number, experiments based on the same concept
741 as gTOW can also be conducted in rich medium (YPD + 500 ng/mL aureobasidin A). In this case, the
742 plasmid pTOW-AUR1d is used (Figure 4—figure supplement 2A).
743
744 **Measuring growth rate**
745 Cellular growth was measured by monitoring OD_{660}, every 10 min using a compact rocking incubator
746 (TVS062CA, ADVANTEC). The max growth rate (MGR) was calculated as described previously
747 (Moriya *et al.* 2006). Average values, SD, and *p*-values of Welch's *t*-test were calculated from at least
748 three biological replicates. The growth data of Figures 2—figure supplement 10A was measured by
749 monitoring OD_{595}, respectively, every 10 min using a microplate reader (Infinite F200, TECAN).
750
751 **Protein analysis**
752 Yeast cells overexpressing a target protein were cultivated in SC–Leu/Ura medium. The total protein
753 was extracted from log-phase cells (OD_{660} = 1.0) with a NuPAGE LDS sample buffer (Thermo Fisher
754 Scientific) after 0.2 mol/l NaOH treatment (Kushnirov 2000). For each analysis, the total protein
755 extracted from 1 optical density (OD) unit of cells with OD_{660} was used. For total protein visualization,
756 the extracted total protein was labeled with Ezlabel FluoroNeo (ATTO), as described in the
757 manufacturer's protocol, and separated by 4–12% sodium-dodecyl sulfate acrylamide gel
758 electrophoresis (SDS-PAGE). Proteins were detected and measured using the LAS-4000 image
759 analyzer (GE Healthcare) in SYBR–green fluorescence detection mode and Image Quant TL software
760 (GE Healthcare). Protein quantification was performed as shown in Figure 2—figure supplement 1B.
761 Average values, SD, and *p*-values of Welch's *t*-test were calculated from three biological replicates.
762
763 **Western blotting of Atg13**

764 Cells overexpressing FPs were collected at OD_{660} = 1 or 2 and fixed with 100 μL of ice–cold alkaline
765 solution (0.2 N NaOH and 0.5% β–mercaptoethanol). After 5 min of incubation on ice, 1 mL of ice–
766 cold acetone was added to the sample and incubated at −20˚C to precipitate proteins. The protein
767 samples were precipitated with a microfuge (15,000 rpm, 5 min), air–dried, suspended in 100 μL of
768 SDS–PAGE sample buffer, and incubated at 65˚C for 15 min. The samples were thoroughly dissolved
769 by sonication and subjected to SDS–PAGE (40 mA, 1h). After ponceau S staining, proteins are
770 transferred to the PVDF membrane (Millipore #IPVH304F0) and blocked in 5% skim milk/TBST.
771 Atg13 was detected using a rabbit anti–Atg13 antibody (1:3000) and peroxidase-conjugated goat anti-
772 rabbit secondary antibodies (Jackson ImmunoResearch, #111–035–003, 1:10,000). Chemiluminescent
773 substrates (Millipore, #WBLUF0100) and Light–Capture II (ATTO) were used for signal detection.
774
775 **Measuring GFP fluorescence**
776 GFP fluorescence (Ex485nm/Em535nm) was measured every 10 min using a microplate reader (Infinite
777 F200, TECAN). Average values, SD, and *p*-values of Welch's *t*-test were calculated from eight
778 biological replicates.
779
780 **RNA-seq analysis**
781 BY4741 cells overexpressing a target protein were cultured in SC–Leu/Ura medium and harvested at
782 the logarithmic growth phase. RNA extraction was performed according to (Köhrer and Domdey, 1991).
783 The purified RNA was quality checked by BioAnalyzer (Agilent) or MultiNA (Shimazu), and the
784 concentration was measured by Qubit (Thermo Fisher Scientific). Purified RNA was stored at −80°C
785 until subsequent experiments. cDNA libraries were prepared using the TruSeq Stranded Total RNA kit
786 (Illumina), using half the protocol of the TruSeq RNA library prep kit. Three biological replicates were
787 analyzed for all strains. The sequences were checked for read quality by FastP (Chen et al., 2018) and
788 then aligned using Hisat2 (Kim et al., 2019). The aligned data were formatted into bam files by Samtools
789 (Li et al., 2009) and quantified by StringTie (Pertea et al., 2015). Finally, expression level variation
790 analysis was performed by EdgeR (Robinson et al., 2010). The raw data were deposited into DDBJ

791 (accession number: PRJDB18064). The processed data (Data_S1) included the average expression
792 levels (log10CPM) of 6685 genes in the vector control, the changes in expression (log2FC) upon
793 overexpression of mox or mox-YG compared to the vector control, and the significance values of
794 expression change (mox_FDR, mox-YG_FDR). Figures 3—figure supplement 1A, B is the
795 visualization of this data using volcano plots. This data is used in subsequent data analyses below.
796

797 **Reporter assay**

798 The strains used for the reporter assay were created by introducing the promoter region of each gene
799 and the sequence of mScarlet-I, a type of RFP, into the *FCY1* locus of the genome as shown in Figure
800 3—figure supplement 2A. Correct integration was checked by histidine prototrophy and 5-FC resistance
801 of the strain. The cell density (OD_{595}) and RFP fluorescence (Ex535nm/Em590nm) of the created strains
802 were measured every 10 min using a microplate reader (Infinite F200PRO, TECAN). Average and SD
803 of max RFP fluorescence, and *p*-values of Welch's *t*-test were calculated from eight biological replicates.
804

805 **Proteome analysis**

806 The vector control and mox-YG overexpressing cells (three biological replicates) were cultured in 5
807 mL of SC–LeuUra medium with shaking and cells were collected at OD_{660} = 1. Cells were washed twice
808 with PBS, frozen on dry ice, and transported to Kazusa DNA Research Institute. The samples were
809 prepared as described in the previous study (Hughes et al., 2019; Kawashima et al., 2022). The cells
810 were dissolved in 100 mM Tris-HCl (pH 8.0) containing 4% SDS and 20 mM NaCl using BIORUPTOR
811 BR-II (SONIC BIO Co., Kanagawa, Japan). The 20 µg of extracted proteins were quantified using
812 Pierce™ BCA Protein Assay Kit (Thermo Fisher Scientific, WA, USA) at 500 ng/µL. The protein
813 extracts were reduced with 20 mM tris (2-carboxyethyl) phosphine for 10 min at 80°C followed by
814 alkylation with 30 mM iodoacetamide for 30 min at room temperature in the dark. Protein purification
815 and digestion were performed using the sample preparation (SP3) method (Kawashima et al., 2022).
816 The tryptic digestion was performed using 500 ng/µL Trypsin/Lys-C Mix (Promega, Madison, WI,
817 USA) for overnight at 37°C. The digests were purified using GL-Tip SDB (GL Sciences, Tokyo, Japan)
818 according to the manufacturer's protocol. The peptides were dissolved again in 2% ACN containing

819 0.1% TFA and quantified using BCA assay at 150 ng/μL. The digested peptides were loaded directly
820 using a 75 μm × 12 cm nanoLC nano-capillary column (Nikkyo Technos Co., Ltd., Tokyo, Japan) at
821 40°C and then separated with a 30-minute gradient (mobile phase A = 0.1% FA in water, B = 0.1% FA
822 in 80% ACN) consisting of 0 min 8% B, 30 min 70% B at a flow rate of 200 nL/min using an UltiMate
823 3000 RSLCnano LC system (Thermo Fisher Scientific). The eluted peptides were detected using a
824 quadrupole Orbitrap Exploris 480 hybrid mass spectrometer (Thermo Fisher Scientific) with normal
825 window DIA. The MS1 scan range was set as a full scan with m/z 490-745 at a mass resolution of
826 15,000 to set an Auto Gain Control (AGC) target for MS1 as 3×10^6 and a maximum injection time of
827 23 msec. The MS2 were collected at more than m/z 200 at 30,000 resolutions to set an AGC target of 3
828 $\times 10^6$, maximum injection time of "auto", and fixed normalized collision energy of 28%. The isolation
829 width for MS2 was set to 4 m/z, and for the 500-740 m/z window pattern, an optimized window
830 arrangement was used in Scaffold DIA (Proteome Software, Inc., Portland, OR, USA). The raw data
831 were searched against an *in silico* predicted spectral library using DIA-NN (Demichev et al., 2020).
832 (version:1.8.1, https://github.com/vdemichev/DiaNN) First, an *in-silico* predicted spectral library was
833 generated from the human protein sequence database (UniProt id UP000005640, reviewed, canonical,
834 20381 entries) using DIA-NN. The DIA-NN search parameters were as follows: protease, trypsin;
835 missed cleavages, 1; peptide length range, 7-45; precursor charge range, 2-4; precursor mass range,
836 495-745; fragment ion m/z range, 200-1800; mass accuracy, 10 ppm; static modification, cysteine
837 carbamidomethylation; enabled "Heuristic protein interferences," "Use isotopologues," "MBR," and
838 "No shared spectra." Additional commands were set as follows: "mass acc cal 10," "peak translation,"
839 and "matrix spec q". The protein identification threshold was set at < 1% for both peptide and protein
840 false discovery rates (FDRs).
841 The signal intensity data for 4241 proteins (Data_S2) was used for further data analysis below.
842
843 **Data analysis**
844 The analysis and visualization of RNA-seq data and proteome data were conducted using custom
845 Python code, and coding and execution were carried out in the Collaboratory. In the RNAseq data,
846 6,685 protein-coding genes were detected (Data_S1). Among these, 4,291 genes assigned to various

847 categories of KEGG Orthology level 3 (Kanehisa et al., 2023) were placed into 77 categories. Analysis
848 was performed on 47 categories that contained more than 10 gene elements. We investigated whether
849 the expression of genes in each category, as a group, was significantly higher or lower upon
850 overexpression of mox and mox-YG compared to the vector control. Specifically, mox/Vector (log2FC)
851 and mox-YG/Vector (log2FC) were calculated along with their FDR values, and each gene was assigned
852 to a KEGG orthology level 3 category. Next, whether the gene groups within each category showed
853 significantly higher or lower expression changes compared to gene groups outside of their category was
854 tested using the Mann-Whitney *U*-test. Significant differences were indicated in the graphs with a red
855 border and red stripes. The graphs showed the overall distribution of genes within each category using
856 violin plots, and only genes showing significant differences in mox/Vector (log2FC) and mox-
857 YG/Vector (log2FC) were highlighted in swarm plots. An asterisk indicated significant differences on
858 the graphs when the expression changes (log2FC) between mox/Vector and mox-YG/Vector were
859 significant by the Mann-Whitney *U*-test. The significance threshold was set at FDR < 0.05 for all. Only
860 categories where either mox or mox-YG overexpression showed significant expression changes were
861 extracted and presented as Figure 3B, and all 47 categories were shown in Figure 3—figure supplement
862 1C.

863 The proteome analysis was conducted using the signal intensity data (Data_S2). This data includes
864 proteins that were detected only in some samples under certain conditions or replicates, especially those
865 with low signals or large expression variations. Additionally, the total protein signal sum excluding
866 mox-YG was almost the same between the vector control and mox-YG overexpression (Figure 4—
867 figure supplement 3A). This result contradicts the SDS−PAGE findings, which indicate that the total
868 protein mass per cell, including mox-YG, is the same between the vector control and mox-YG
869 overexpression (Figure 4A). Therefore, it is considered necessary to adjust the total protein signal sum,
870 including mox-YG, to match that of the vector control to understand the proteome change per cell. In
871 this study, however, we used the most conservative approach by removing proteins with zero values
872 and not applying any overall corrections (Figure 4—figure supplement 3B), which allowed the analysis
873 of 3,588 proteins. Although this may not correctly analyze "per cell" proteome change, it enables us to

874 capture the change in proteome composition (excluding mox-YG), thus providing information about
875 cellular responses. If the total correction is applied, only 138 proteins were increased (Figure 4—figure
876 supplement 3C), most of which are mitochondrial proteins.

877 For the detected 3,588 proteins above, we compared the increase or decrease of protein groups within
878 each category of KEGG Orthology Level 3 with those outside the category. Analysis was performed on
879 45 categories, each containing more than 10 proteins, to investigate whether the expression of protein
880 groups in each category was significantly higher or lower under mox-YG overexpression compared to
881 the vector control. Specifically, the average log2FC and its FDR values were calculated using data from
882 three replicates for mox-YG/Vector, and each protein was assigned to a KEGG orthology level 3
883 category. Next, whether the protein groups within each category showed significantly higher or lower
884 expression changes compared to protein groups outside of their category was tested using the Mann-
885 Whitney *U*-test. Significant differences were indicated in the graphs with a red border and red stripes.
886 The graphs showed the overall distribution of proteins within each category using violin plots, and only
887 proteins showing significant differences in mox-YG/Vector (log2FC) were highlighted in swarm plots.
888 The significance threshold was set at FDR < 0.05 for all. Only categories where mox-YG
889 overexpression showed significant expression changes were extracted and presented in Figure 4C and
890 all 47 categories were shown in Figure 4—figure supplement 6. Published data (Gowans et al., 2018)
891 was used to separate protein groups into rapamycin-responsive and non-responsive, and similar analysis
892 and visualization were conducted (Figures 4—figure supplement 6A, B).

893

894 **Fluorescence microscopic observation**

895 Cells overexpressing target proteins were cultured in SC–LeuUra medium and observed under an
896 inverted microscope (DMI 6000 B, Leica) at log phase ($OD_{660} = 1.0$). Images were acquired with Leica
897 Application Suite and processed with Leica Application Suite X software (Leica Microsystems). Cells
898 in brightfield images were separated from the images using yeast_segmentation-master_v3 (Lu et al.,
899 2019). Cell morphological traits were assessed using parameters obtained when analysed using

900 CellProfiler (Ver. 4.2.6) (Carpenter et al., 2006). "AreaShape_Area" was used to analyse FP-
901 overexpressing cell size (arbitrary unit; AU) in Figure 2—figure supplement 6B, Nsr1-GFP in Figure
902 5—figure supplement 2C and Nsr1-mScarlet-I in Figure 5—figure supplement 5E, 6F, and Figure 6—
903 figure supplement 7C. For analysis of the fluorescence intensity of Rip1-mScarlet-I in Figure 4—figure
904 supplement 8B and Figure 6—figure supplement 5A. "Intensity_ IntegratedIntensity" was used.
905 Intensity_MeanIntensity" was used to analyze the fluorescence intensity of Nsr1-GFP in Figure 5—
906 figure supplement 2D and Figure 6—figure supplement 7C. Ten images per experiment were used for
907 analysis. The axis ratio in Figure 6—figure supplement 3 was calculated as the ratio of
908 "AreaShape_MajorAxisLength" to "AreaShape_MinorAxisLength" in the data
909

910 **Measurement of oxygen consumption**

911 Cells overexpressing the target protein were collected at OD_{660} = 1. The cells (0.05 OD unit) were
912 treated with oxygen probe in SC–LeuUra and 50μM antimycin A in SC–LeuUra. Oxygen consumption
913 was measured according to the instruction manual of the Extracellular OCR Plate Assay Kit (Dojindo,
914 #E297). The fluorescence intensity (Ex500nm/Em650 nm) was recorded at 10 min intervals using a
915 microplate reader (Infinite F200, TECAN). The oxygen consumption rate (AU) was calculated as the
916 slope of a linear approximation of the kinetic data.
917

918 **Electron microscopic observation**

919 Cells grown to log phase (OD_{600} = 1.0) at 30°C in SC–LeuUra medium were collected and transported
920 to Tokai Electron Microscope Co. Transported samples were sandwiched between copper plates, flash-
921 frozen with liquefied propane, and then dehydrated with anhydrous ethanol. cells were fixed with a 5:5
922 mixture of propylene oxide and resin (Quetol-651, Nissin EM Co.). Fixed cells were cut with an
923 ultramicrotome (Ultracut UCT, Leica) to prepare 80 nm thick sections, stained with 2% uranyl acetate
924 and lead stain solution (Sigma-Aldrich Co.), and observed with a transmission electron microscope
925 (JEM-1400 Plus, JEOL Ltd.).
926

927 **Data availability**

928 All raw data, analysis code, and omics analysis pipelines used for generating the figures have been
929 deposited in GitHub (https://github.com/hisaomlab/Fujita_eLife_2025).

Acknowledgments

We thank the members of the Moriya laboratory (Okayama University) for their helpful discussions.

Funding

This work was partly supported by the Nagase Science and Technology Foundation, Institute for Fermentation, Osaka (IFO) General Research Funding, JSPS KAKENHI Grant Numbers 22K19294, and 24K02313, JST SPRING Japan Grant Number JPMJSP2126.

937 # References

938 Amberg DC, Burke DJ, Burke D, Strathern JN. 2005. Methods in Yeast Genetics: A Cold Spring Harbor
939 Laboratory Course Manual. CSHL Press.

940 Bolognesi B, Lorenzo Gotor N, Dhar R, Cirillo D, Baldrighi M, Tartaglia GG, Lehner B. 2016. A
941 Concentration-Dependent Liquid Phase Separation Can Cause Toxicity upon Increased Protein
942 Expression. *Cell Rep* **16**:222–231.

943 Brachmann CB, Davies A, Cost GJ, Caputo E, Li J, Hieter P, Boeke JD. 1998. Designer deletion strains
944 derived from Saccharomyces cerevisiae S288C: a useful set of strains and plasmids for PCR-
945 mediated gene disruption and other applications. *Yeast* **14**:115–132.

946 Bruggeman FJ, Planqué R, Molenaar D, Teusink B. 2020. Searching for principles of microbial
947 physiology. *FEMS Microbiol Rev* **44**:821–844.

948 Carpenter AE, Jones TR, Lamprecht MR, Clarke C, Kang IH, Friman O, Guertin DA, Chang JH,
949 Lindquist RA, Moffat J, Golland P, Sabatini DM. 2006. CellProfiler: image analysis software for
950 identifying and quantifying cell phenotypes. *Genome Biol* **7**:R100.

951 Chen S, Zhou Y, Chen Y, Gu J. 2018. fastp: an ultra-fast all-in-one FASTQ preprocessor.
952 *Bioinformatics* **34**:i884–i890.

953 Costantini LM, Baloban M, Markwardt ML, Rizzo M, Guo F, Verkhusha VV, Snapp EL. 2015. A
954 palette of fluorescent proteins optimized for diverse cellular environments. *Nat Commun* **6**:7670.

955 Craggs TD. 2009. Green fluorescent protein: structure, folding and chromophore maturation. *Chem Soc*
956 *Rev* **38**:2865–2875.

957 Delarue M, Brittingham GP, Pfeffer S, Surovtsev IV, Pinglay S, Kennedy KJ, Schaffer M, Gutierrez JI,
958 Sang D, Poterewicz G, Chung JK, Plitzko JM, Groves JT, Jacobs-Wagner C, Engel BD, Holt LJ.
959 2018. mTORC1 Controls Phase Separation and the Biophysical Properties of the Cytoplasm by
960 Tuning Crowding. *Cell* **174**:338–349.e20.

961 Demichev V, Messner CB, Vernardis SI, Lilley KS, Ralser M. 2020. DIA-NN: neural networks and
962 interference correction enable deep proteome coverage in high throughput. *Nat Methods* **17**:41–
963 44.

964 Dong H, Nilsson L, Kurland CG. 1995. Gratuitous overexpression of genes in Escherichia coli leads to
965 growth inhibition and ribosome destruction. *J Bacteriol* **177**:1497–1504.
966 Eguchi Y, Makanae K, Hasunuma T, Ishibashi Y, Kito K, Moriya H. 2018. Estimating the protein
967 burden limit of yeast cells by measuring the expression limits of glycolytic proteins. *Elife* **7**.
968 doi:10.7554/eLife.34595
969 Farkas Z, Kalapis D, Bódi Z, Szamecz B, Daraba A, Almási K, Kovács K, Boross G, Pál F, Horváth P,
970 Balassa T, Molnár C, Pettkó-Szandtner A, Klement É, Rutkai E, Szvetnik A, Papp B, Pál C. 2018.
971 Hsp70-associated chaperones have a critical role in buffering protein production costs. *Elife* **7**.
972 doi:10.7554/eLife.29845
973 Frumkin I, Schirman D, Rotman A, Li F, Zahavi L, Mordret E, Asraf O, Wu S, Levy SF, Pilpel Y. 2017.
974 Gene Architectures that Minimize Cost of Gene Expression. *Mol Cell* **65**:142–153.
975 Gowans GJ, Schep AN, Wong KM, King DA, Greenleaf WJ, Morrison AJ. 2018. INO80 Chromatin
976 Remodeling Coordinates Metabolic Homeostasis with Cell Division. *Cell Rep* **22**:611–623.
977 Hausser J, Mayo A, Keren L, Alon U. 2019. Central dogma rates and the trade-off between precision
978 and economy in gene expression. *Nat Commun* **10**:68.
979 Hughes CS, Moggridge S, Müller T, Sorensen PH, Morin GB, Krijgsveld J. 2019. Single-pot, solid-
980 phase-enhanced sample preparation for proteomics experiments. *Nat Protoc* **14**:68–85.
981 Kafri M, Metzl-Raz E, Jona G, Barkai N. 2016. The Cost of Protein Production. *Cell Rep* **14**:22–31.
982 Kaizu K, Moriya H, Kitano H. 2010. Fragilities caused by dosage imbalance in regulation of the
983 budding yeast cell cycle. *PLoS Genet* **6**:e1000919.
984 Kamada Y, Funakoshi T, Shintani T, Nagano K, Ohsumi M, Ohsumi Y. 2000. Tor-mediated induction
985 of autophagy via an Apg1 protein kinase complex. J Cell Biol 150:1507–1513.
986 Kanehisa M, Furumichi M, Sato Y, Kawashima M, Ishiguro-Watanabe M. 2023. KEGG for taxonomy-
987 based analysis of pathways and genomes. *Nucleic Acids Res* **51**:D587–D592.
988 Kastberg LLB, Ard R, Jensen MK, Workman CT. 2022. Burden Imposed by Heterologous Protein
989 Production in Two Major Industrial Yeast Cell Factories: Identifying Sources and Mitigation
990 Strategies. *Front Fungal Biol* **3**:827704.
991 Kawashima Y, Nagai H, Konno R, Ishikawa M, Nakajima D, Sato H, Nakamura R, Furuyashiki T,

992 Ohara O. 2022. Single-Shot 10K Proteome Approach: Over 10,000 Protein Identifications by
993 Data-Independent Acquisition-Based Single-Shot Proteomics with Ion Mobility Spectrometry. *J*
994 *Proteome Res* **21**:1418–1427.
995 Keppler-Ross S, Noffz C, Dean N. 2008. A new purple fluorescent color marker for genetic studies in
996 Saccharomyces cerevisiae and Candida albicans. *Genetics* **179**:705–710.
997 Keren L, Hausser J, Lotan-Pompan M, Vainberg Slutskin I, Alisar H, Kaminski S, Weinberger A, Alon
998 U, Milo R, Segal E. 2016. Massively Parallel Interrogation of the Effects of Gene Expression
999 Levels on Fitness. *Cell* **166**:1282–1294.e18.
1000 Kim D, Paggi JM, Park C, Bennett C, Salzberg SL. 2019. Graph-based genome alignment and
1001 genotyping with HISAT2 and HISAT-genotype. *Nat Biotechnol* **37**:907–915.
1002 Kintaka R, Makanae K, Moriya H. 2016. Cellular growth defects triggered by an overload of protein
1003 localization processes. *Scientific Reports*. doi:10.1038/srep31774
1004 Kintaka R, Makanae K, Namba S, Kato H, Kito K, Ohnuki S, Ohya Y, Andrews BJ, Boone C, Moriya
1005 H. 2020. Genetic profiling of protein burden and nuclear export overload. *Elife* **9**.
1006 doi:10.7554/eLife.54080
1007 Koch AL. 1983. The protein burden oflac operon products. *J Mol Evol* **19**:455–462.
1008 Köhrer K, Domdey H. 1991. [27] Preparation of high molecular weight RNAMethods in Enzymology.
1009 Academic Press. pp. 398–405.
1010 Kummer AD, Wiehler J, Rehaber H, Kompa C, Steipe B, Michel-Beyerle ME. 2000. Effects of
1011 Threonine 203 Replacements on Excited-State Dynamics and Fluorescence Properties of the Green
1012 Fluorescent Protein (GFP). *J Phys Chem B* **104**:4791–4798.
1013 Lafontaine DLJ. 2015. Noncoding RNAs in eukaryotic ribosome biogenesis and function. *Nat Struct*
1014 *Mol Biol* **22**:11–19.
1015 Liebermeister W, Noor E, Flamholz A, Davidi D, Bernhardt J, Milo R. 2014. Visual account of protein
1016 investment in cellular functions. *Proc Natl Acad Sci U S A* **111**:8488–8493.
1017 Li H, Handsaker B, Wysoker A, Fennell T, Ruan J, Homer N, Marth G, Abecasis G, Durbin R, 1000
1018 Genome Project Data Processing Subgroup. 2009. The Sequence Alignment/Map format and
1019 SAMtools. *Bioinformatics* **25**:2078–2079.

1020 Lu AX, Zarin T, Hsu IS, Moses AM. 2019. YeastSpotter: accurate and parameter-free web segmentation
1021 for microscopy images of yeast cells. *Bioinformatics* **35**:4525–4527.
1022 Mahima, Sharma AK. 2023. Optimization of ribosome utilization in Saccharomyces cerevisiae. *PNAS*
1023 *Nexus* **2**:gad074.
1024 Makanae K, Kintaka R, Makino T, Kitano H, Moriya H. 2013. Identification of dosage-sensitive genes
1025 in Saccharomyces cerevisiae using the genetic tug-of-war method. *Genome Res* **23**:300–311.
1026 Ma L, Pang CNI, Li SS, Wilkins MR. 2010. Proteins Deleterious on Overexpression Are Associated
1027 with High Intrinsic Disorder, Specific Interaction Domains, and Low Abundance. *J Proteome Res*
1028 **9**:1218–1225.
1029 Martin DE, Soulard A, Hall MN. 2004. TOR regulates ribosomal protein gene expression via PKA and
1030 the Forkhead transcription factor FHL1. *Cell* **119**:969–979.
1031 Meng EC, Goddard TD, Pettersen EF, Couch GS, Pearson ZJ, Morris JH, Ferrin TE. 2023. UCSF
1032 ChimeraX: Tools for structure building and analysis. *Protein Sci* **32**:e4792.
1033 Metzl-Raz E, Kafri M, Yaakov G, Barkai N. 2020. Gene Transcription as a Limiting Factor in Protein
1034 Production and Cell Growth. *G3* **10**:3229–3242.
1035 Metzl-Raz E, Kafri M, Yaakov G, Soifer I, Gurvich Y, Barkai N. 2017. Principles of cellular resource
1036 allocation revealed by condition-dependent proteome profiling. *Elife* **6**. doi:10.7554/eLife.28034
1037 Moriya H. 2015. Quantitative nature of overexpression experiments. *Mol Biol Cell* **26**:3932–3939.
1038 Moriya H, Makanae K, Watanabe K, Chino A, Shimizu-Yoshida Y. 2012. Robustness analysis of
1039 cellular systems using the genetic tug-of-war method. *Mol Biosyst* **8**:2513–2522.
1040 Moriya H, Shimizu-Yoshida Y, Kitano H. 2006. In vivo robustness analysis of cell division cycle genes
1041 in Saccharomyces cerevisiae. *PLoS Genet* **2**:e111.
1042 Namba S, Kato H, Shigenobu S, Makino T, Moriya H. 2022. Massive expression of cysteine-containing
1043 proteins causes abnormal elongation of yeast cells by perturbing the proteasome. *G3* **12**.
1044 doi:10.1093/g3journal/jkac106
1045 Oldenburg K. 1997. Recombination-mediated PCR-directed plasmid construction in vivo in yeast.
1046 *Nucleic Acids Research*. doi:10.1093/nar/25.2.451
1047 Papp B, Pál C, Hurst LD. 2003. Dosage sensitivity and the evolution of gene families in yeast. *Nature*

1048 **424**:194–197.

1049 Pellegrino S, Demeshkina N, Mancera-Martinez E, Melnikov S, Simonetti A, Myasnikov A, Yusupov
1050 M, Yusupova G, Hashem Y. 2018. Structural Insights into the Role of Diphthamide on Elongation
1051 Factor 2 in mRNA Reading-Frame Maintenance. *J Mol Biol* **430**:2677–2687.

1052 Peralta D, Bronowska AK, Morgan B, Dóka É, Van Laer K, Nagy P, Gräter F, Dick TP. 2015. A proton
1053 relay enhances H2O2 sensitivity of GAPDH to facilitate metabolic adaptation. *Nat Chem Biol*
1054 **11**:156–163.

1055 Pertea M, Pertea GM, Antonescu CM, Chang T-C, Mendell JT, Salzberg SL. 2015. StringTie enables
1056 improved reconstruction of a transcriptome from RNA-seq reads. *Nat Biotechnol* **33**:290–295.

1057 Prelich G. 2012. Gene overexpression: uses, mechanisms, and interpretation. *Genetics* **190**:841–854.

1058 Robinson MD, McCarthy DJ, Smyth GK. 2010. edgeR: a Bioconductor package for differential
1059 expression analysis of digital gene expression data. *Bioinformatics* **26**:139–140.

1060 Scott M, Gunderson CW, Mateescu EM, Zhang Z, Hwa T. 2010. Interdependence of cell growth and
1061 gene expression: origins and consequences. *Science* **330**:1099–1102.

1062 Shachrai I, Zaslaver A, Alon U, Dekel E. 2010. Cost of unneeded proteins in E. coli is reduced after
1063 several generations in exponential growth. *Mol Cell* **38**:758–767.

1064 Stoebel DM, Dean AM, Dykhuizen DE. 2008. The cost of expression of Escherichia coli lac operon
1065 proteins is in the process, not in the products. *Genetics* **178**:1653–1660.

1066 Vavouri T, Semple JI, Garcia-Verdugo R, Lehner B. 2009. Intrinsic protein disorder and interaction
1067 promiscuity are widely associated with dosage sensitivity. *Cell* **138**:198–208.

1068 Watson JL, Seinkmane E, Styles CT, Mihut A, Krüger LK, McNally KE, Planelles-Herrero VJ, Dudek
1069 M, McCall PM, Barbiero S, Vanden Oever M, Peak-Chew SY, Porebski BT, Zeng A, Rzechorzek
1070 NM, Wong DCS, Beale AD, Stangherlin A, Riggi M, Iwasa J, Morf J, Miliotis C, Guna A, Inglis
1071 AJ, Brugués J, Voorhees RM, Chambers JE, Meng Q-J, O'Neill JS, Edgar RS, Derivery E. 2023.
1072 Macromolecular condensation buffers intracellular water potential. *Nature* **623**:842–852.

1073 White MF, Fothergill-Gilmore LA. 1992. Development of a mutagenesis, expression and purification
1074 system for yeast phosphoglycerate mutase. Investigation of the role of active-site His181. *Eur*
1075 *J Biochem* **207**:709–714.

1076 Youn J-Y, Friesen H, Nguyen Ba AN, Liang W, Messier V, Cox MJ, Moses AM, Andrews B. 2017.
1077 Functional Analysis of Kinases and Transcription Factors in Saccharomyces cerevisiae Using an
1078 Integrated Overexpression Library. *G3* **7**:911–921.

1079 # Figure supplements

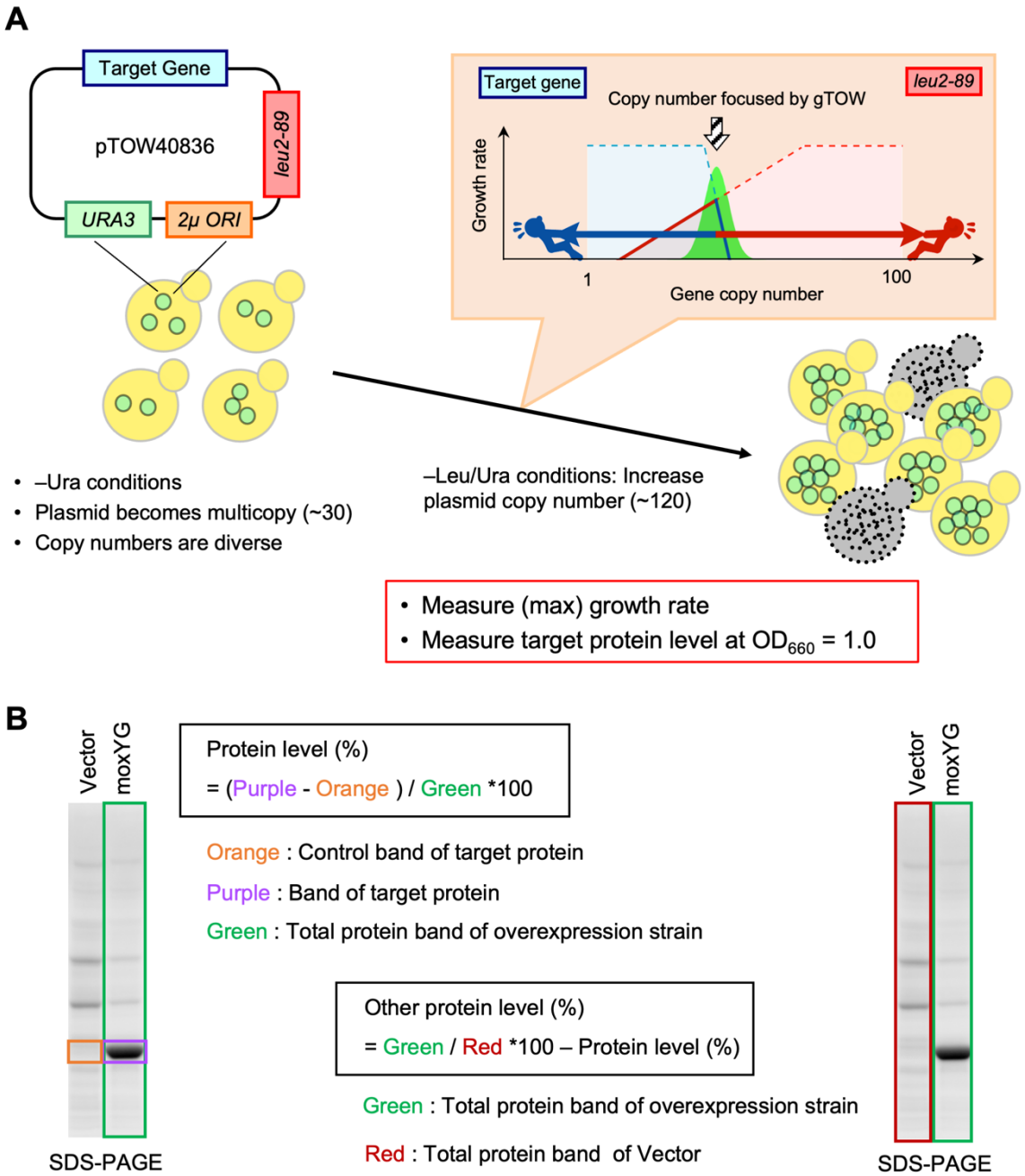

1080

1081 **Figure 2—figure supplement 1. Methods used for overexpression and protein expression**

1082 **quantification.**

1083 **A**) The genetic tug-of-war (gTOW) method. See Materials and Methods for details.

1084 **B**) Protein quantification method. All proteins present in the cells were labeled with a fluorescent dye
1085 (Ezlabel FluoroNeo) and separated by SDS-PAGE. The protein level of the target protein (Protein level)
1086 was calculated by subtracting the band at the same position of the vector control (Orange) from the band
1087 of the target protein on the gel (Purple), which was estimated from the molecular weight, and dividing
1088 the result by the total protein (Green). Other protein (Other protein level) was calculated by subtracting
1089 Protein level (%) from the value obtained by normalizing the total protein (Green) of the overexpression
1090 strain by the total protein (Red) of the vector control.

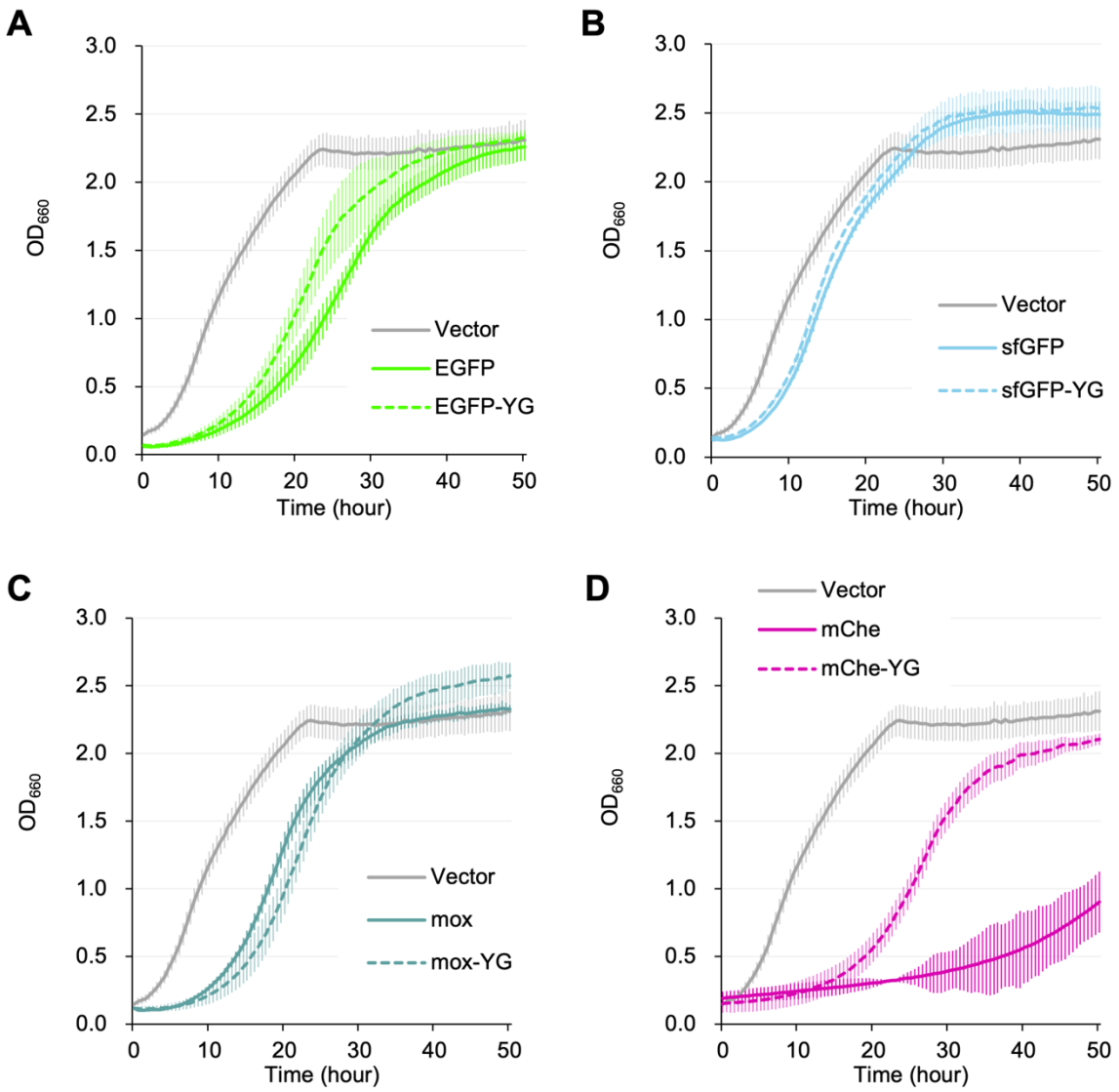

1091

1092 **Figure 2—figure supplement 2. Comparison of growth of fluorescent protein overexpressing**
1093 **strains**

1094 Growth curves of the cells with the vector (pTOW40836) and the cells overexpressing fluorescent
1095 proteins and their non-fluorescent YG mutants in synthetic medium (–LeuUra). The solid or dotted lines
1096 show the average calculated from three biological replicates. Shaded zones indicate their standard
1097 deviations. **A**: EGFP and EGFP-YG, **B**: sfGFP and sfGFP-YG, **C**: moxGFP (mox) and mox-YG, **D**:
1098 mCherry (mCche) and mCche-YG.

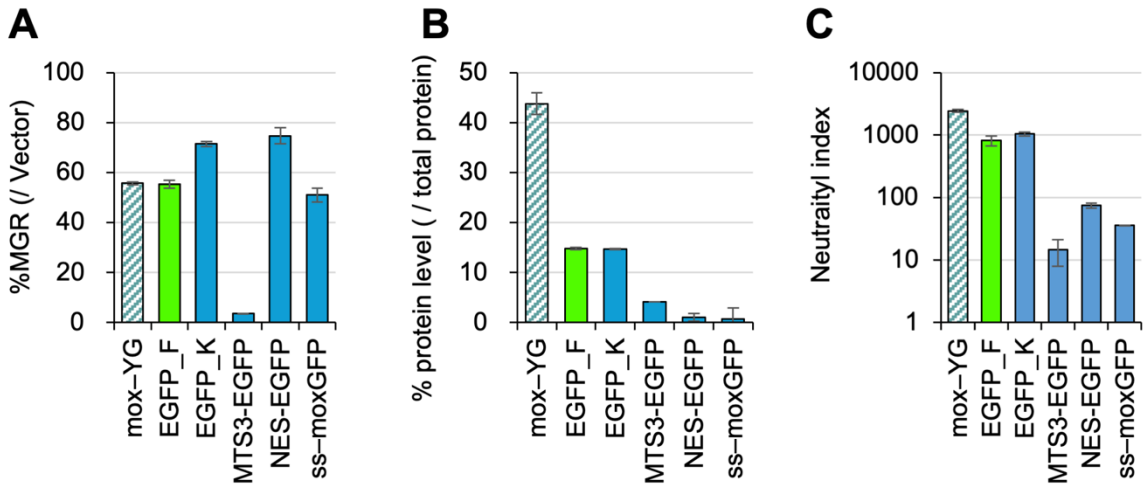

1099

1100 **Figure 2—figure supplement 3. Neutrality indexes of constrained proteins**

1101 **A**) MGRs of cells overexpressing indicated proteins.

1102 **B**) Protein levels of the indicated target proteins (percent over the total proteins).

1103 **C**) The neutrality index for the indicated proteins.

1104 MTS3–EGFP: EGFP targeted to mitochondria; cultured in SC–LeuUra; expressed by the *PYK1*
1105 promoter. NES–EGFP: EGFP with nuclear export signal; cultured in SC–Ura; expressed by the *HXT7*
1106 promoter. ss–moxGFP: moxGFP targeted to the endoplasmic reticulum; cultured in SC–Ura; expressed
1107 by the *PYK1* promoter. EGFP_K: the EGFP result of Kintaka *et al*. (Kintaka et al., 2016); cultured in
1108 SC–LeuUra; expressed by the *PYK1* promoter. EGFP_F: the EGFP result of this paper.

1109 In **A** and **B**, the data was obtained from Kintaka *et al*. (Kintaka et al., 2016), except mox-YG and
1110 EGFP_F (same as Figure 2 in this paper). The bars and error bars show the means and SDs calculated
1111 from three biological replicates.

moxGFP

```
  1  M  S  K  G  E  E  L  F  T  G  V  V  P  I  L  V  E  L  D  G  20
  1 ATGTCTAAAGGTGAAGAATTATTCACTGGTGTTGTCCCAATTTTGGTTGAATTAGATGGT 60

 21  D  V  N  G  H  K  F  S  V  R  G  E  G  E  G  D  A  T  N  G  40
 61 GATGTTAATGGTCACAAATTTTCTGTCcgtGGTGAAGGTGAAGGTGATGCTACTaAtGGT 120

 41  K  L  T  L  K  F  I  S  T  T  G  K  L  P  V  P  W  P  T  L  60
121 AAATTGACCTTAAAATTTATTTcTACTACTGGTAAATTGCCAGTTCCATGGCCAACCTTA 180

 61  V  T  T  L  T  Y  G  V  Q  S  F  S  R  Y  P  D  H  M  K  R  80
181 GTCACTACTTTAACTTATGGTGTTCAATcTTTTTCTAGATACCCAGATCATATGAAACgt 240

 81  H  D  F  F  K  S  A  M  P  E  G  Y  V  Q  E  R  T  I  S  F  100
241 CATGACTTTTTCAAGTCTGCCATGCCAGAAGGTTATGTTCAAGAAAGAACTATTTcTTTC 300

101  K  D  D  G  T  Y  K  T  R  A  E  V  K  F  E  G  D  T  L  V  120
301 AAAGATGACGGTActTACAAGACCAGAGCTGAAGTCAAGTTTGAAGGTGATACCTTAGTT 360

121  N  R  I  E  L  K  G  I  D  F  K  E  D  G  N  I  L  G  H  K  140
361 AATAGAATCGAATTAAAAGGTATTGATTTTAAAGAAGATGGTAACATTTTAGGTCACAAA 420

141  L  E  Y  N  F  N  S  H  N  V  Y  I  T  A  D  K  Q  K  N  G  160
421 TTGGAATACAACTtcAACTCTCACAATGTTTACATCActGCTGACAAACAAAAGAATGGT 480

161  I  K  A  N  F  K  I  R  H  N  V  E  D  G  S  V  Q  L  A  D  180
481 ATCAAAGcTAACTTCAAAATTAGACACAACgtTGAAGATGGTTCTGTTCAATTAGCTGAC 540

181  H  Y  Q  Q  N  T  P  I  G  D  G  P  V  L  L  P  D  N  H  Y  200
541 CATTATCAACAAAATACTCCAATTGGTGATGGTCCAGTCTTGTTACCAGACAACCATTAC 600

201  L  S  T  Q  S  R  L  S  K  D  P  N  E  K  R  D  H  M  V  L  220
601 TTATCCACTCAATCTcgtTTATCCAAAGATCCAAACGAAAAGAGAGACCACATGGTCTTG 660

221  L  E  F  V  T  A  A  G  I  T  H  G  M  D  E  L  Y  K  *  239
661 TTAGAATTTGTTACTGCTGCTGGTATTACCCATGGTATGGATGAATTGTACAAATAA 717
```

sfGFP

```
  1  M  S  K  G  E  E  L  F  T  G  V  V  P  I  L  V  E  L  D  G  20
  1 ATGTCTAAAGGTGAAGAATTATTCACTGGTGTTGTCCCAATTTTGGTTGAATTAGATGGT 60

 21  D  V  N  G  H  K  F  S  V  R  G  E  G  E  G  D  A  T  N  G  40
 61 GATGTTAATGGTCACAAATTTTCTGTCcgtGGTGAAGGTGAAGGTGATGCTACTaAtGGT 120

 41  K  L  T  L  K  F  I  C  T  T  G  K  L  P  V  P  W  P  T  L  60
121 AAATTGACCTTAAAATTTATTTgTACTACTGGTAAATTGCCAGTTCCATGGCCAACCTTA 180

 61  V  T  T  L  T  Y  G  V  Q  C  F  S  R  Y  P  D  H  M  K  R  80
181 GTCACTACTTTAACTTATGGTGTTCAATgTTTTTCTAGATACCCAGATCATATGAAACgt 240

 81  H  D  F  F  K  S  A  M  P  E  G  Y  V  Q  E  R  T  I  S  F  100
241 CATGACTTTTTCAAGTCTGCCATGCCAGAAGGTTATGTTCAAGAAAGAACTATTTcTTTC 300

101  K  D  D  G  T  Y  K  T  R  A  E  V  K  F  E  G  D  T  L  V  120
301 AAAGATGACGGTActTACAAGACCAGAGCTGAAGTCAAGTTTGAAGGTGATACCTTAGTT 360

121  N  R  I  E  L  K  G  I  D  F  K  E  D  G  N  I  L  G  H  K  140
361 AATAGAATCGAATTAAAAGGTATTGATTTTAAAGAAGATGGTAACATTTTAGGTCACAAA 420

141  L  E  Y  N  F  N  S  H  N  V  Y  I  T  A  D  K  Q  K  N  G  160
421 TTGGAATACAACTtcAACTCTCACAATGTTTACATCActGCTGACAAACAAAAGAATGGT 480

161  I  K  A  N  F  K  I  R  H  N  V  E  D  G  S  V  Q  L  A  D  180
481 ATCAAAGcTAACTTCAAAATTAGACACAACgtTGAAGATGGTTCTGTTCAATTAGCTGAC 540

181  H  Y  Q  Q  N  T  P  I  G  D  G  P  V  L  L  P  D  N  H  Y  200
541 CATTATCAACAAAATACTCCAATTGGTGATGGTCCAGTCTTGTTACCAGACAACCATTAC 600

201  L  S  T  Q  S  R  L  S  K  D  P  N  E  K  R  D  H  M  V  L  220
601 TTATCCACTCAATCTcgtTTATCCAAAGATCCAAACGAAAAGAGAGACCACATGGTCTTG 660

221  L  E  F  V  T  A  A  G  I  T  H  G  M  D  E  L  Y  K  *  239
661 TTAGAATTTGTTACTGCTGCTGGTATTACCCATGGTATGGATGAATTGTACAAATAA 717
```

1112

1113 **Figure 2—figure supplement 4. Base and amino acid sequences of moxGFP and sfGFP.**

1114 **Amino acids relevant to the text are shown in red.**

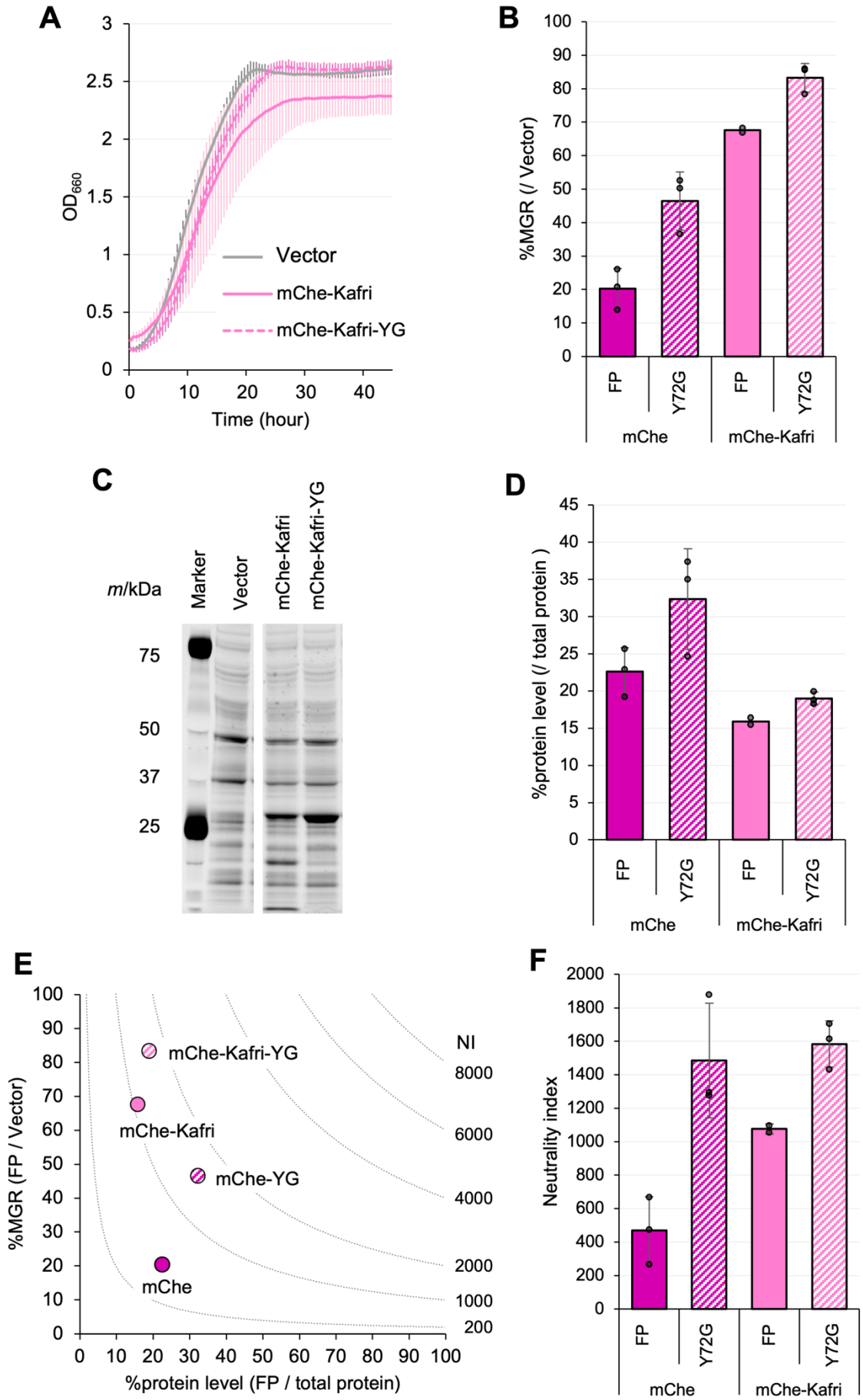
A
OD660
Time (hour)
Vector
mCh-Kafri
mCh-Kafri-YG
B
%MGR (/ Vector)
FP
Y72G
mCh
mCh-Kafri
C
m/kDa
Marker
Vector
mCh-Kafri
mCh-Kafri-YG
75
50
37
25
D
%protein level (/ total protein)
E
%MGR (FP / Vector)
%protein level (FP / total protein)
mCh-Kafri-YG
mCh-Kafri
mCh-YG
mCh
NI
8000
6000
4000
2000
1000
200
F
Neutrality index

1115

1116 **Figure 2—figure supplement 5. Comparative evaluation of mCherry (mCherry-Kafri) used in**
1117 **previous studies and this study.**
1118 **A)** Growth curves of cells overexpressing WT and YG mutants of mCherry used in Kafri *et al*. (Kafri
1119 et al. 2016) in synthetic medium (–LeuUra). The solid or dotted lines show the average calculated from
1120 three biological replicates.
1121 **B)** Ratio of MGR of cells overexpressing FPs and their mutants over the vector control.
1122 **C)** Gel images of SDS-PAGE-separated proteins extracted from cells overexpressing FPs. All proteins
1123 were separated after staining with a fluorescent dye.
1124 **D)** Protein level of the target protein (percent over the total protein). The amount was calculated from
1125 the intensity of the target bands separated by SDS-PAGE of **D**. Note that mChe may not be accurately
1126 measured due to molecular cleavage of the protein.
1127 **E**) Relationship between MGR and the protein level. MGR data are the same as in **B**, and the protein
1128 level data are the same as in **D**. The neutrality indexes (NIs), calculated from the products of MGR
1129 and %protein levels, are indicated by the lines. If the investigated proteins have the same NI, they are
1130 located on the same dotted line segment.
1131 **F**) The neutrality index for the FPs and mutants. The neutrality index is the product of %MGR (/Vector)
1132 and %protein level (/total protein).
1133 The bars and error bars in **B**, **D**, and **F** show the means and SDs calculated from three biological
1134 replicates. The raw data is shown with dot plots.

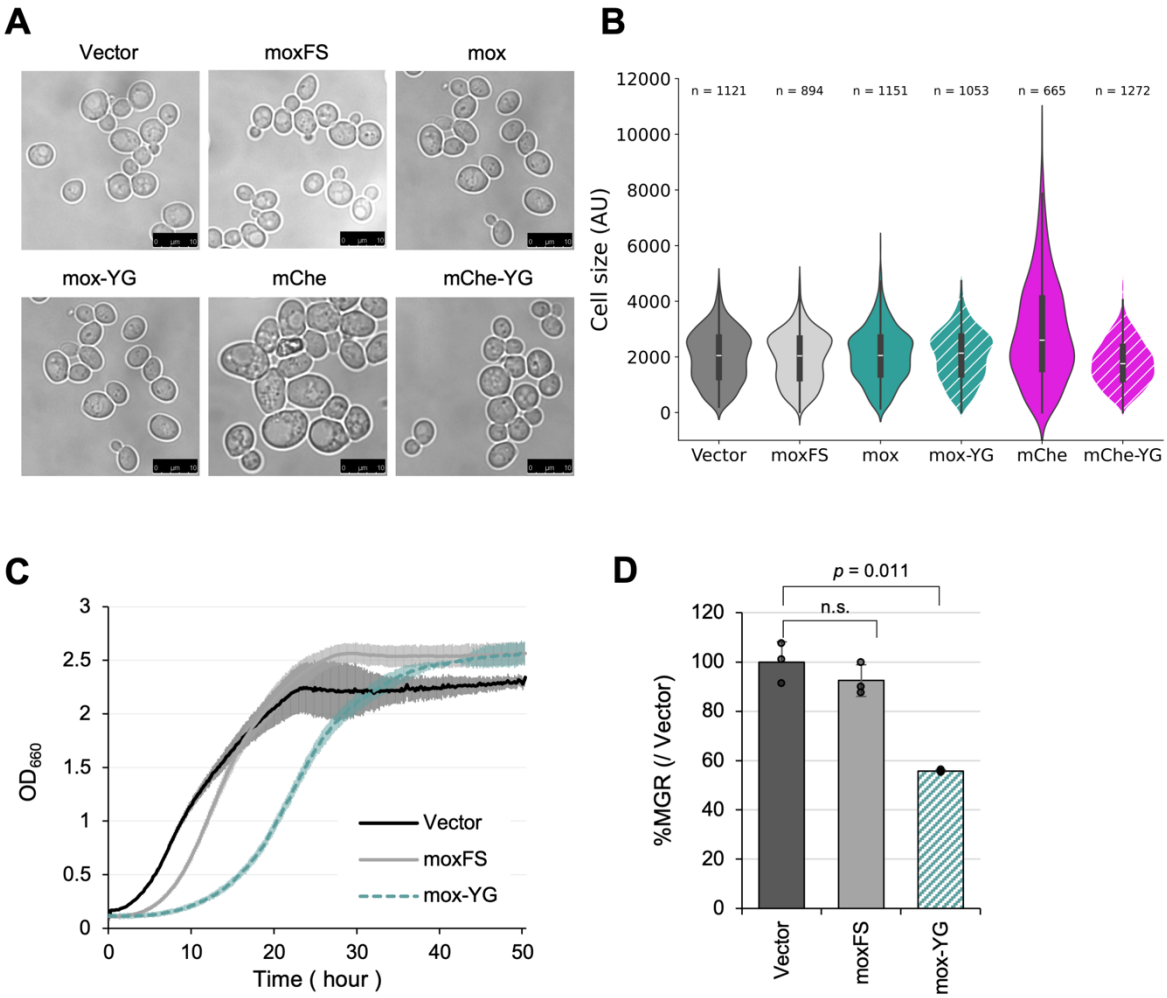

Figure 2—figure supplement 6. Overexpression of mox-YG does not cause cell enlargement or burden on transcription.

A) Representative microscopic images of cells overexpressing indicated target proteins or moxFS (a frameshift mutant of mox).

B) Violin plots showing the cell size quantified from microscopic images. The number of cells used for the quantification is shown.

C) Growth curves of the vector control and cells overexpressing moxFS and mox-YG in synthetic medium (–LeuUra). The solid or dotted lines show the average calculated from three biological replicates.

D) MGR of cells overexpressing moxFS and mox-YG (percent over the vector control). The bars and error bars show the means and SDs of the MGR calculated from three biological replicates. The raw data is shown with dot plots. The *p*-value of Welch's *t*-test is shown. n.s: not significant.

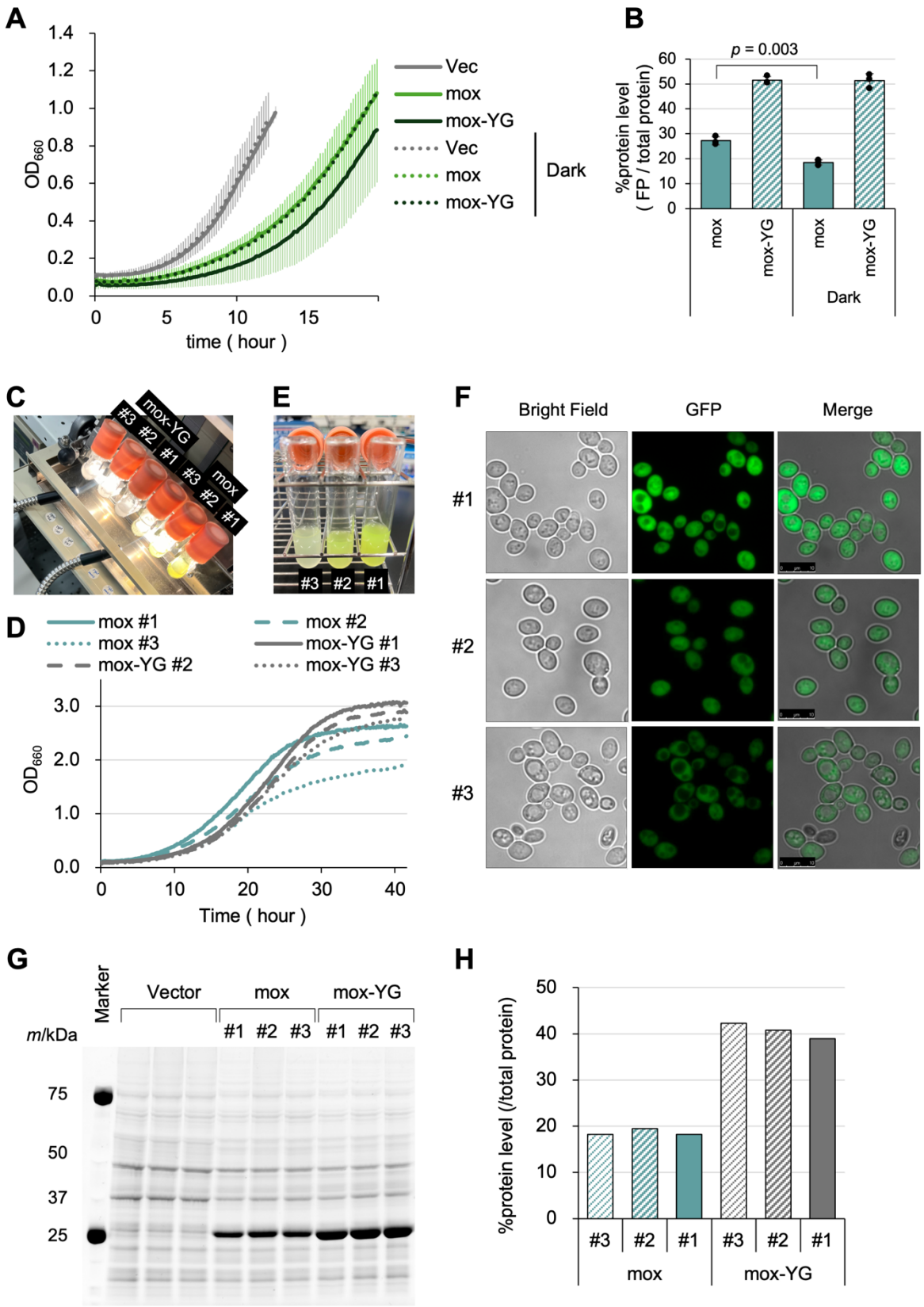

Figure 2—figure supplement 7. Phototoxicity is not the constraint of mox expression.

1150 **A**) Growth curves of the vector control and cells overexpressing mox and mox-YG grown under room
1151 light or in the dark (Dark) in synthetic medium (–LeuUra). The solid or dotted lines show the average
1152 calculated from three biological replicates.
1153 **B**) Protein level of mox and mox-YG (percent over the total protein) under room light or in the dark
1154 (Dark) in synthetic medium (–LeuUra).
1155 **C**) Experimental setup for the cultivation of cells under strong light. Strong light was irradiated using a
1156 halogen lighting source (Megalight 100, HOYA-SCHOTT). Among the three cultures of cells
1157 overexpressing mox and mox-YG, culture #3 was closest to the light, followed by #2 and #1 in
1158 decreasing order. Cells were cultured in SC–LeuUra medium. Note that the light does not affect the
1159 OD_{660} measurement itself in this setup.
1160 **D**) Growth curves of the cells overexpressing mox and mox-YG grown under the strong light. Growth
1161 curves of cells at the positions (#1, #2, and #3) in **C** are shown.
1162 **E**) Color of the culture of cells overexpressing mox cultivated at the positions in **C**. The photo was
1163 taken after 40 hrs cultivation.
1164 **F**) Fluorescence microscopy images of the cells cultivated under strong light. The cells were cultivated
1165 at the position in **C** for 40 hrs.
1166 **G**) Gel images of SDS-PAGE-separated proteins extracted from cells overexpressing mox and mox-
1167 YG cultured under the light. Cells were cultured at the position in **C** to OD_{660} = 1 and analyzed. All
1168 proteins were separated after staining with a fluorescent dye.
1169 **H**) Protein level of mox and mox-YG level in **G** (percent over the total protein).

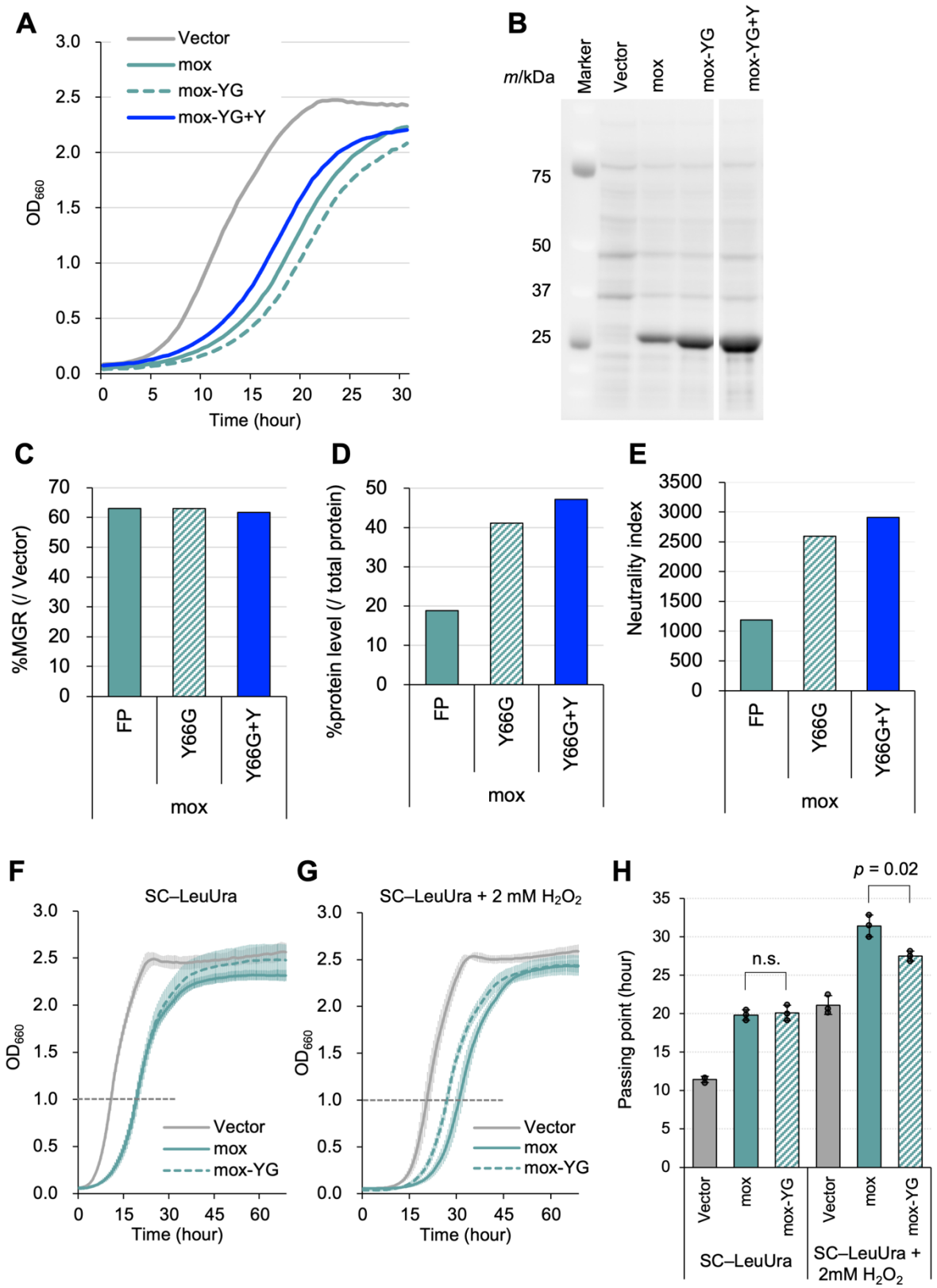

Figure 2—figure supplement 8. Effect of Tyr and oxidative stress for the expression limits of mox and mox-YG.

1173 **A)** Growth curves of cells with the vector (Vector) and overexpressing mox, mox-YG, and mox-YG
1174 with one Tyr added to the C-terminal (mox-YG+Y) (n = 1 for each).
1175 **B)** Gel images of SDS-PAGE-separated proteins extracted from cells overexpressing FPs. All proteins
1176 were separated after staining with a fluorescent dye.
1177 **C-E)** Quantification of MGR (**C**), the protein level (**D**), and the neutrality index (**E**) of cells
1178 overexpressing mox (FP), mox-YG (Y66G), and mox-YG+Y (Y66G+Y). The MGR was calculated
1179 from the growth curve in **A**. The protein level was calculated from the band in **B**. The neutrality index
1180 was calculated as the product of %MGR in **C** and the %protein level in **D**. The results for n = 1 are
1181 shown.
1182 **F, G)** Growth curves of the vector control (Vector) and cells overexpressing mox and mox-YG in
1183 synthetic medium (**F**) and medium with 2 mM H_2O_2 (**G**). Solid or dotted lines indicate mean values
1184 calculated from three biological replicates.
1185 **H)** Passing point when the time for Vector, mox, and mox-YG overexpressing cell cultures to reach
1186 OD_{660} = 1 (the intersection of the dotted line in **F** and **G** with the respective growth curves).

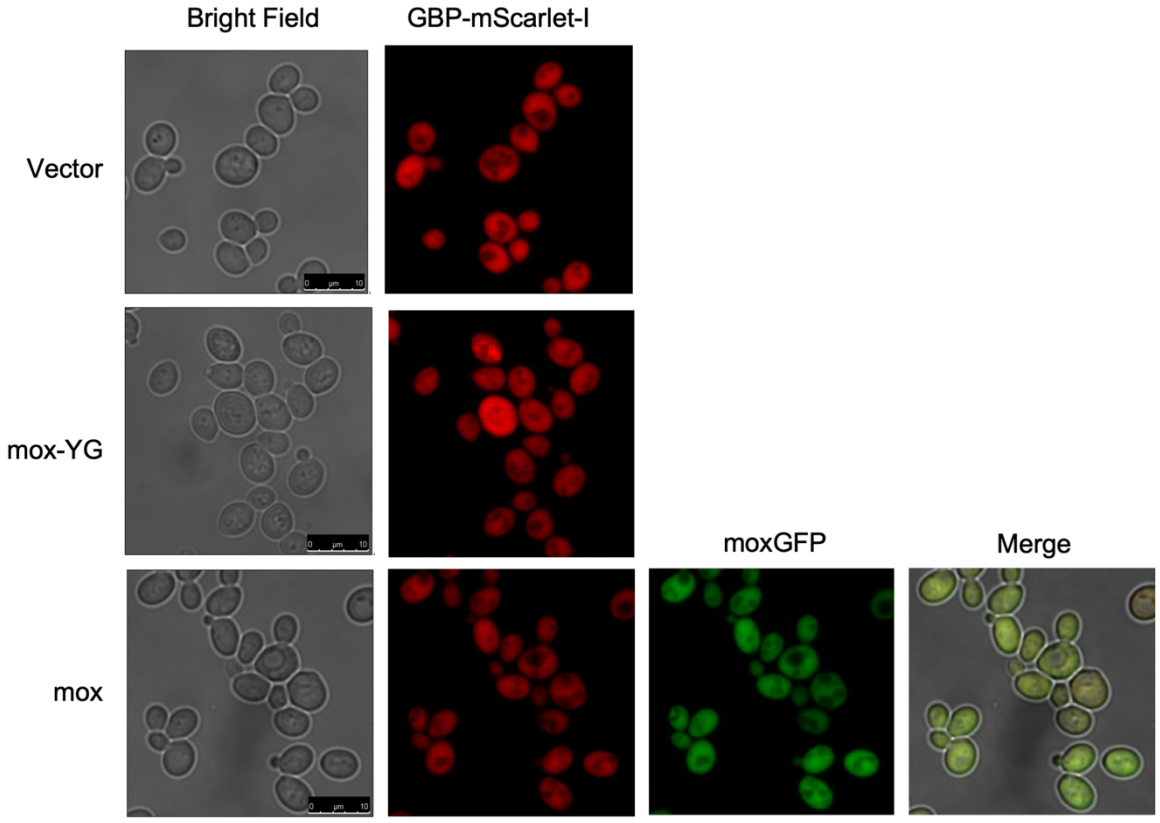

1187

1188 **Figure 2—figure supplement 9. Overexpressed mox-YG does not show any specific localization.**

1189 Fluorescence microscopy images of the cells with the vector (Vector) and overexpressing mox and

1190 mox-YG in a strain expressing a GFP-binding protein (GBP) fused to mScarlet-I under the control of

1191 *ACT1* promoter.

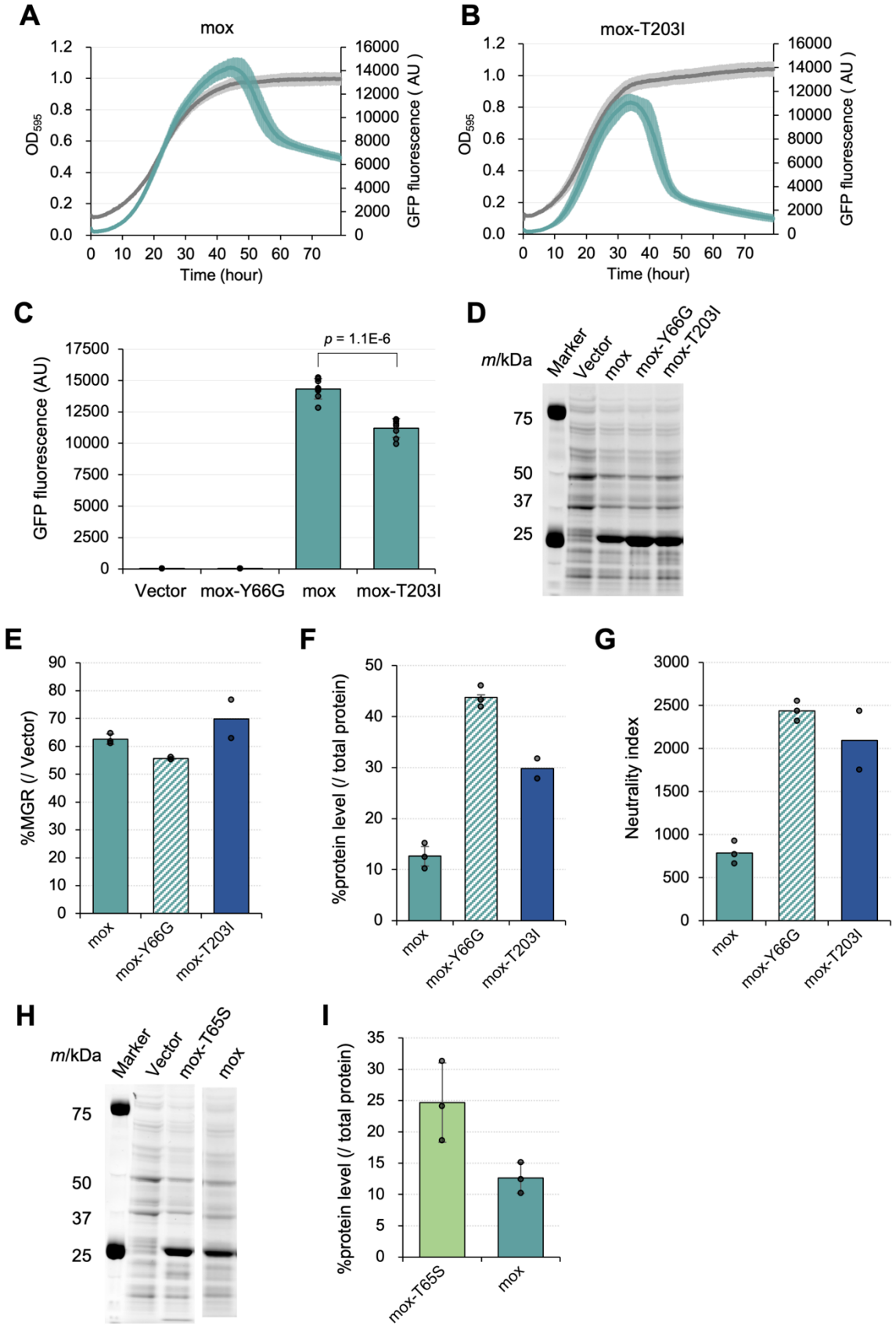

1192

1193 **Figure 2—figure supplement 10. Mutational analysis of mox.**

1194 **A, B)** Curves representing time series data of cell growth (gray, OD_{595}) and GFP fluorescence (green)
1195 overexpressing mox and mox-T203I mutant in the synthetic medium (–LeuUra). Solid lines are means
1196 calculated from eight biological replicates.
1197 **C)** Bar graph comparing the maximum value of GFP fluorescence obtained from the GFP fluorescence
1198 curves shown in **A** and **B**. GFP fluorescence values for the vector control and mox-YG overexpressing
1199 cells were also shown as controls. Average values, SD, and *p*-values of Welch's *t*-test were calculated
1200 from eight biological replicates.
1201 **D)** Gel images of SDS-PAGE-separated proteins extracted from cells overexpressing modified GFP.
1202 All proteins were separated after staining with a fluorescent dye.
1203 **E**) MGR of cells overexpressing modified moxGFP and their mutants (percent over the vector control).
1204 **F)** Protein levels of the mox variants (percent over the total protein). The amount was calculated from
1205 the intensity of the target bands separated by SDS-PAGE of **D**.
1206 **G**) The neutrality index for the modified GFP. The neutrality index was calculated as the product of
1207 the %MGR in **E** and the %protein level in **F**.
1208 **H)** Gel images of SDS-PAGE-separated proteins extracted from cells overexpressing mox-T65S mutant
1209 and mox of WT. All proteins were separated after staining with a fluorescent dye.
1210 **I)** Protein levels of mox-T65S mutant and mox (percent over the total protein). The amount was
1211 calculated from the intensity of the target bands separated by SDS-PAGE of **H**.
1212 The bars and error bars in **E**, **F**, **G**, and **I** show the means and SDs calculated from three biological
1213 replicates, except the T203I mutant (n = 2). The raw data is shown with dot plots.

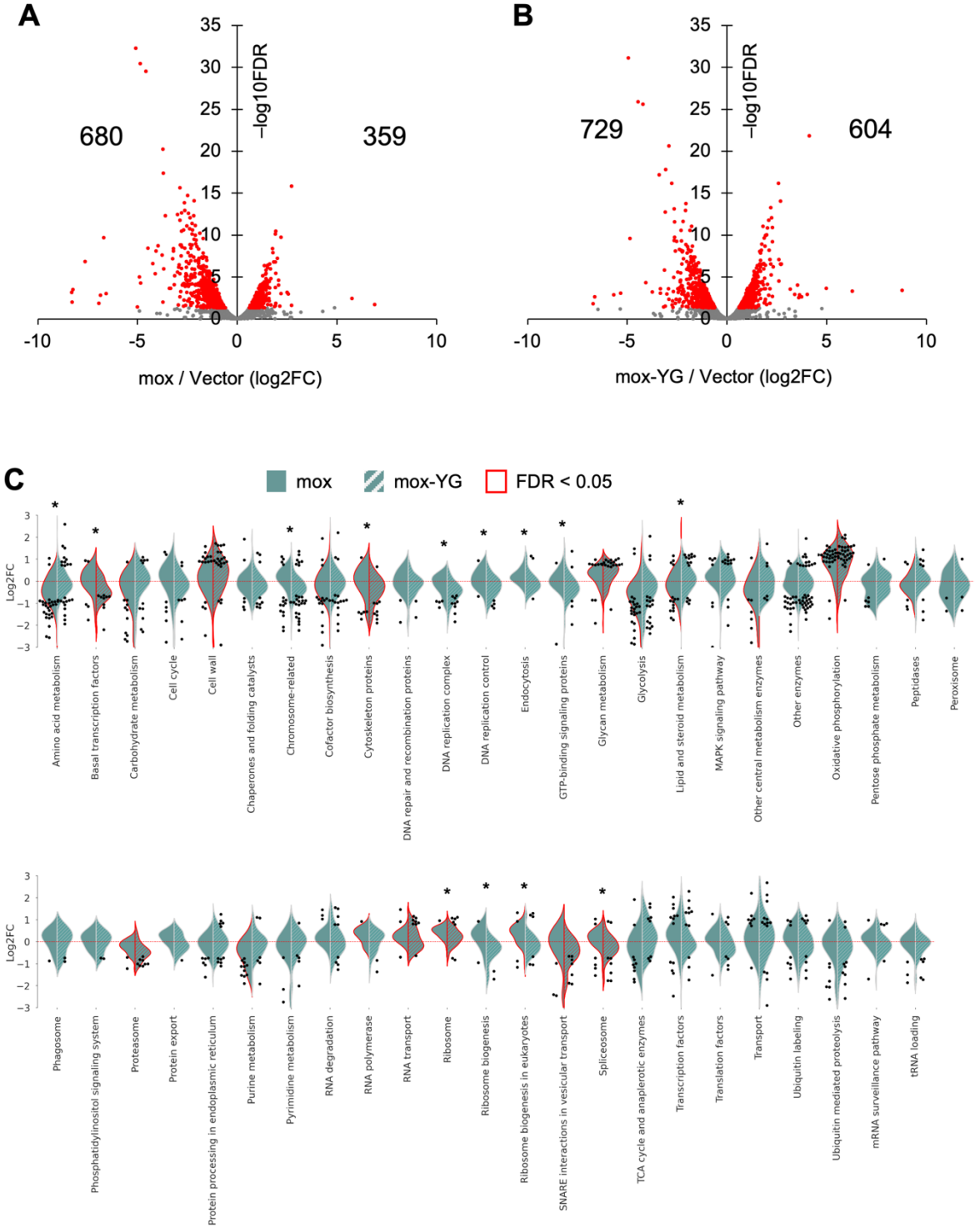

Figure 3—figure supplement 1. Comparison of the transcriptional response of mox and mox-YG overexpressing cells.

1217 **A, B)** Transcriptome changes in mox (**A**) and mox-YG (**B**) overexpressing cells. Significantly altered
1218 ORFs (FDR < 0.05) compared to the vector control are shown in red. The number of ORFs that were
1219 significantly increased and decreased are shown.
1220 **C)** Violin plots showing transcriptome results for each category of KEGG orthology level 3. Categories
1221 that were significantly up or down-regulated (FDR < 0.05) are indicated by red violin plots. Genes that
1222 showed significant expression changes (FDR < 0.05) within the same category are indicated by swarm
1223 plots. Asterisks indicate significant differences (FDR < 0.05) between mox and mox-YG comparisons
1224 for groups of genes in the same category.

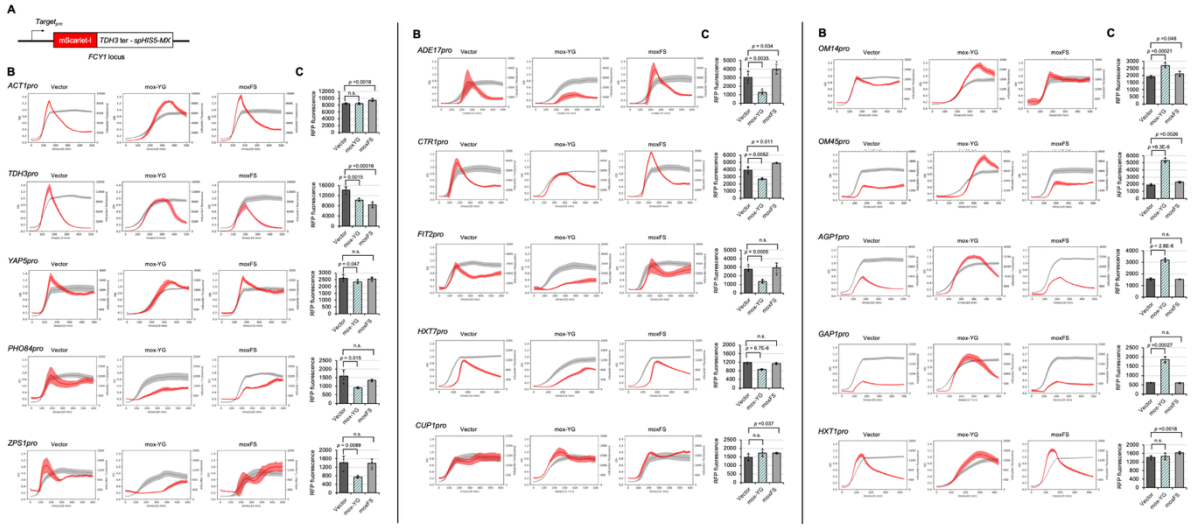

1225

1226 **Figure 3—figure supplement 2. Verification of promoter activity by the reporter assay.**
1227 **A)** The constructs used for promoter analysis by the transcriptional reporter included a sequence of RFP
1228 (mScarlet-I) behind each promoter, a terminator for *TDH3*, and a sequence incorporating *spHIS5MX* as
1229 a selection marker, which was integrated into the genomic *FCY1* locus. "moxFS" means the frameshift
1230 mutant of mox-YG is overexpressed.
1231 **B)** Curves representing time series data of cell growth (gray, OD_{595}) and mScarlet-I fluorescence (red,
1232 arbitrary unit) overexpressing mox-YG and moxFS in SC–LeuUra medium for each promoter. Solid
1233 lines are averages calculated from four biological replicates.
1234 **C)** Quantitative results of mScarlet-I fluorescence values for each promoter. Bars and error bars indicate
1235 the mean and SD of maximum fluorescence values (arbitrary unit) for mScarlet-I calculated from four

1236 biological replicates. Raw data are shown as dot plots. The *p*-values were calculated by performing

1237 Welch's *t*-test and applying the Bonferroni correction. “n.s.” means $p > 0.05$.

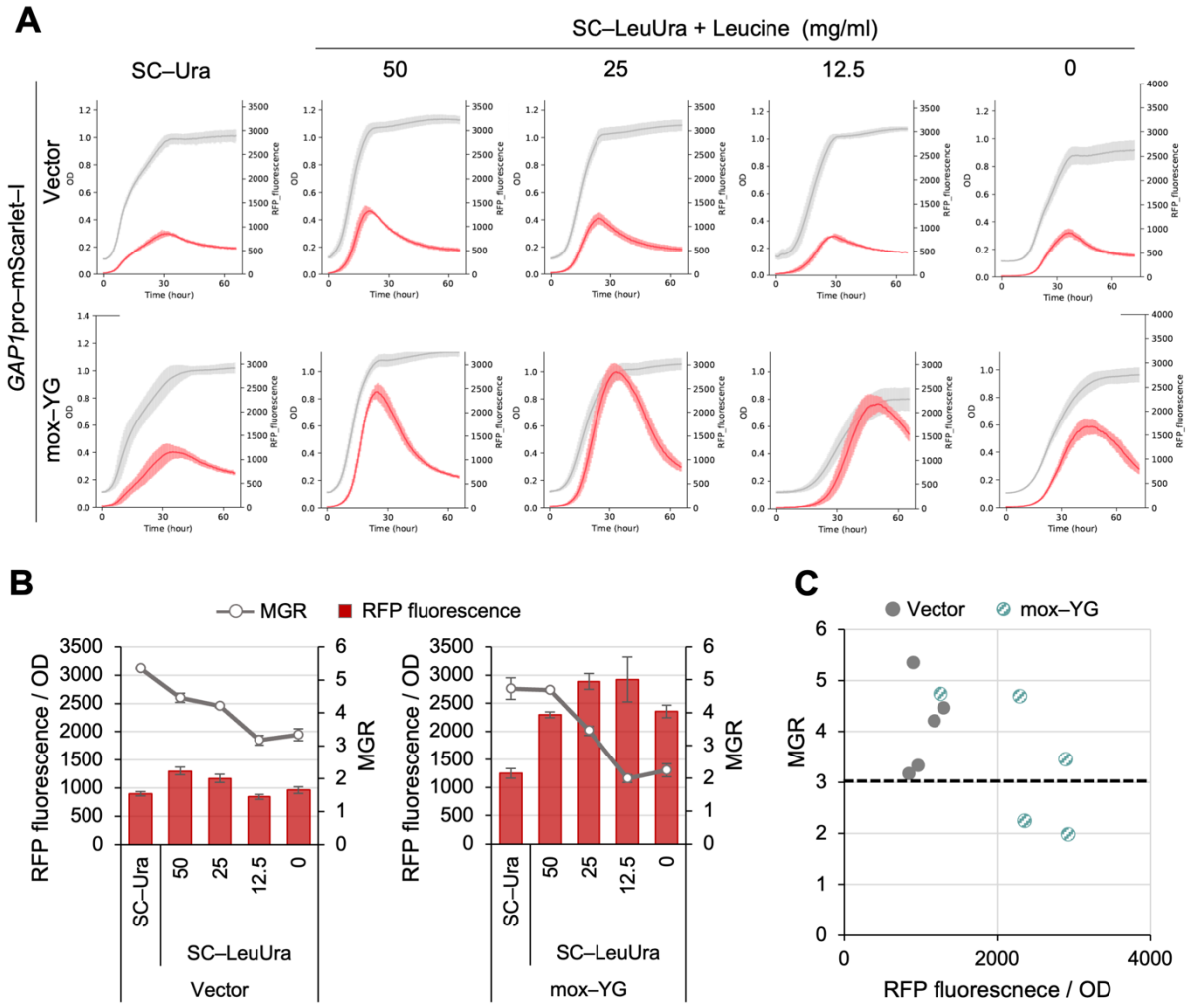

1238

1239 **Figure 3—figure supplement 3. Depletion of leucine in the gTOW experiment does not induce the**

1240 ***GAP1* promoter.**

1241 **A**) Reporter assay of the *GAP1* promoter in media with different concentrations of leucine. Curves

1242 representing time series data of cell growth (gray, OD595) and mScarlet–I fluorescence (red, arbitrary

1243 unit) overexpressing mox–YG. Solid lines are averages calculated from four biological replicates.

1244 **B**) Quantification of the maximum growth rate (MGR) and maximum RFP fluorescence derived from

1245 the results in A. Bar graphs indicate the mean maximum RFP fluorescence, and error bars represent the

1246 SD. Line graphs indicate the MGR, with error bars representing SD. Means and SDs were calculated

1247 from four biological replicates.

1248 **C**) Scatter plots of maximum fluorescence values and MGRs created using the values in **B**. Note that
1249 *GAP1* induction was observed only in mox-YG overexpression, even under conditions where the MGR
1250 was reduced to around three due to leucine depletion (the dotted line).

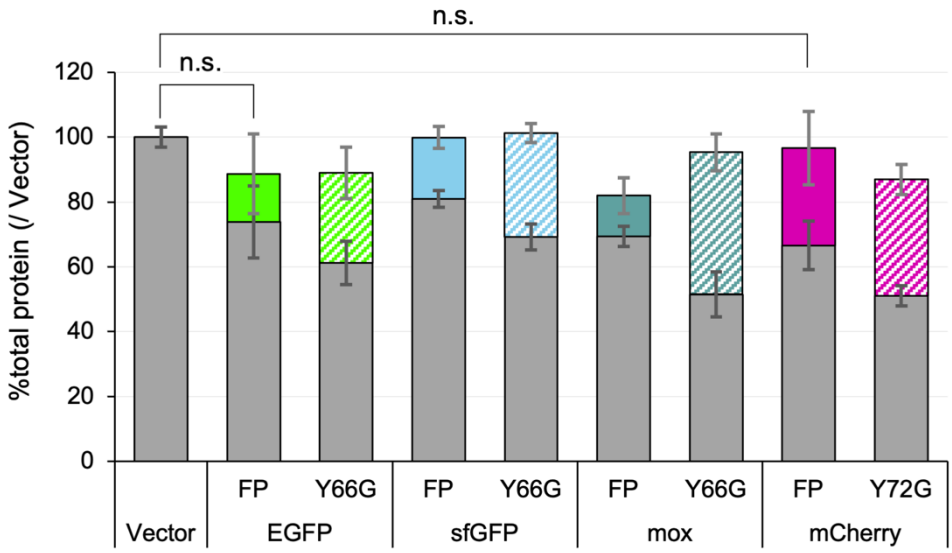

1251

1252 **Figure 4—figure supplement 1. Change in total protein levels upon overexpression of target**
1253 **proteins.**

1254 Ratio of total protein content of cells overexpressing FPs over the vector control. Gray bars and error
1255 bars indicate expression levels and SDs for proteins other than FPs; non-gray bars and error bars indicate
1256 expression levels and SDs for each overexpressed protein. The mean and SD are calculated from three
1257 biological replicates. The *p*-values were calculated by performing Welch's *t*-test and applying
1258 Bonferroni correction. “n.s.” means $p > 0.05$.

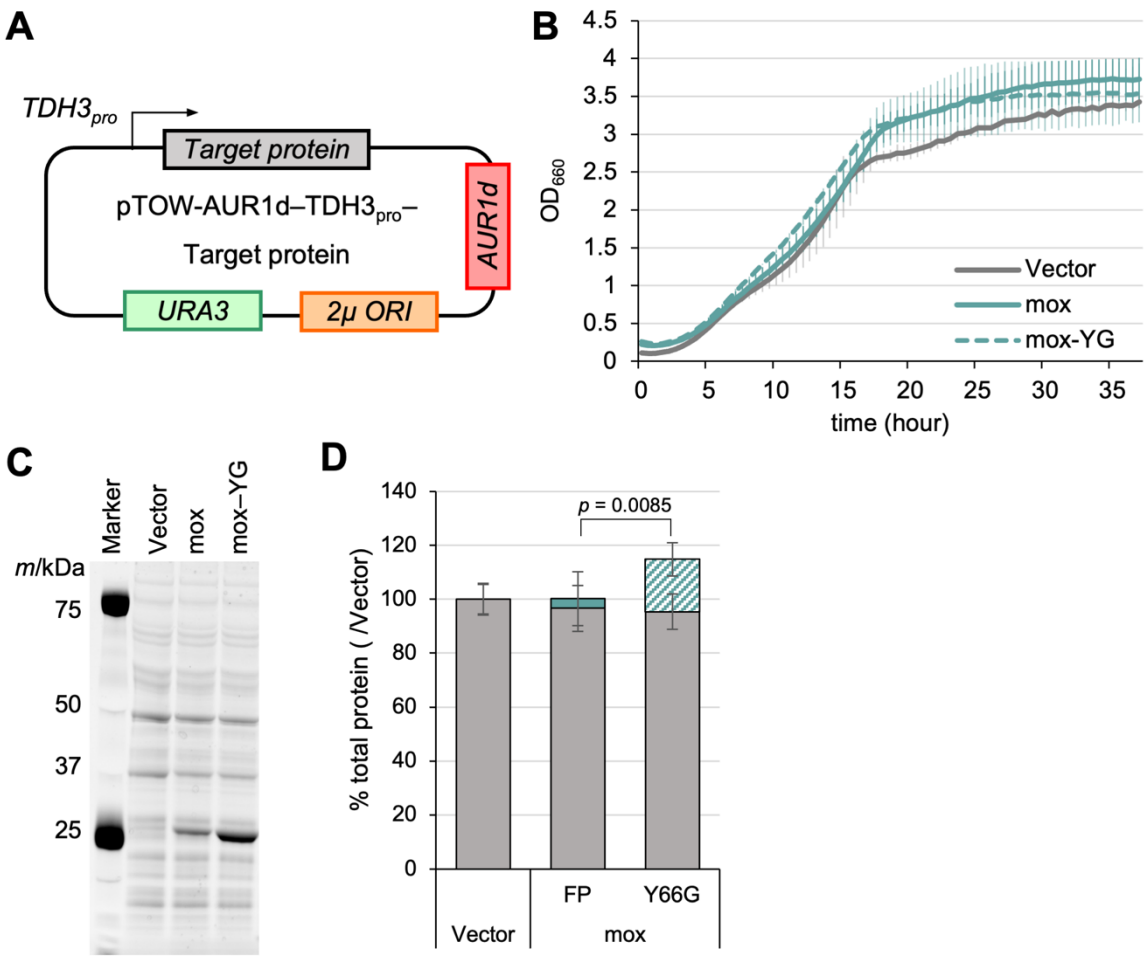

1259

1260 **Figure 4—figure supplement 2. Evaluation of expression constraint of fluorescent proteins under**

1261 **nutrient–rich medium.**

1262 **A**) Experimental setup of the analysis. Target proteins were expressed under the control of the *TDH3*

1263 promoter (*TDH3pro*) using the multicopy plasmid pTOW-AUR1d. This plasmid uses the aureobasidin

1264 resistance gene *AUR1d*, which has a short promoter region, replacing the *leu2–89* used in the plasmid

1265 shown in Figure 2A.

1266 **B**) Growth curves of the vector control and cells overexpressing FPs in YPD included 500 ng/mL

1267 aureobasidin A. The solid or dotted lines show the average calculated from three biological replicates.

1268 Shaded zones indicate their standard deviations.

1269 **C**) Gel images of SDS–PAGE–separated proteins extracted from cells overexpressing FPs. All proteins

1270 were separated after staining with a fluorescent dye.

1271 **D**) Ratio of total protein content of cells overexpressing FPs over the vector control in YPD added
1272 aureobasidin A and SC–LeuUra. Gray bars and error bars indicate expression levels and SDs for
1273 proteins other than; non–gray bars and error bars indicate expression levels and SDs for each
1274 overexpressed protein. The mean and SD are calculated from three biological replicates. The *p*-values
1275 were calculated by performing Welch's *t*-test.

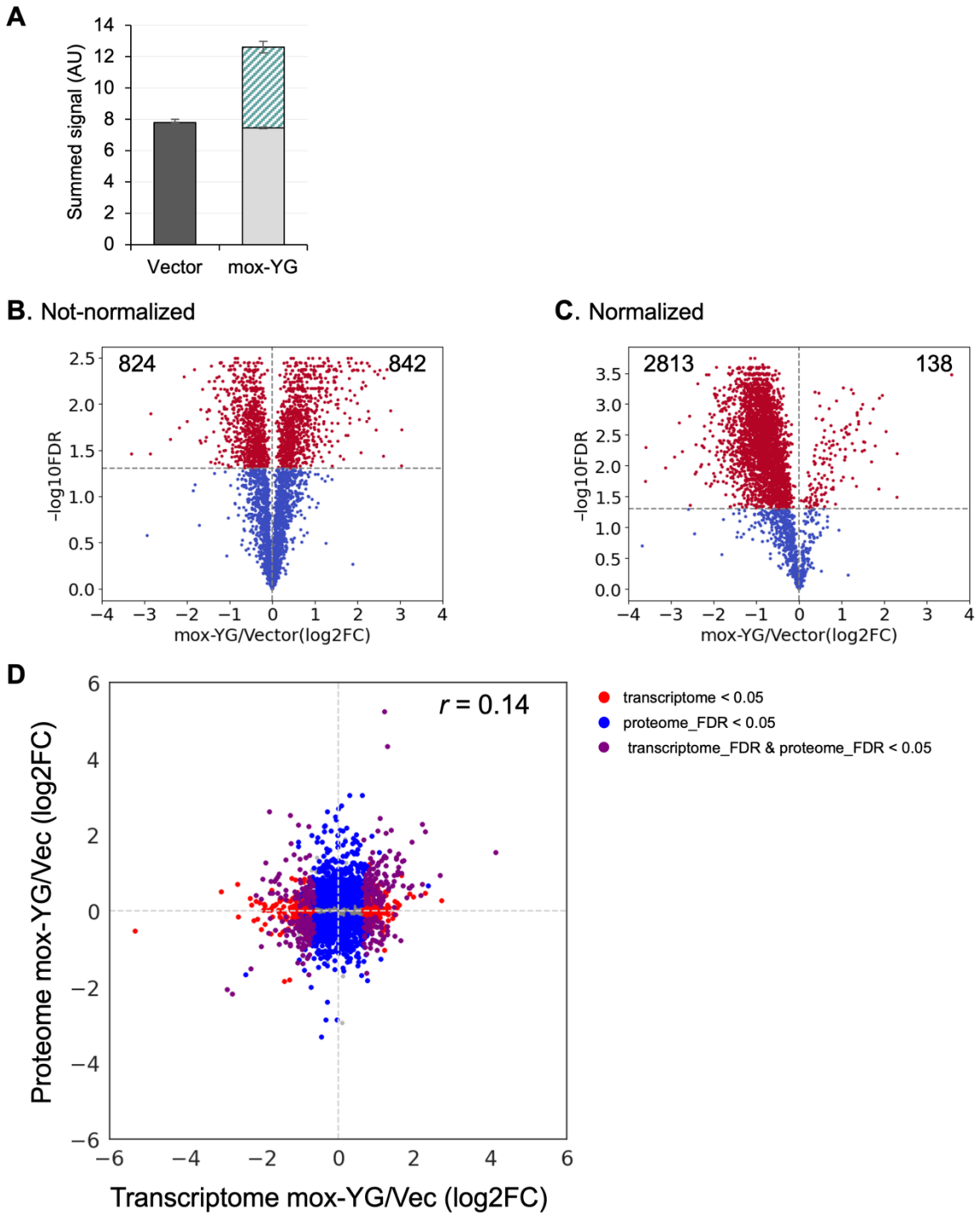

1276

1277 **Figure 4—figure supplement 3. Comparison of normalized or not-normalized proteome results.**

1278 **A)** Bar graph showing the sum of signals for each gene detected by proteome analysis. Black or light
1279 gray bars indicate the sum of signals other than mox-YG, and green-shaded bars indicate mox-YG
1280 signals. The error bar indicates the SD calculated from three biological replicates.

1281 **B)** Volcano plot of proteome results excluding proteins not detected in either condition.

1282 **C)** Volcano plot of **B**'s results normalized so that the sum of mox-YG signals equals the sum of the
1283 vector control signals. Significantly changed proteins (FDR < 0.05) are shown in red. The number of
1284 genes whose expression decreased or increased during mox-YG overexpression compared to the vector
1285 control is indicated in the upper left or upper right of the graph.

1286 **D**) Comparison of proteome and transcriptome changes in cells overexpressing mox-YG.
1287 The transcriptome data used are the same as those in Figure 3—figure supplement 1B, and the proteome
1288 data are the same as those in Figure 4—figure supplement 3B. The Pearson correlation coefficient (*r*)
1289 is shown.

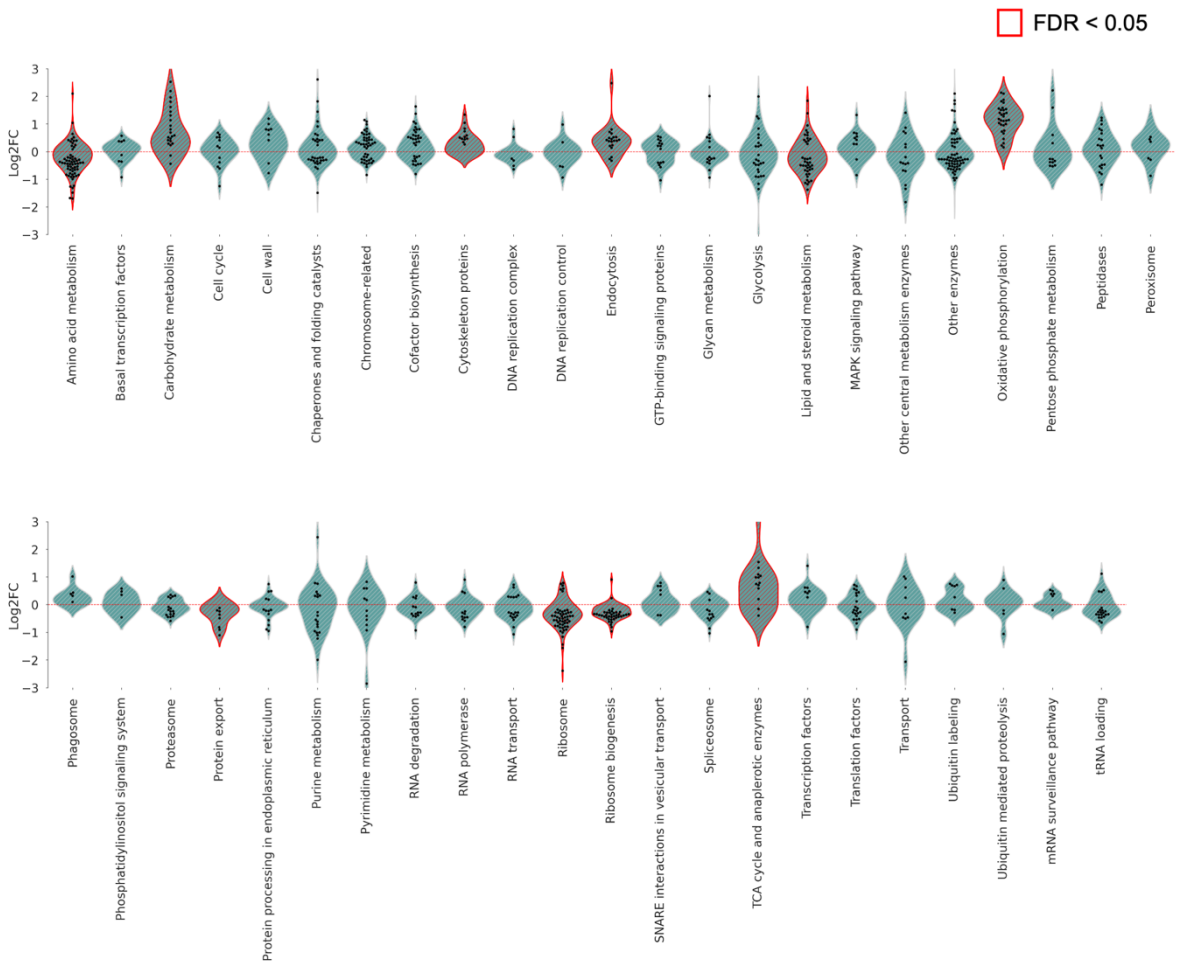

Figure 4—figure supplement 4. Violin plots showing groups of proteins whose expression was changed by mox-YG overexpression.

Protein groups with significantly altered expression (FDR < 0.05) upon mox-YG overexpression over the vector control are shown in red violin plots. Proteins with significant expression changes (FDR < 0.05) within the same category are shown by swarm plots.

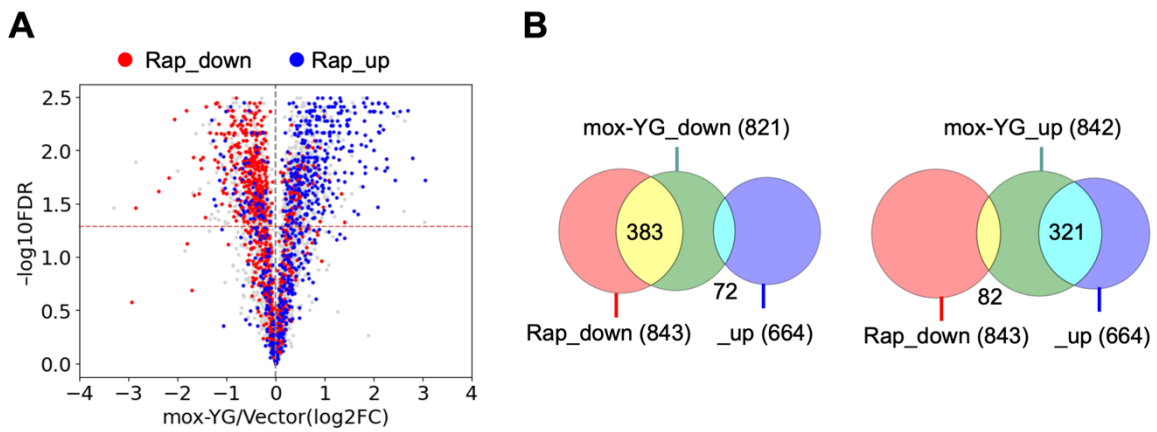

1297 **Figure 4—figure supplement 5. Cells overexpressing mox-YG exhibit proteomic changes that**
1298 **overlap with those observed in rapamycin-treated cells.**

1299 **A**) Volcano plots showing genes whose expression levels were altered by rapamycin treatment in the
1300 proteome results of mox-YG overexpressing cells.

1301 **B**) Venn diagram representing the overlap of the proteome during mox-YG overexpression and
1302 rapamycin treatment. The number of genes in each area is shown.

1303 Published data (Gowans et al., 2018) was used for comparison with the rapamycin response genes.

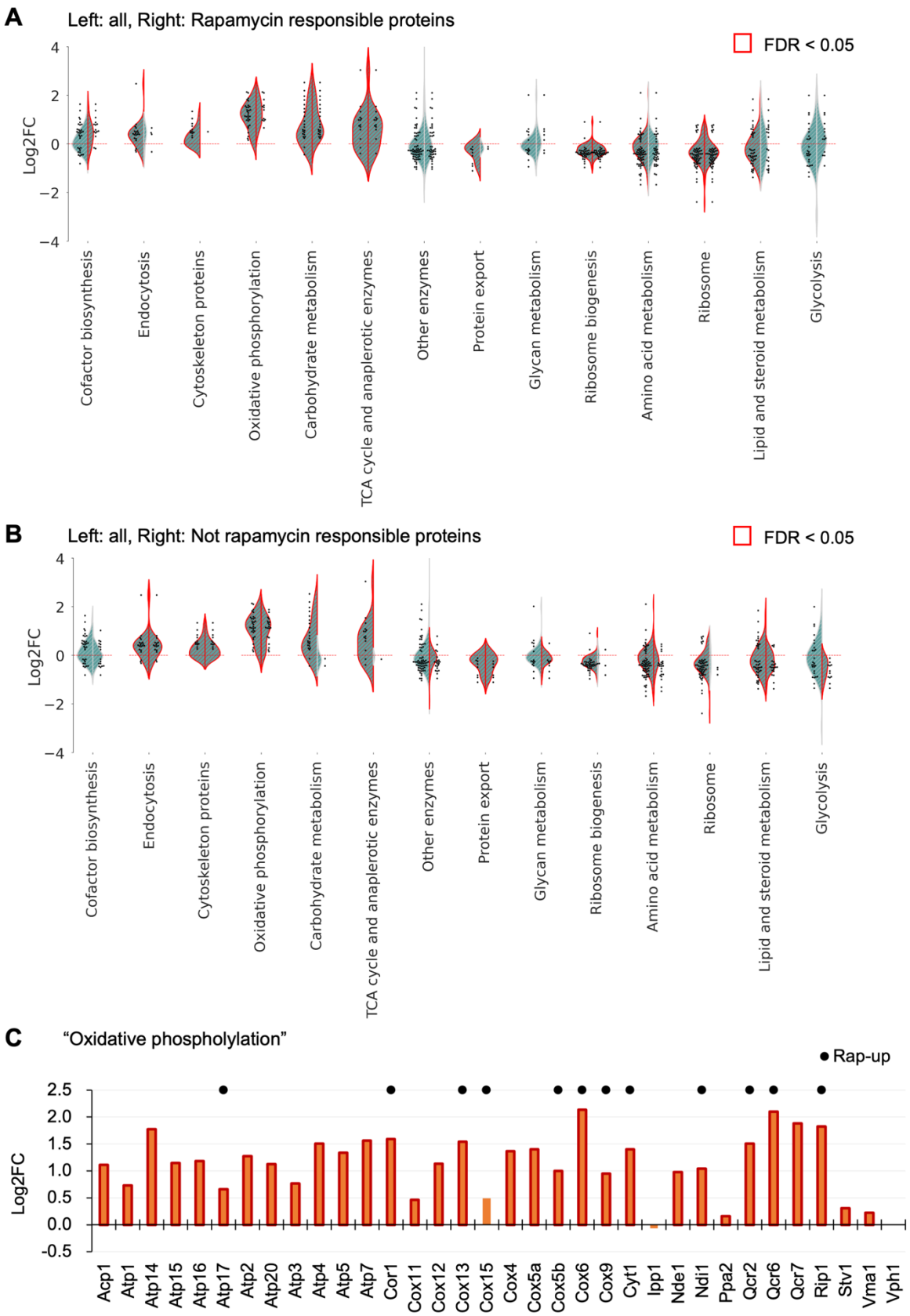

1304

1305 **Figure 4—figure supplement 6. Comparison of groups of proteins whose expression levels are**

1306 **changed by mox-YG overexpression and rapamycin treatment.**

1307 **A, B)** Violin plots showing protein expression changes upon mox-YG overexpression for each KEGG
1308 ontology level 3 category. Plots with red borders represent categories that changed significantly (FDR
1309 < 0.05). Proteins with significantly (FDR < 0.05) altered expression within a category are shown in the
1310 swarm plot. The left side of the violin plot shows the analysis with all the data. The right side of the
1311 plot shows the analysis with only rapamycin-responsive protein (**A**) and rapamycin-non-responsive
1312 protein (**B**).
1313 **C)** Bar graph showing the results for proteins in the "Oxidative phosphorylation" category. Proteins
1314 whose expression is also increased during rapamycin treatment (Rap-up) are marked.

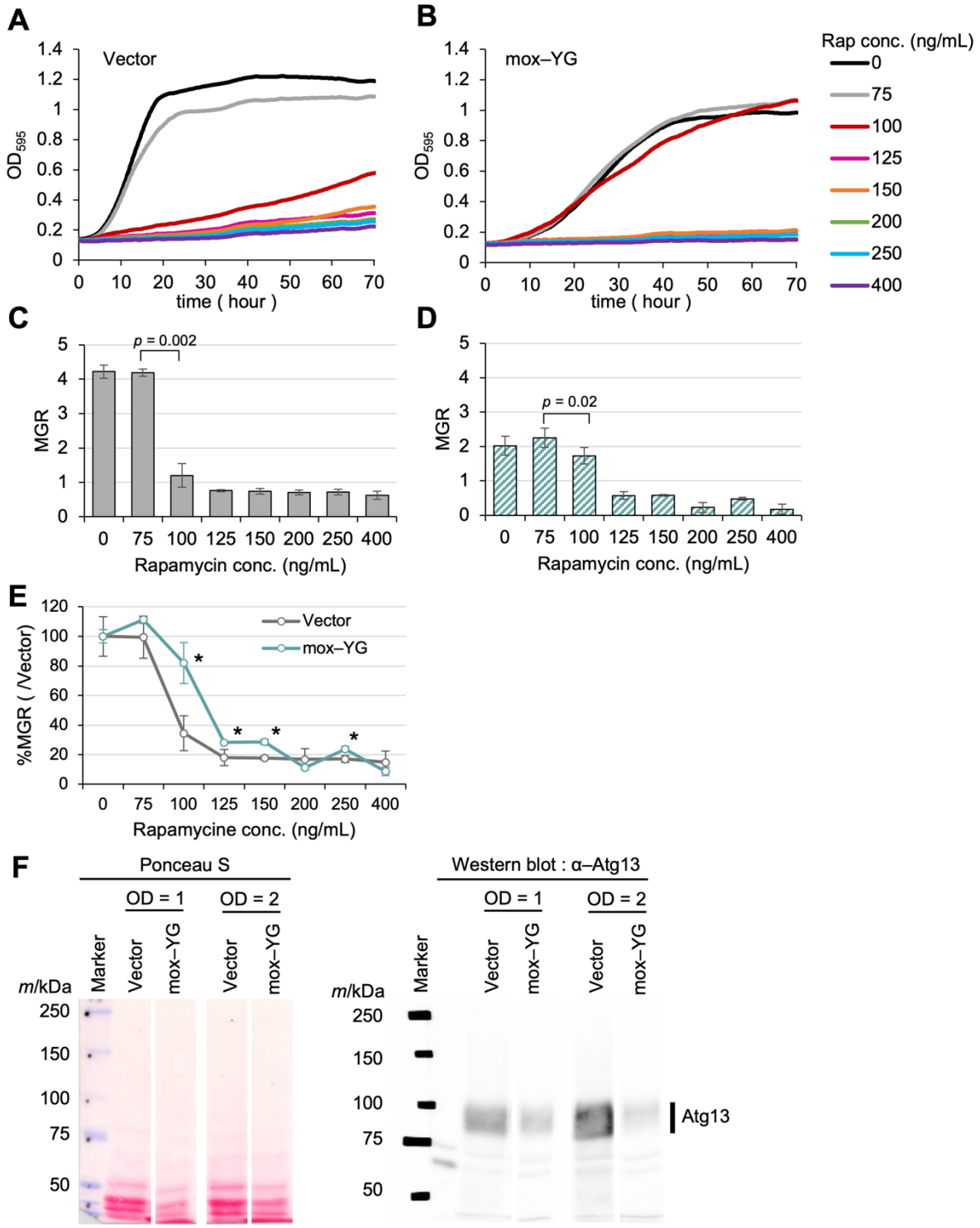

Figure 4—figure supplement 7. Assessment of TORC1 pathway activity in mox-YG overexpressing cells

A, **B**) Growth curves of the vector control (**A**) or mox–YG overexpressing (**B**) cells under different rapamycin concentrations. The solid lines show the average calculated from four biological replicates.

1320 **C**, **D**) Max growth rate of the vector control (**C**) or mox–YG overexpressing (**D**) cells under different
1321 rapamycin concentrations. The bars and error bars show the means and SDs of the MGR calculated
1322 from four biological replicates. The *p*–values were calculated by performing Welch's *t*–test.
1323 **E**) Line graph showing the change in MGR with increasing rapamycin concentration, using 0 ng/mL of
1324 rapamycin concentration as reference. Rapamycin concentrations with significant differences ($p < 0.05$)
1325 between the vector control and mox–YG are marked with * above the mox–YG marker. The *p*–values
1326 were calculated by performing Welch's *t*–test. In the vector control, the addition of 100 ng/mL
1327 rapamycin caused significant growth inhibition, whereas in mox-YG overexpressing cells, the
1328 inhibitory effect was limited. This highlights a decreased sensitivity to rapamycin in mox-YG
1329 overexpressing cells.
1330 **F**) Detection of Atg13 phosphorylation in the vector control and mox-YG overexpressing cells cultured
1331 in SC–LeuUra medium to the indicated optical density (OD_{660}). Total protein was visualized by ponceau
1332 S staining (left), and Atg13 was detected by Western blotting using an anti-Atg13 antibody (right).
1333 Atg13 phosphorylated by TORC1 appears as a broad band (indicated by a line).

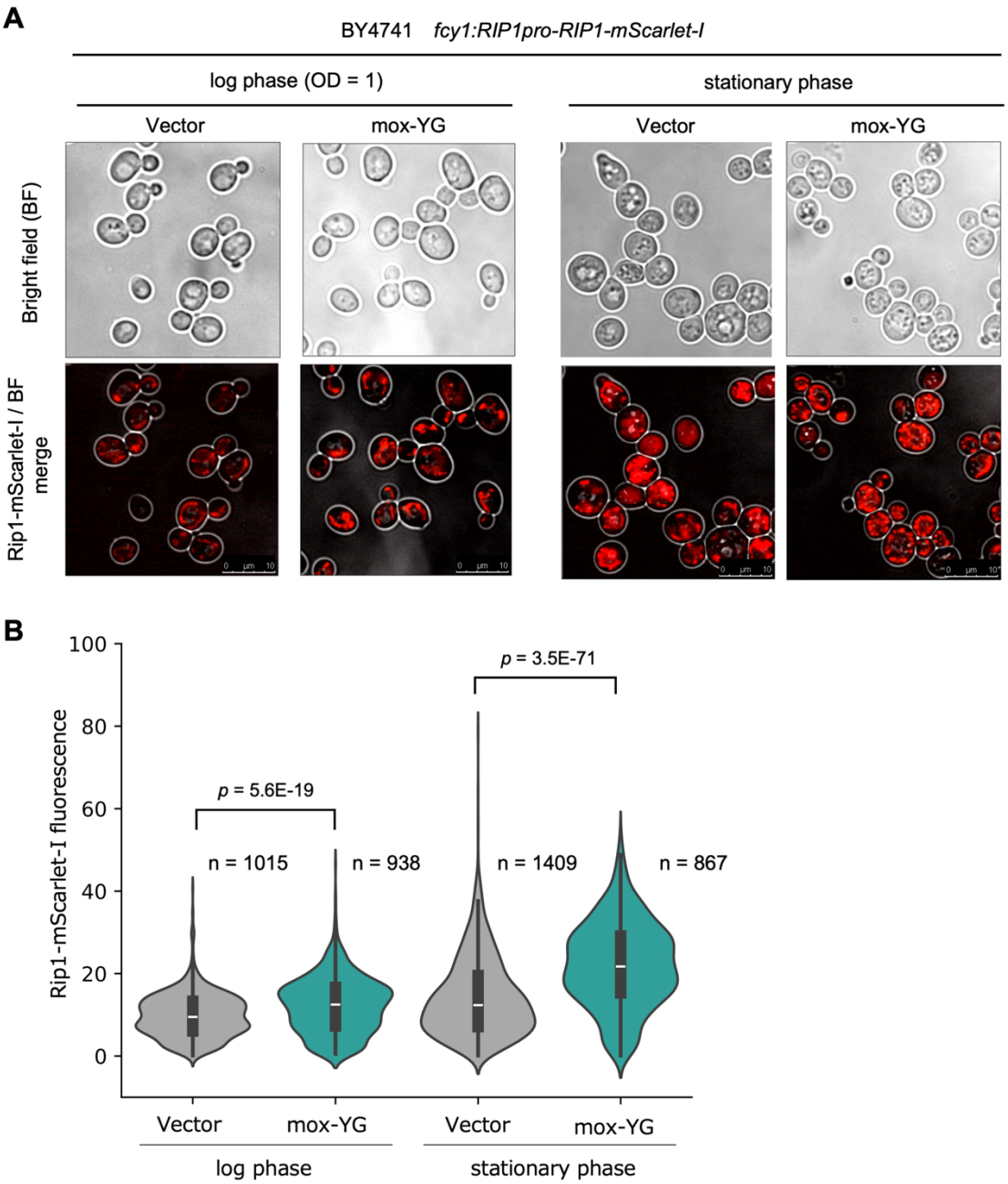

1334

1335 **Figure 4—figure supplement 8. Observation of mitochondria in mox-YG overexpressing cells**

1336 **A)** Fluorescence microscopy image showing the localization of Rip1-mScarlet-I. The vector control and

1337 mox-YG overexpressing cells were observed in the log phase and stationary phase. The upper panel is

1338 a bright-field (BF) image, and the lower panel is a merged image of the BF and fluorescence images.

1339 **B)** Violin plots showing the quantified fluorescence values of Rip1-mScarlet-I from fluorescence

1340 microscopy images taken in the log phase and stationary phase. The number (n) of observed cells is

1341 shown. The *p*-values were calculated by Welch's *t*-test.

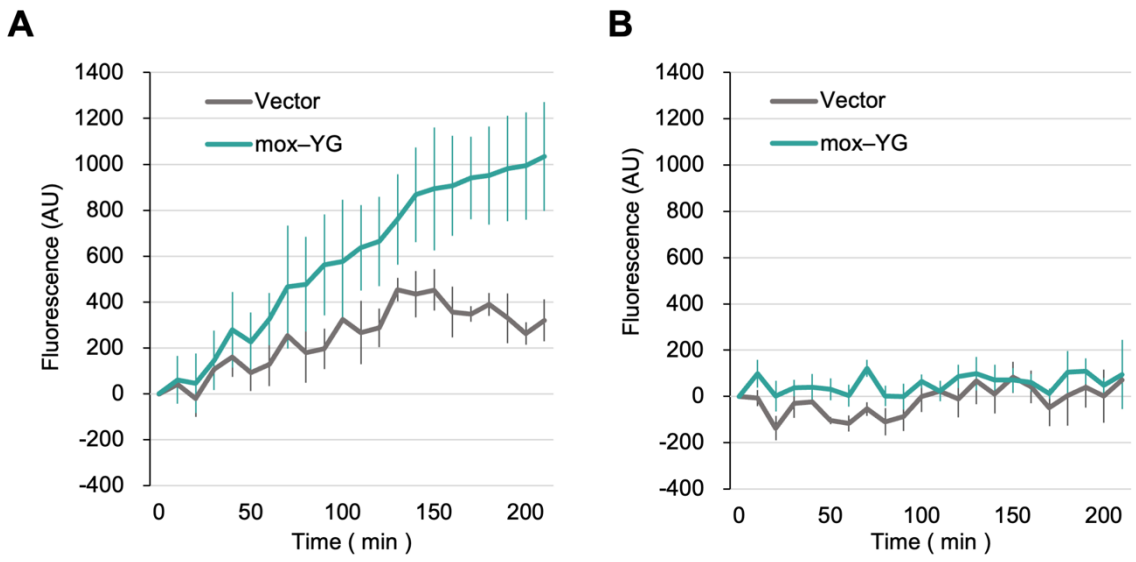

1342

1343 **Figure 4—figure supplement 9. Time-course analysis of oxygen consumption in mox-YG**

1344 **overexpressing cells.**

1345 **A**, **B**) Line graphs showing changes in the fluorescence of an oxygen-sensitive probe, measured in

1346 synthetic medium (**A**) and in medium containing 50 µM antimycin A (**B**). Solid lines represent the mean

1347 values from three biological replicates; Error bars indicate standard deviations.

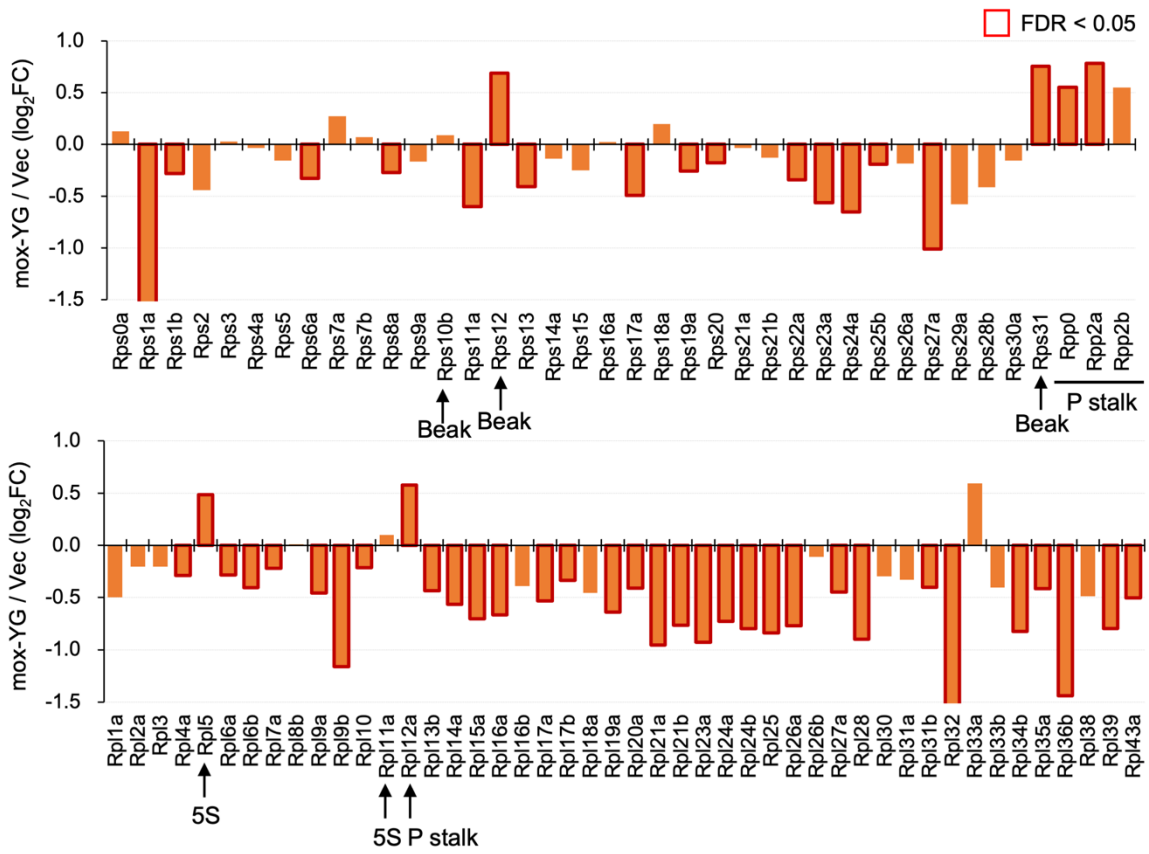

1348

1349 **Figure 5—figure supplement 1. Expression changes of ribosomal proteins upon mox-YG**
1350 **overexpression.**
1351 Bar graphs show the changes in the expression of ribosomal proteins in the proteome analysis of **Figure**
1352 **4**. Significantly changed proteins are boxed in red. Structure names containing increased proteins are
1353 shown. Note that when the amino acid sequences of paralogs are identical, they cannot be distinguished
1354 by proteomic analysis, and the protein abundance of both members of the paralog pair is represented
1355 under the name of only one.

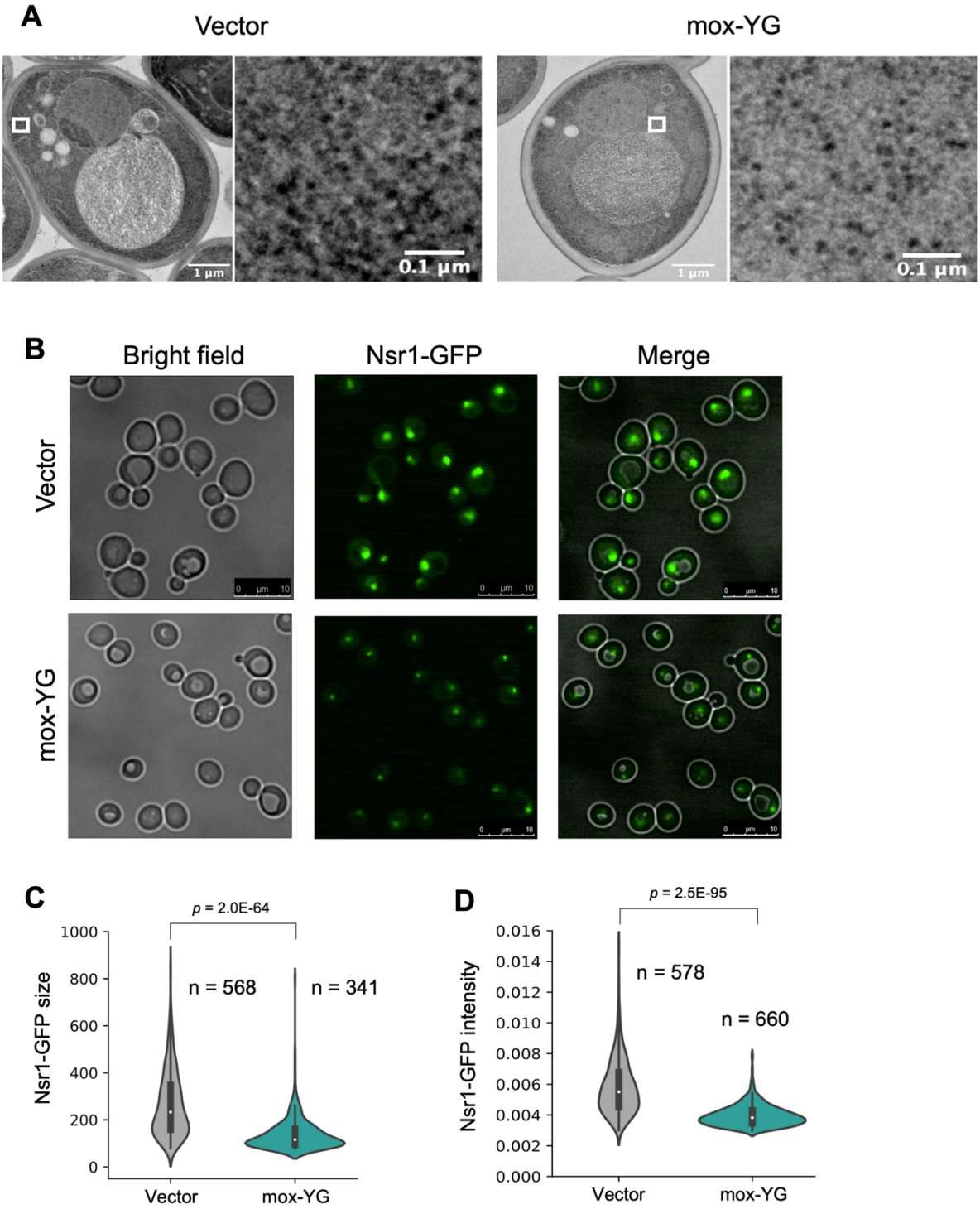

Figure 5—figure supplement 2. Microscopic analysis of the cells under mox-YG overexpression. **A**) Electron microscopic images of the cells with the vector or under mox-YG overexpression. The white rectangular area in each left image is magnified to show the cytoplasmic density (shown in each right image).

1361 **B**) Fluorescence microscopy image showing the size of nucleolus with Nsr1-EGFP. Log phase cells

1362 (OD_{660} = 1.0) with the vector or under mox-YG overexpression were observed.

1363 **C, D)** Quantification of the size of Nsr1-GFP fluorescent region (**C**) and fluorescence value of Nsr1-

1364 GFP (**D**) in the cells with the vector or mox-YG overexpression. The number (n) of observed cells is

1365 shown. The *p*-values were calculated by Welch's *t*-test.

1366

1367

A Vector

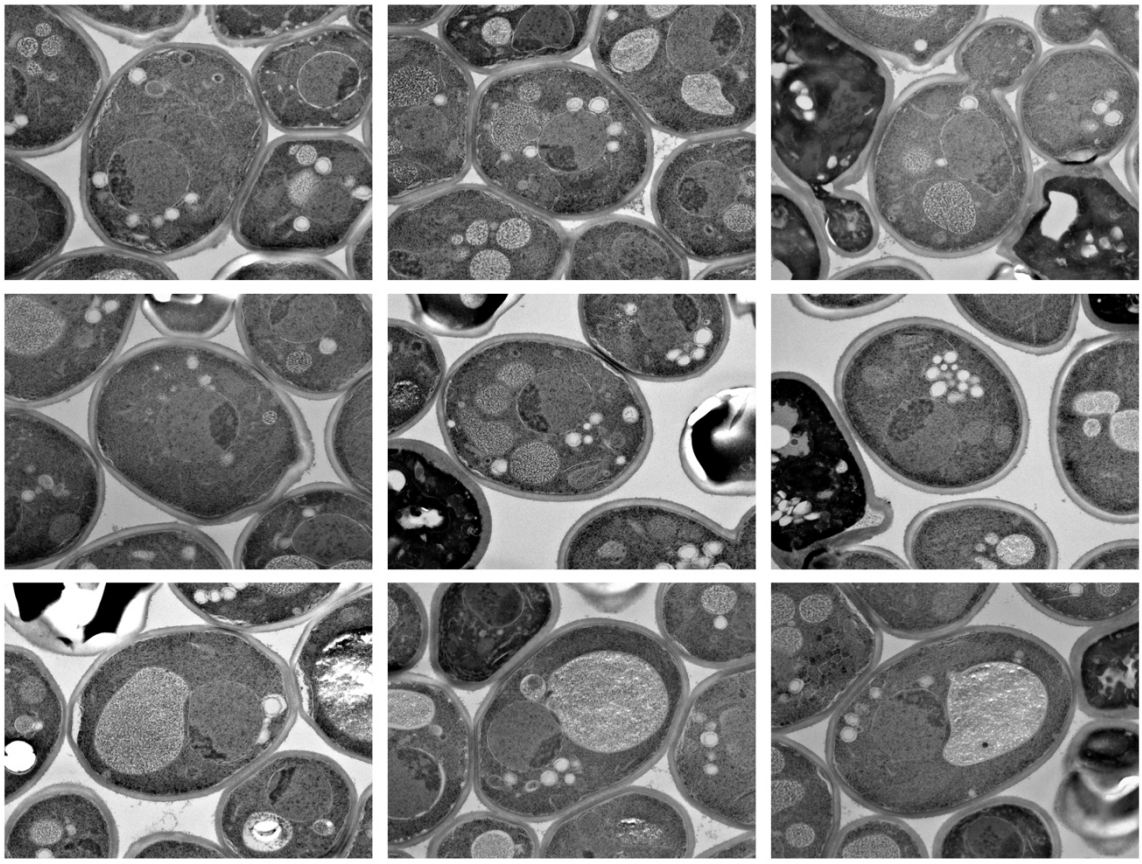

B mox-YG

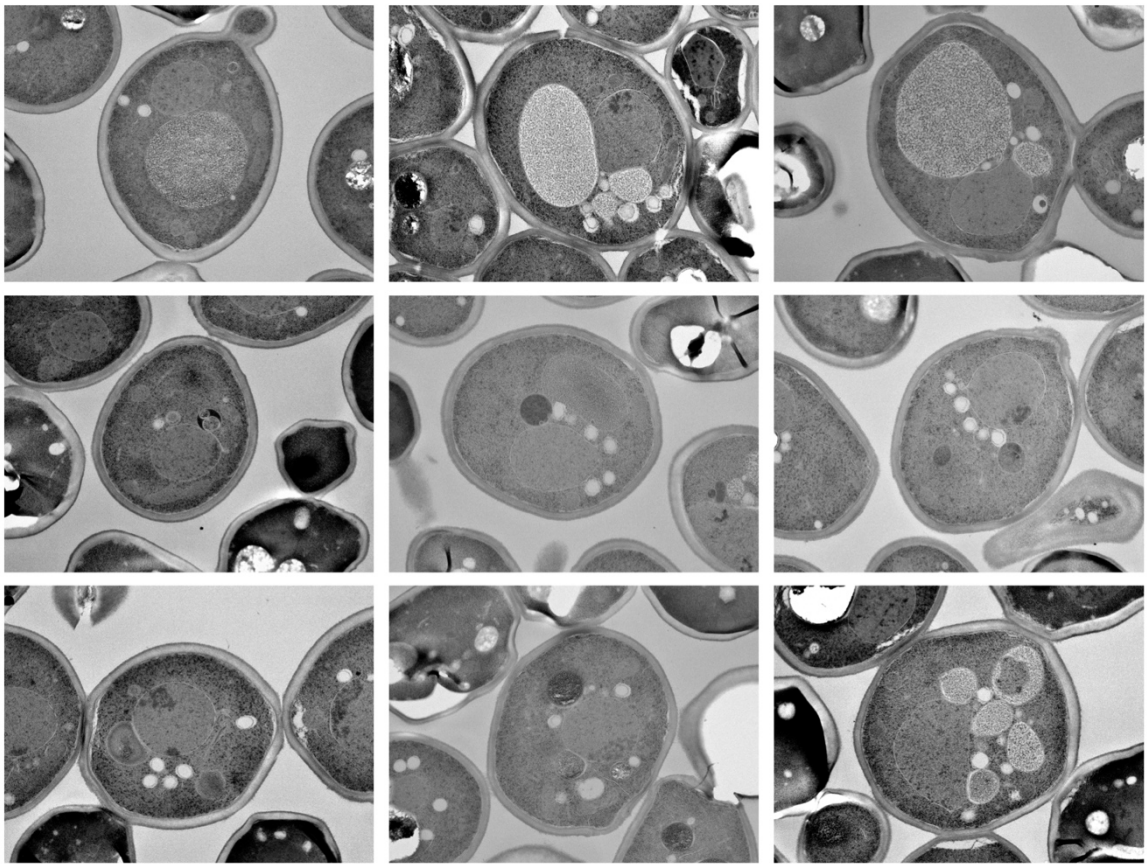

1368

1369 **Figure 5—figure supplement 3. Electron microscopic images of the cells with the vector (A) or**

1370 **under mox-YG overexpression (B).**

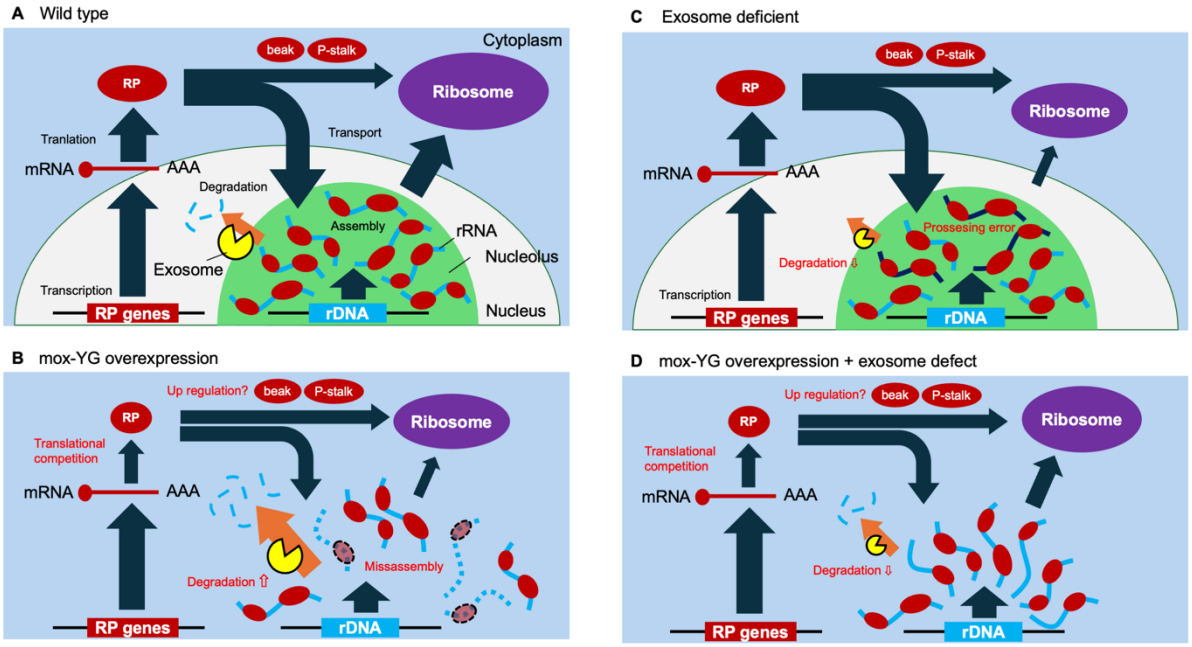

1371

1372 **Figure 5—figure supplement 4. Model diagrams showing the hypothetical situation of the cells.**

1373 **A**) In the wild type cells, enough ribosomal proteins (RPs) are produced, resulting in RP-assembled

1374 rRNAs and the formation of nucleolus with normal morphology.

1375 **B**) In mox-YG overexpressing cells, the amount of RP is reduced due to translation competition,

1376 increasing misassembled rRNA. As a result, degradation of rRNA by exosomes may be accelerated,

1377 resulting in abnormal nucleolus morphology and reduction of ribosomes.

1378 **C**) In exosome-deficient cells like the *mtr4-1* cells, errors in rRNA processing occur due to the reduction

1379 of degradation by exosomes, resulting in the reduction of ribosomes and growth defects.

1380 **D**) In mox-YG overexpressing, exosome-deficient cells, degradation of misassembled rRNA is reduced,

1381 and nucleolus formation and ribosome biosynthesis are partially recovered.

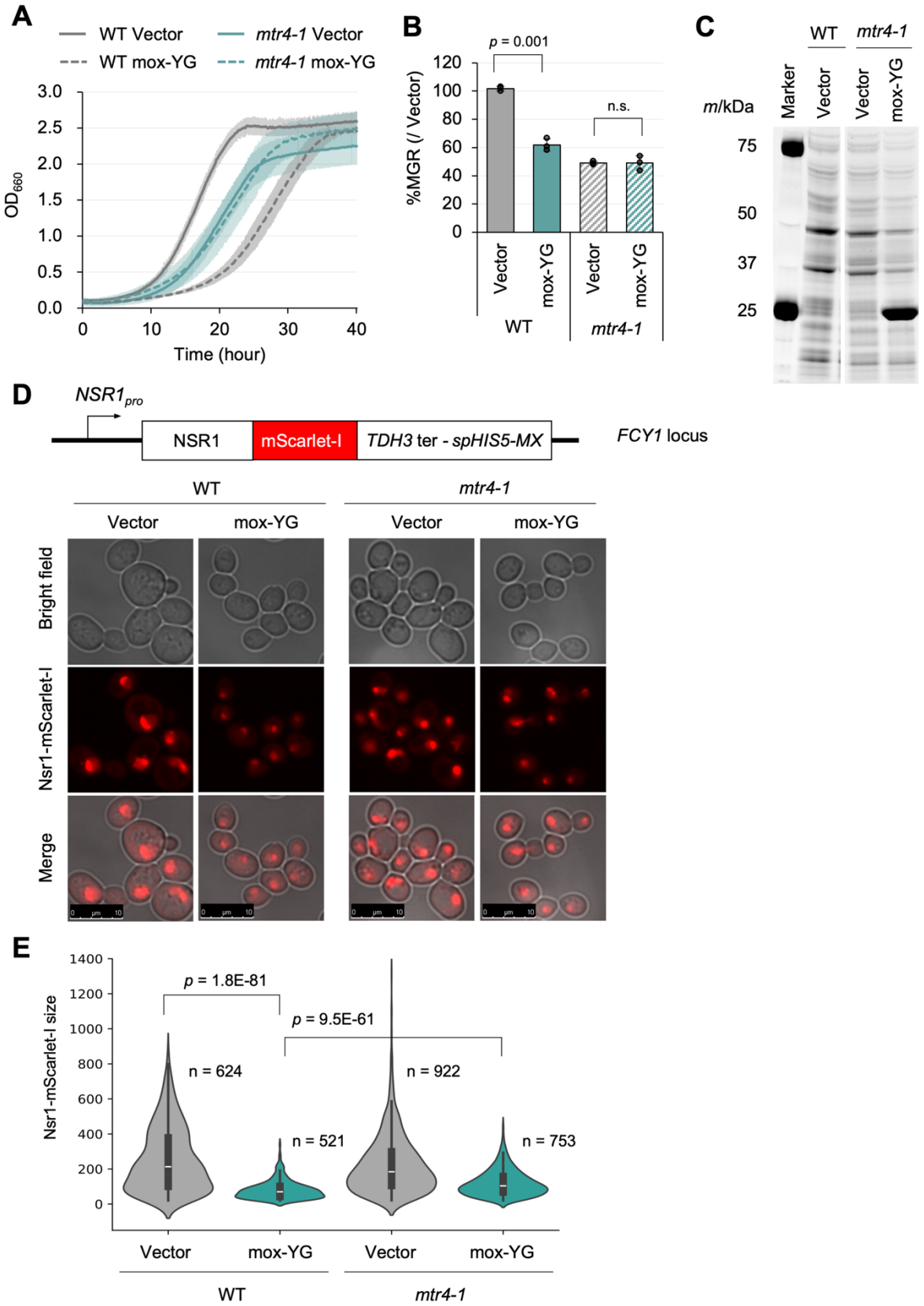

Figure 5—figure supplement 5. Positive genetic interaction between exosome mutation (*mtr4-1*) and mox-YG overexpression

1385 **A**) Growth curves of the wild type (WT) and *mtr4-1* mutant cells with the vector or under
1386 overexpression of mox-YG in SC–LeuUra medium at 30˚C. The solid or dotted lines show the average
1387 calculated from three biological replicates. Shaded zones indicate their SDs.
1388 **B**) MGR of the wild type (WT) and *mtr4-1* mutant cells with the vector or under overexpression of
1389 mox-YG (percent over the vector control). The bars and error bars show the means and SDs calculated
1390 from three biological replicates. The raw data is shown with dot plots. The *p*-value of Welch's *t*-test is
1391 shown. n.s.: $p > 0.05$.
1392 **C)** Gel images of SDS-PAGE-separated proteins extracted from the wild type (WT) and *mtr4-1* mutant
1393 cells with the vector or under overexpression of mox-YG. All proteins were separated after staining
1394 with a fluorescent dye.
1395 **D)** Observation of nucleolus. The construct to observe nucleolus (Nsr1-mScarlet-I fusion gene) was
1396 integrated into the genomic *FCY1* locus. Fluorescence microscopy image of nucleolus-localized protein
1397 Nsr1-mScarlet-I of the WT and *mtr4-1* mutant cells with the vector or mox-YG overexpression.
1398 **E)** Quantification of the size of Nsr1-mScarlet-I fluorescent region in WT and *mtr4-1* cells with the
1399 vector or mox-YG overexpression. The number (n) of observed cells is shown. The *p*-values were
1400 calculated by Welch's *t*-test.

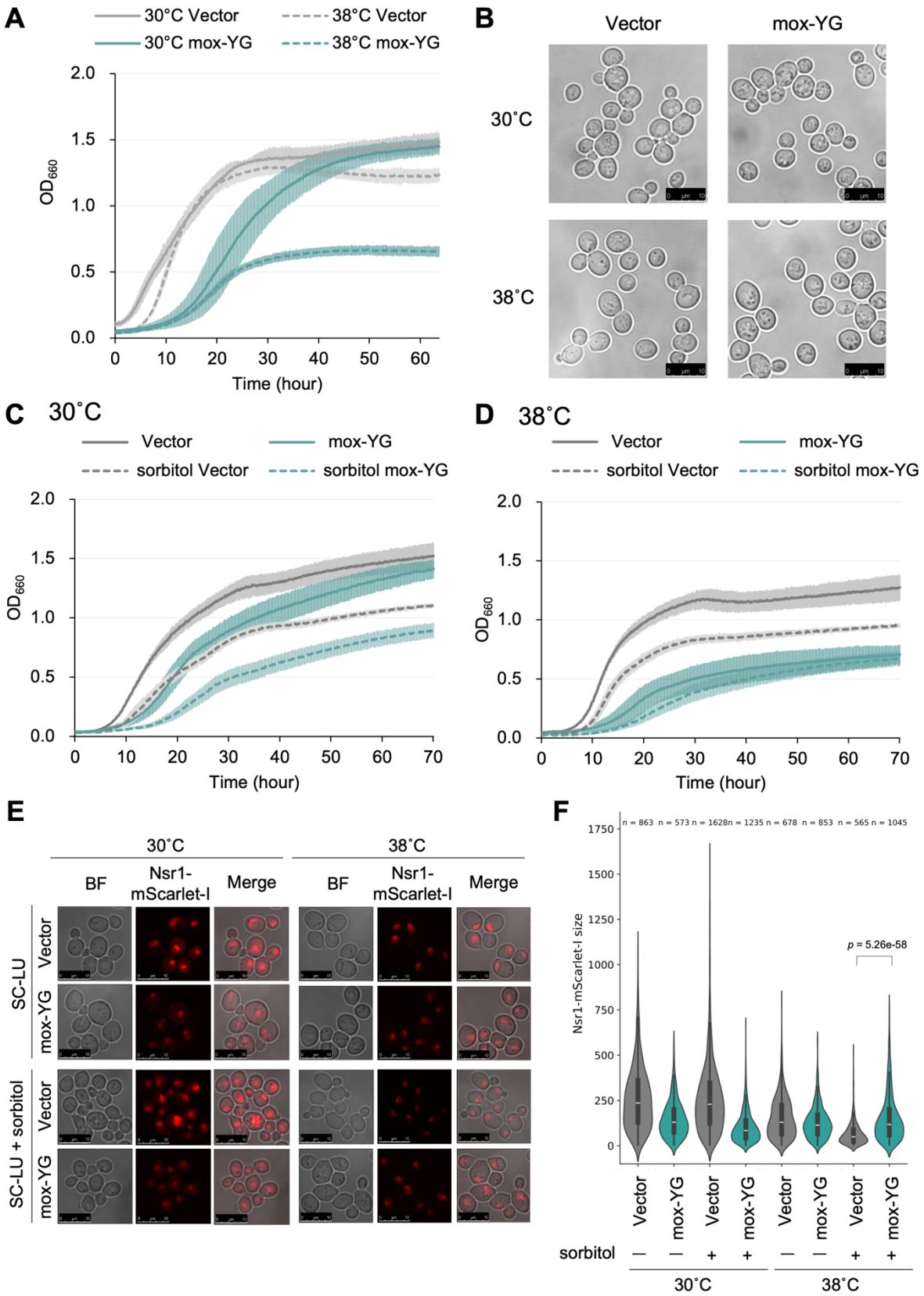

Figure 5—figure supplement 6. Comparison of growth of glycolytic enzymes overexpressing strains.

1404 **A**, **C**, **D**) Growth curves of cells with the vector or under mox-YG overexpression in SC–LeuUra
1405 medium at the indicated temperature. In the indicated culture, sorbitol (1 M) is added. The solid or
1406 dotted lines show the average calculated from three biological replicates. Shaded zones indicate their
1407 standard deviations.
1408 **B**) Bright-field microscopic images of cells with the vector or under mox-YG overexpression cultured
1409 at the indicated temperature.
1410 **E)** Fluorescence microscopy image showing the size of the Nsr1-mScarlet-I nucleolus, observed in the
1411 vector control or mox-YG over-expressing cells (OD_{660} = 1.0) when cultured at 38°C or in sorbitol-
1412 enriched medium.
1413 **F**) Quantification results of the Nsr1-mScarlet-I regions observed in the eight conditions indicated in **E**.
1414 Number of cells observed (n) is shown. The *p*-value was calculated by the Mann-Whitney *U*-test.

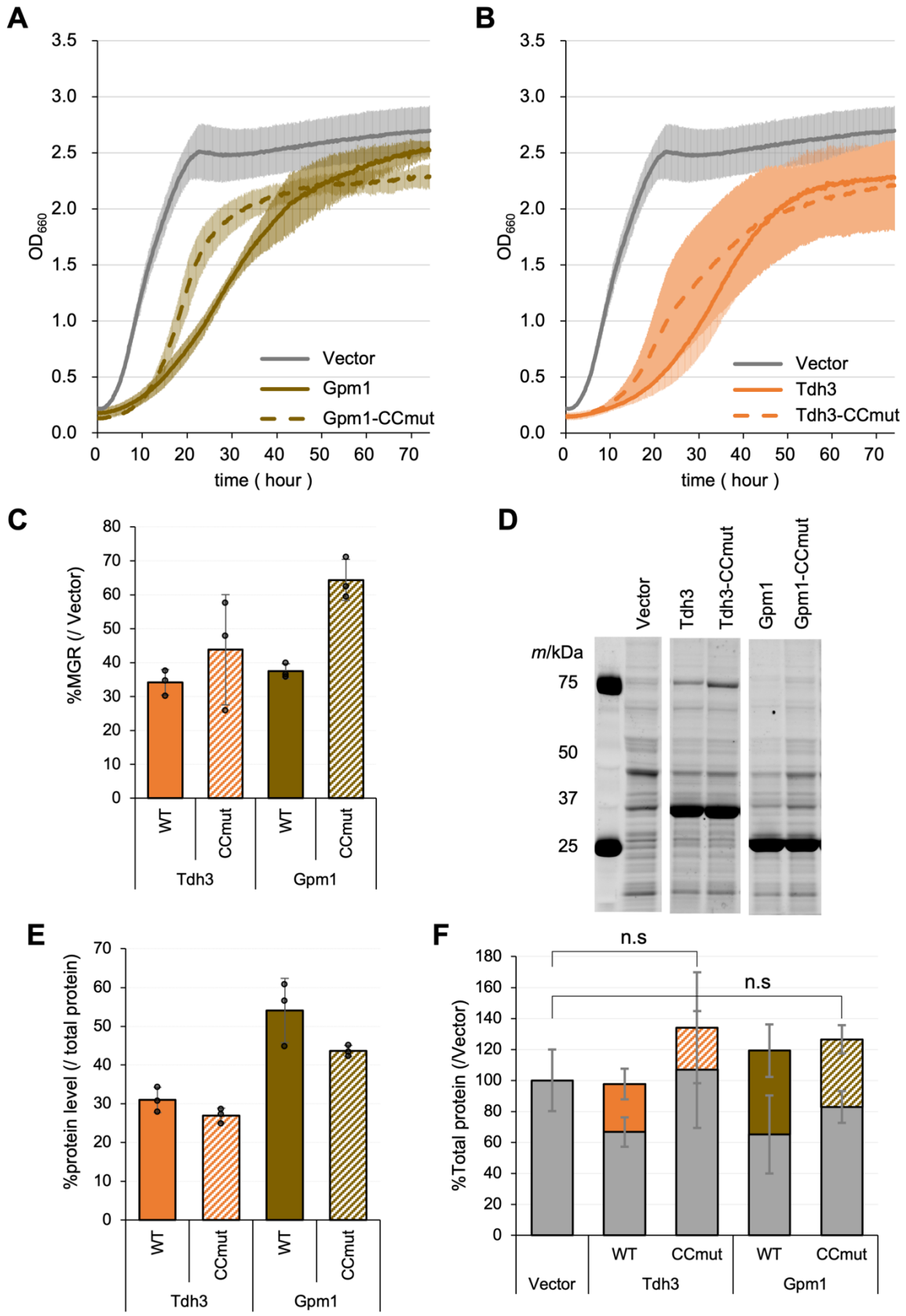

1415

1416 **Figure 6—figure supplement 1. Evaluation of the neutrality of Tdh3 and Gpm1.**

1417 **A**, **B**) Growth curves of cells with the vector (Vector) and overexpressing Gpm1 and Tdp3 and their
1418 catalytic center mutants (CCmut) in synthetic medium (–LeuUra). The solid or dotted lines show the
1419 average calculated from three biological replicates. Shaded zones indicate their SD.
1420 **C**) MGR of cells overexpressing indicated proteins (percent over the vector control).
1421 **D**) Gel images of SDS-PAGE-separated proteins extracted from cells overexpressing indicated proteins.
1422 All proteins were separated after staining with a fluorescent dye.
1423 **E**) Protein levels of the target protein (percent over the total protein). The amount was calculated from
1424 the intensity of the target bands separated by SDS-PAGE of **D**.
1425 **F**) Ratio of total protein content of cells overexpressing glycolytic enzymes over the vector control.
1426 Gray bars and error bars indicate expression levels and SDs for proteins other than glycolytic enzymes;
1427 non-gray bars and error bars indicate expression levels and SDs for each overexpressed protein.
1428 The bars and error bars in **C, E**, and **F** show the means and SDs calculated from three biological
1429 replicates. The raw data is shown with dot plots.

Gpm1

```
   1  M  P  K  L  V  L  V  R  H  G  Q  S  E  W  N  E  K  N  L  F  20
 959 ATGCCAAAGTTAGTTTTAGTTAGACACGGTCAATCCGAATGGAACGAAAAGAACTTATTC 1018

  21  T  G  W  V  D  V  K  L  S  A  K  G  Q  Q  E  A  A  R  A  G  40
1019 ACCGGTTGGGTTGATGTTAAATTGTCTGCCAAGGGTCAACAAGAAGCCGCTAGAGCCGGT 1078

  41  E  L  L  K  E  K  K  V  Y  P  D  V  L  Y  T  S  K  L  S  R  60
1079 GAATTGTTGAAGGAAAAGAAGGTCTACCCAGACGTCTTGTACACTTCCAAGTTGTCCAGA 1138

  61  A  I  Q  T  A  N  I  A  L  E  K  A  D  R  L  W  I  P  V  N  80
1139 GCTATCCAAACTGCTAACATTGCTTTGGAAAAGGCTGACAGATTATGGATTCCAGTCAAC 1198

  81  R  S  W  R  L  N  E  R  H  Y  G  D  L  Q  G  K  D  K  A  E  100
1199 AGATCCTGGAGATTGAACGAAAGACATTACGGTGACTTACAAGGTAAGGACAAGGCTGAA 1258

 101  T  L  K  K  F  G  E  E  K  F  N  T  Y  R  R  S  F  D  V  P  120
1259 ACTTTGAAGAAGTTCGGTGAAGAAAAATTCAACACCTACAGAAGATCCTTCGATGTTCCA 1318

 121  P  P  P  I  D  A  S  S  P  F  S  Q  K  G  D  E  R  Y  K  Y  140
1319 CCTCCCCCAATCGACGCTTCTTCTCCATTCTCTCAAAAGGGTGATGAAAGATACAAGTAC 1378

 141  V  D  P  N  V  L  P  E  T  E  S  L  A  L  V  I  D  R  L  L  160
1379 GTTGACCCAAATGTCTTGCCAGAAACTGAATCTTTGGCTTTGGTCATTGACAGATTGTTG 1438

 161  P  Y  W  Q  D  V  I  A  K  D  L  L  S  G  K  T  V  M  I  A  180
1439 CCATACTGGCAAGATGTCATTGCCAAGGACTTGTTGAGTGGTAAGACCGTCATGATCGCC 1498

 181  A  A  G  N  S  L  R  G  L  V  K  H  L  E  G  I  S  D  A  D  200
1499 GCTgcCGGTAACTCCTTGAGAGGTTTGGTTAAGCACTTGGAAGGTATCTCTGATGCTGAC 1558

 201  I  A  K  L  N  I  P  T  G  I  P  L  V  F  E  L  D  E  N  L  220
1559 ATTGCTAAGTTGAACATCCCAACTGGTATTCCATTGGTCTTCGAATTGGACGAAAACTTG 1618

 221  K  P  S  K  P  S  Y  Y  L  D  P  E  A  A  A  A  G  A  A  A  240
1619 AAGCCATCTAAGCCATCTTACTACTTGGACCCAGAAGCTGCCGCTGCTGGTGCCGCTGCT 1678

 241  V  A  N  Q  G  K  K  *  248
1679 GTTGCCAACCAAGGTAAGAAATAA 1702
```

Tdh3

```
   1  M  V  R  V  A  I  N  G  F  G  R  I  G  R  L  V  M  R  I  A  20
 959 ATGGTTAGAGTTGCTATTAACGGTTTCGGTAGAATCGGTAGATTGGTCATGAGAATTGCT 1018

  21  L  S  R  P  N  V  E  V  V  A  L  N  D  P  F  I  T  N  D  Y  40
1019 TTGTCTAGACCAAACGTCGAAGTTGTTGCTTTGAACGACCCATTCATCACCAACGACTAC 1078

  41  A  A  Y  M  F  K  Y  D  S  T  H  G  R  Y  A  G  E  V  S  H  60
1079 GCTGCTTACATGTTCAAGTACGACTCCACTCACGGTAGATACGCTGGTGAAGTTTCCCAC 1138

  61  D  D  K  H  I  I  V  D  G  K  K  I  A  T  Y  Q  E  R  D  P  80
1139 GATGACAAGCACATCATTGTCGATGGTAAGAAGATTGCTACTTACCAAGAAAGAGACCCA 1198

  81  A  N  L  P  W  G  S  S  N  V  D  I  A  I  D  S  T  G  V  F  100
1199 GCTAACTTGCCATGGGGTTCTTCCAACGTTGACATCGCCATTGACTCCACTGGTGTTTTC 1258

 101  K  E  L  D  T  A  Q  K  H  I  D  A  G  A  K  K  V  V  I  T  120
1259 AAGGAATTAGACACTGCTCAAAAGCACATTGACGCTGGTGCCAAGAAGGTTGTTATCACT 1318

 121  A  P  S  S  T  A  P  M  F  V  M  G  V  N  E  E  K  Y  T  S  140
1319 GCTCCATCTTCCACCGCCCCAATGTTCGTCATGGGTGTTAACGAAGAAAAATACACTTCT 1378

 141  D  L  K  I  V  S  N  A  S  S  T  T  N  C  L  A  P  L  A  K  160
1379 GACTTGAAGATTGTTTCCAACGCTTCTTcTACCACCAACTGTTTGGCTCCATTGGCCAAG 1438

 161  V  I  N  D  A  F  G  I  E  E  G  L  M  T  T  V  H  S  L  T  180
1439 GTTATCAACGATGCTTTCGGTATTGAAGAAGGTTTGATGACCACTGTCCACTCTTTGACT 1498

 181  A  T  Q  K  T  V  D  G  P  S  H  K  D  W  R  G  G  R  T  A  200
1499 GCTACTCAAAAGACTGTTGACGGTCCATCCCACAAGGACTGGAGAGGTGGTAGAACCGCT 1558

 201  S  G  N  I  I  P  S  S  T  G  A  A  K  A  V  G  K  V  L  P  220
1559 TCCGGTAACATCATCCCATCCTCCACCGGTGCTGCTAAGGCTGTCGGTAAGGTCTTGCCA 1618

 221  E  L  Q  G  K  L  T  G  M  A  F  R  V  P  T  V  D  V  S  V  240
1619 GAATTGCAAGGTAAGTTGACCGGTATGGCTTTCAGAGTCCCAACCGTCGATGTCTCCGTT 1678

 241  V  D  L  T  V  K  L  N  K  E  T  T  Y  D  E  I  K  K  V  V  260
1679 GTTGACTTGACTGTCAAGTTGAACAAGGAAACCACCTACGATGAAATCAAGAAGGTTGTT 1738

 261  K  A  A  A  E  G  K  L  K  G  V  L  G  Y  T  E  D  A  V  V  280
1739 AAGGCTGCCGCTGAAGGTAAGTTGAAGGGTGTTTTGGGTTACACCGAAGACGCTGTTGTC 1798

 281  S  S  D  F  L  G  D  S  H  S  S  I  F  D  A  S  A  G  I  Q  300
1799 TCCTCTGACTTCTTGGGTGACTCTCACTCTTCCATCTTCGATGCTTCCGCTGGTATCCAA 1858

 301  L  S  P  K  F  V  K  L  V  S  W  Y  D  N  E  Y  G  Y  S  T  320
1859 TTGTCTCCAAAGTTCGTCAAGTTGGTCTCCTGGTACGACAACGAATACGGTTACTCTACC 1918

 321  R  V  V  D  L  V  E  H  V  A  K  A  *  333
1919 AGAGTTGTCGACTTGGTTGAACACGTTGCCAAGGCTTAA 1957
```

1430

1431 **Figure 6—figure supplement 2. Nucleotide and amino acid sequences of Gpm1 and Tdh3.**

1432 The amino acid substitutions introduced to eliminate enzyme activity are shown in red. The H182A

1433 mutation in Gpm1 was referred to the study by White *et al*. (White and Fothergill-Gilmore, 1992), and

1434 the C150S mutation in Tdh3 was referred to the study by Peralta et al. (Peralta et al., 2015).

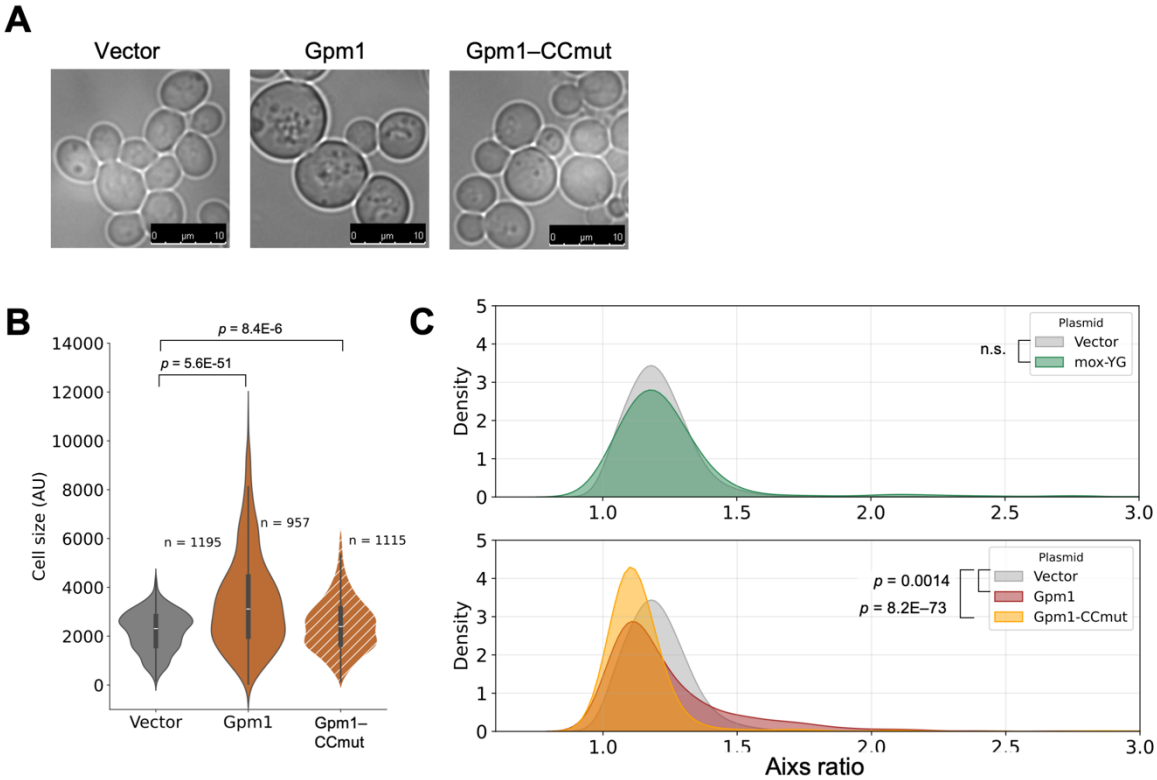

1435

1436 **Figure 6—figure supplement 3. Overexpression of Gpm1 and its CC-mutant induces abnormal**

1437 **cell morphology.**

1438 **A**) Representative microscopic images of cells overexpressing Gpm1 or Gpm1–CCmut.

1439 **B**) Violin plots showing cell size quantified from microscopic images. The number of cells used for

1440 the quantification is shown. The *p*–values were calculated by the Mann–Whitney *U*–test.

1441 **C**) Distribution of cell axis ratios upon overexpression of mox–YG, Gpm1, and Gpm1–CCmut,

1442 compared with the vector control. The *p*–values were calculated by the Mann–Whitney *U*–test. "n.s."

1443 means $p > 0.05$.

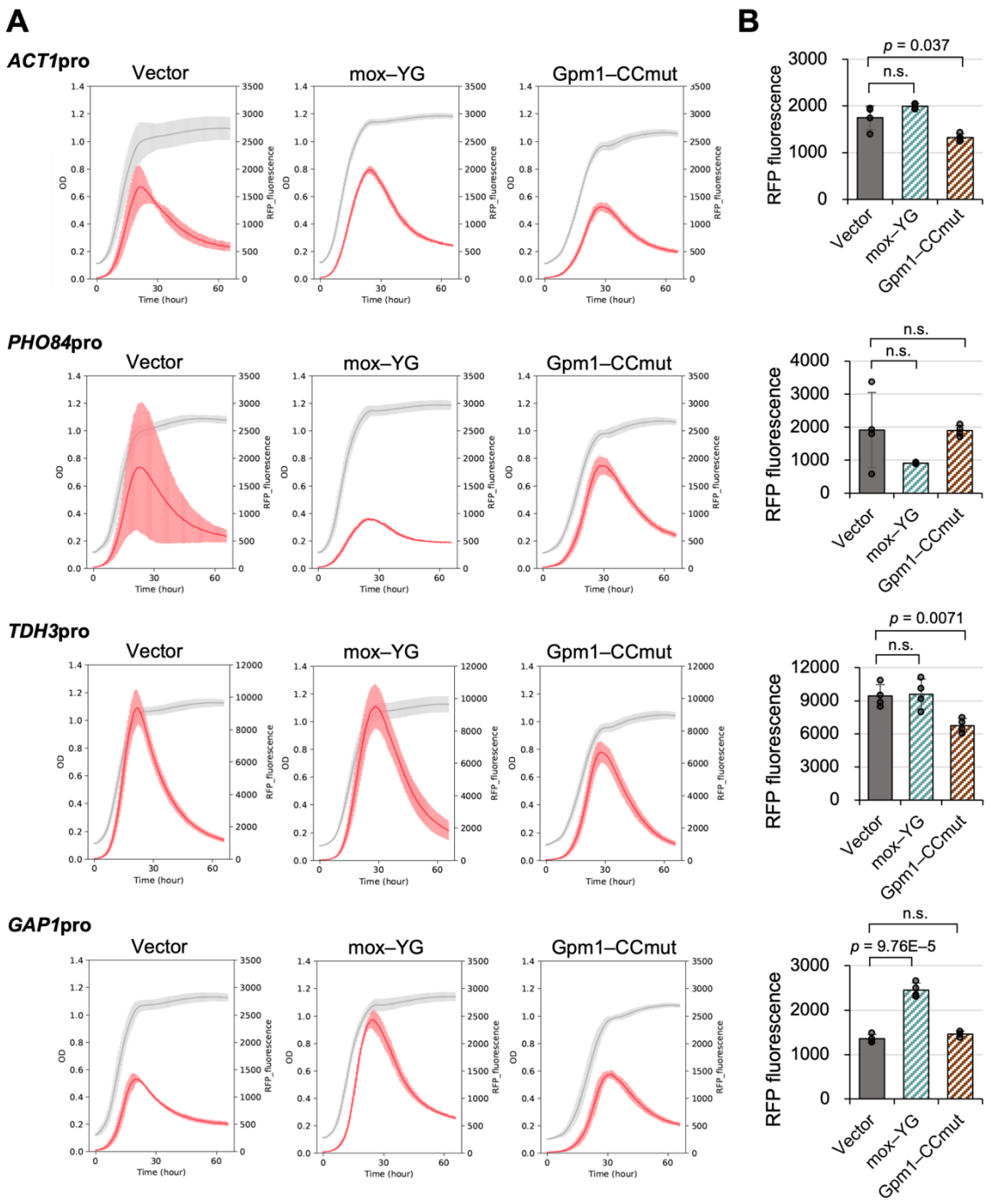

1444

1445 **Figure 6—figure supplement 4. Transcriptional response under mox–YG and Gpm1 CC-mutant**

1446 **overexpression.**

1447 **A**) Curves representing time series data of cell growth (gray, OD_{595}) and mScarlet–I fluorescence (red,

1448 arbitrary unit) overexpressing mox–YG and Gpm1–CCmut in SC–LeuUra + 50 mg/mL leucine medium

1449 for each promoter. Solid lines are averages calculated from four biological replicates.

1450 **B**) Quantitative results of mScarlet–I fluorescence values for each promoter. Bars and error bars indicate

1451 the mean and SD of maximum fluorescence values (arbitrary unit) for mScarlet–I calculated from four

1452 biological replicates. Raw data are shown as dot plots. The *p*–values were calculated by performing

1453 Welch's *t*–test and applying the Bonferroni correction. “n.s.” means $p > 0.05$.

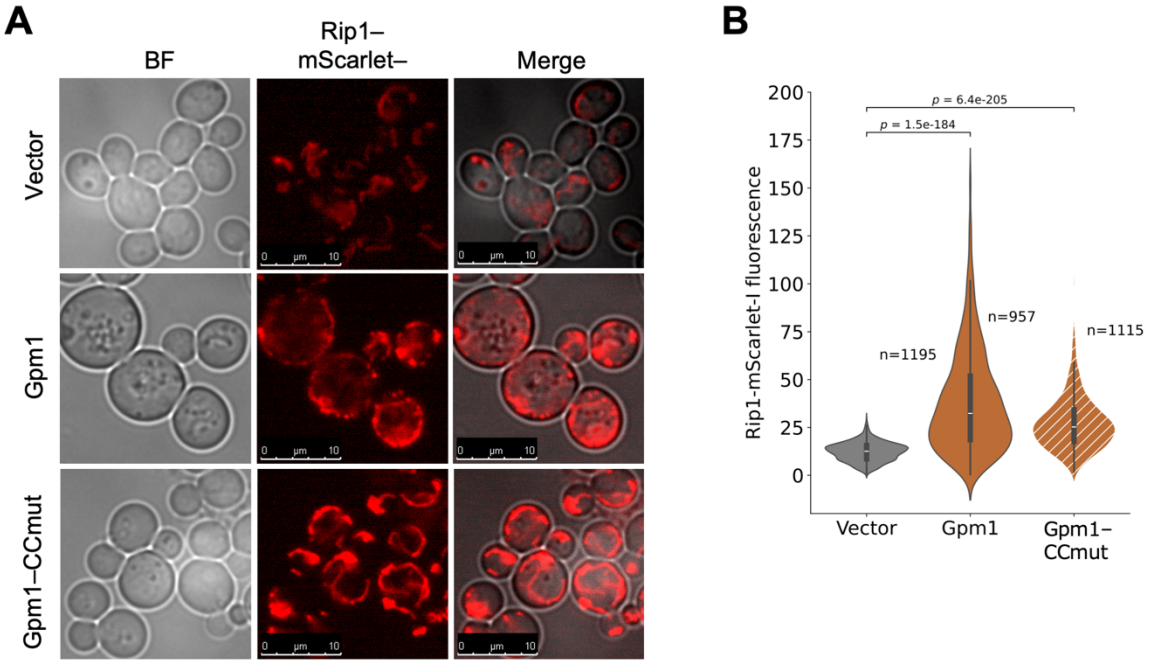

1454

1455 **Figure 6—figure supplement 5. Microscopic observation of mitochondria in cells overexpressing**

1456 **Gpm1 or Gpm1-CCmut.**

1457 **A**) Fluorescence microscopy image showing the size of nucleolus with Rip1–mScarlet–I. Log phase

1458 cells (OD_{660} = 1.0) with the vector or under Gpm1 or Gpm1–CCmut overexpression were observed.

1459 **B**) Quantification of the fluorescence value of Rip1–mScarlet–I in the cells with the vector or Gpm1 or

1460 Gpm1–CCmut overexpression. The number of cells used for the quantification is shown. The *p*–values

1461 were calculated by Mann–Whitney *U* test.

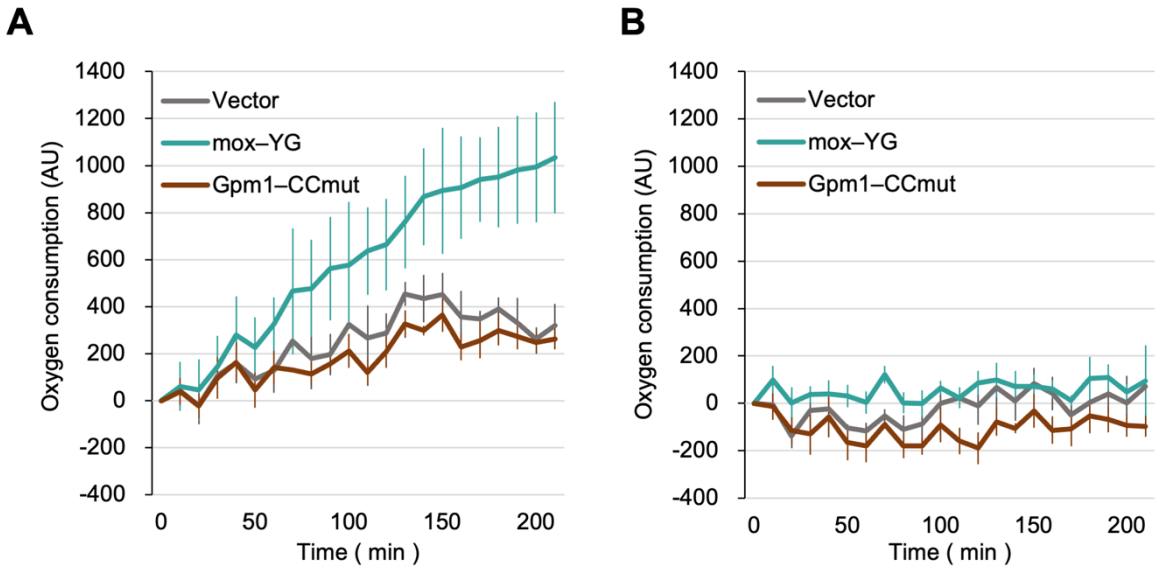

1462

1463 **Figure 6—figure supplement 6. Time-course analysis of oxygen consumption in Gpm1-CCmut**

1464 **overexpressing cells.**

1465 **A**, **B**) Line graphs showing changes in the fluorescence of an oxygen-sensitive probe, measured in

1466 synthetic medium (**A**) and in medium containing 50 µM antimycin A (**B**). Solid lines represent the mean

1467 values from three biological replicates; error bars indicate standard deviations.

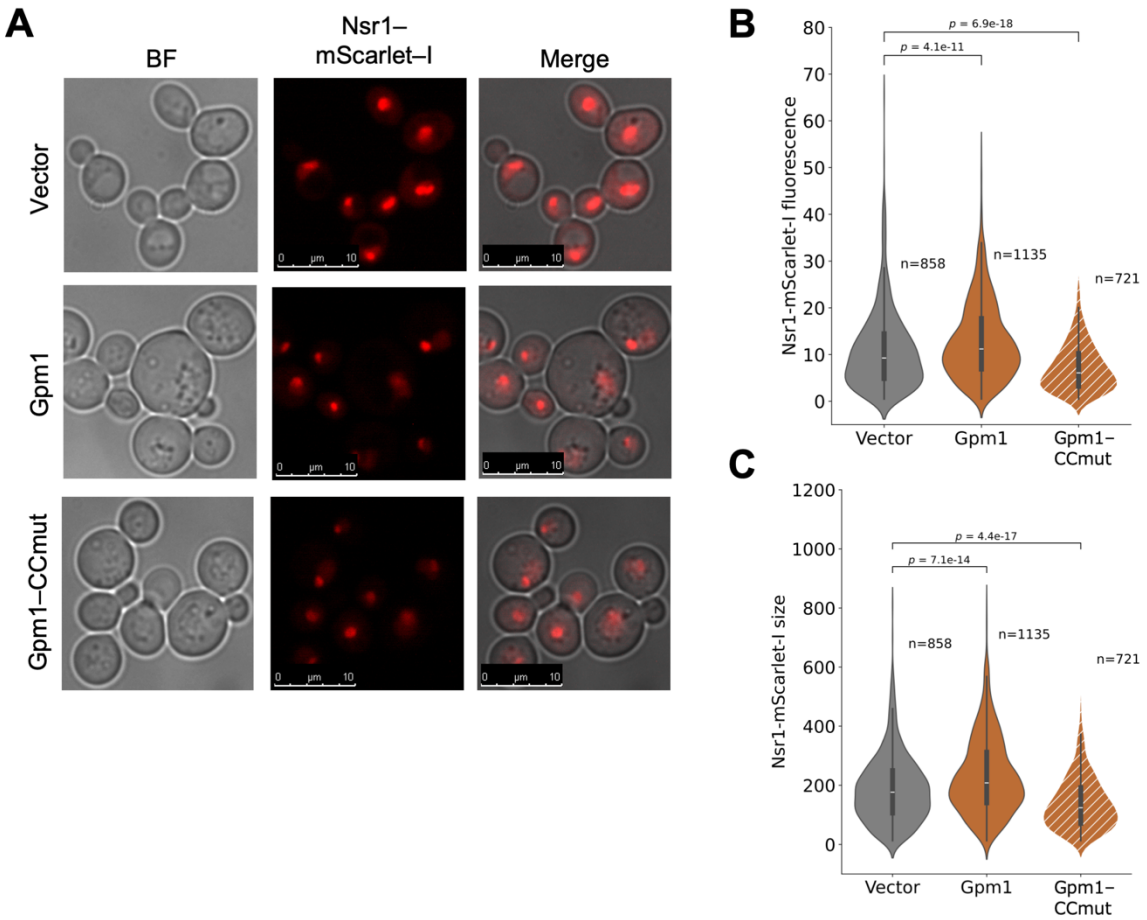

Figure 6—figure supplement 7. Microscopic observation of nucleoli in cells overexpressing Gpm1 or Gpm1-CCmut.

A) Fluorescence microscopy images showing the size of nucleolus with Nsr1–mScarlet–I. Log phase cells (OD_{660} = 1.0) with the vector or under Gpm1 or Gpm1–CCmut overexpression were observed.

B, **C**) Quantification of the size of Nsr1–mScarlet–I fluorescent region (**B**) and fluorescence value of Nsr1–mScarlet–I (**C**) in the cells with the vector or Gpm1 or Gpm1–CCmut overexpression. The number of cells used for the quantification is shown. The *p*–values were calculated by Mann–Whitney *U* test.